University of Southampton

Faculty of Medicine

Clinical and Experimental Sciences

The profile of cerebral T cells in dementia with Lewy bodies

by

Claire Louise Gee

ORCID ID: 0000-0002-2215-5949

Thesis for the degree of Doctor of Medicine

October 2025

University of Southampton

Abstract

Faculty of Medicine

Clinical and Experimental Sciences

Thesis for the degree of Doctor of Medicine

The profile of cerebral T cells in dementia with Lewy bodies

Claire Louise Gee

Dementia with Lewy bodies (DLB) is the second most common neurodegenerative cause of dementia, behind Alzheimer's disease (AD). Neuroinflammation has been implicated in the aetiology of AD, with the involvement of both innate and adaptive immune responses. A potential role for adaptive immune cells is supported by T cell recruitment into the brain parenchyma in AD, however, this has not yet been extensively investigated in DLB.

To determine the cerebral profile of T cells in DLB, a human *post-mortem* study was conducted to examine T cell populations in brain tissue from 30 DLB and 29 control cases using immunohistochemistry. Specific markers were used to identify T cell populations: CD4 (T helper cells), CD8 (T cytotoxic cells), Foxp3 (Treg), Tbet (T helper/cytotoxic 1 cells) and GATA3 (T helper/cytotoxic 2 cells). T cell numbers were quantified and categorised by location (grey or white matter) and compartment (parenchyma or perivascular). Markers of neuropathology and inflammation were correlated with T cell markers.

The study revealed increased numbers of CD4+ T cells in the grey matter parenchyma in DLB compared to controls. Although no significant difference was observed in the number of CD8+ T cells between groups, there was a trend towards increased numbers of CD8+ T cells in the DLB group. Within grey matter in DLB, the number of CD8+ T cells was associated with increased neuronal expression of CD32b. Further exploration of T cell subsets revealed increased numbers of Tbet+ and GATA3+ T cells in the grey matter parenchyma in DLB. In contrast, there was no significant difference in the number of Foxp3+ T cells between groups. Increased numbers of Tbet+ T cells were associated with increased expression of the inflammatory markers, CD64 and CD32b in DLB. No associations were found between CD4, Foxp3, GATA3 and markers of inflammation. Correlations with markers of neuropathology revealed no associations with any T cell marker.

This project provides evidence of an altered profile of T cells in the DLB brain with increased recruitment of CD4+ T cells into the grey matter parenchyma, potentially contributing to neuroinflammation and neurodegeneration in DLB. The increased presence of Tbet+ and GATA3+ T cells within the grey matter parenchyma implicate T helper 1 and T helper 2 cells as the infiltrating CD4+ T cell subsets. The association between Tbet+ T cells and CD64 may represent interactions with microglia to promote proinflammatory responses in DLB. Interactions between CD8+ and Tbet+ T cells with neurons are inferred by associations with CD32b, potentially contributing to synaptic dysfunction. The lack of association with markers of neuropathology in DLB suggests that T cell responses occur independently of neuropathological changes. Further exploration of T cell subsets in the brain, cerebrospinal fluid and blood compartments is warranted in DLB to improve our understanding of disease mechanisms and to guide the development of therapeutic strategies such as T cell modulation.

Table of Contents

Table of Tables

Table of Figures

List of Accompanying Materials

Suppporting data via University of Southampton repository:

http://doi.org/10.5258/SOTON/D3908

Research Thesis: Declaration of Authorship

Print name: Claire Louise Gee

Title of thesis: The profile of cerebral T cells in dementia with Lewy bodies

I declare that this thesis and the work presented in it are my own and has been generated by me as the result of my own original research.

I confirm that:

1. This work was done wholly or mainly while in candidature for a research degree at this University;
2. Where any part of this thesis has previously been submitted for a degree or any other qualification at this University or any other institution, this has been clearly stated;
3. Where I have consulted the published work of others, this is always clearly attributed;
4. Where I have quoted from the work of others, the source is always given. With the exception of such quotations, this thesis is entirely my own work;
5. I have acknowledged all main sources of help;
6. Where the thesis is based on work done by myself jointly with others, I have made clear exactly what was done by others and what I have contributed myself;
7. Parts of this work have been published as:-

Amin J, Gee C, Stowell K, Coulthard D, Boche D. T lymphocytes and Their Potential Role in Dementia with Lewy Bodies. *Cells* 2023; 12(18):2283. https://doi.org/10.3390/cells12182283

Signature: .....

Date:

Acknowledgements

This work was funded through grants awarded from the University of Southampton Research Management Committee and the British Neuropathological Society.

I am very grateful to my supervisors Dr Jay Amin and Prof Delphine Boche for their invaluable guidance, support and encouragement throughout the course of this work. Dr Amin provided access to an existing cohort of cases and data from a previous study which provided an important foundation for this project.

Thank you to the staff at the Biomedical Imaging Unit and Histochemistry Research Unit for their assistance in digital image acquisition and immunostaining. Regan Doherty provided training and supervision for automated slide scanning. Jon Ward and Jenny Norman trained me to optimise and conduct immunohistochemistry experiments for GATA3. I am grateful to Dr Jin Wang and the staff at the Clinical Pathology Department for their assistance in performing immunohistochemistry experiments for additional T cell markers. Acknowledgements also go Iain Hartnell for his guidance on the use of QuPath for T cell detection.

Staff at the Memory Assessment and Research Centre have supported me to complete this study during my research post, for which I am very thankful.

Lastly, a huge thank you to my family. This work would not have been possible without the incredible support I have received from my husband, Sam and three children, Sophie, Holly and Thomas.

Definitions and Abbreviations

α -syn..... Alpha-synuclein

ABC ..... Avidin-biotin complex

ACE-R ..... Addenbrooke's cognitive examination – revised

ACKR3 ..... Atypical chemokine receptor 3

AD ..... Alzheimer's disease

APC ..... Antigen presenting cell

APOE ..... Apolipoprotein E

APP..... Amyloid precursor protein

Aβ..... Amyloid-beta

BBB ..... Blood-brain barrier

CD ..... Cluster of differentiation

cDNA ..... Complementary deoxyribonucleic acid

CHI31 ..... Chitinase-3-like-1

CNS..... Central nervous system

CSF ..... Cerebrospinal fluid

CT..... Computerised tomography

CXCR4 ..... C-X-C motif chemokine receptor 4

CXCL12 ..... C-X-C motif chemokine ligand 12

DAB ..... Diaminobenzidine

DAMP ..... Damage associated molecular pattern

DLB ..... Dementia with Lewy bodies

DNA..... Deoxyribonucleic acid

EDTA..... Ethylenediaminetetraacetic acid

EEG ..... Electroencephalography

ERGO..... Ethics and Research Governance Online

FcγR ..... Fc gamma receptor

FDG ..... Fluorodeoxyglucose

FFPE ..... Formalin fixed and paraffin embedded

Foxp3..... Forkhead box P3

GATA3..... GATA3 binding protein 3

GFAP ..... Glial fibrillary acidic protein

GI ..... Gastrointestinal

GWAS ..... Genome-wide association study

HLA-DR..... Human leukocyte antigen – antigen D related

HRU..... Histochemistry research unit

Iba1 ..... Ionized calcium-binding adapter molecule 1

IFN..... Interferon

Ig ..... Immunoglobulin

IL ..... Interleukin

Ki-67 ..... Kiel 67

LB ..... Lewy body

LBD ..... Lewy body disease

LN..... Lewy neurite

LNDBB..... London Neurodegenerative Brain Bank

LRP..... Lewy-related pathology

MCI..... Mild cognitive impairment

MHC ..... Major histocompatibility complex

MHCI ..... Major histocompatibility complex class 1

MHCII ..... Major histocompatibility complex class 2

MIBG ..... Metaiodobenzylguanidine

MRI ..... Magnetic resonance imaging

mRNA ..... messenger ribonucleic acid

NIA-AA..... National Institute on Ageing-Alzheimer's Association

NFT..... Neurofibrillary tangles

NK ..... Natural killer

NREC ..... National Research Ethics Committee

PAMP ..... Pathogen associated molecular pattern

PD ..... Parkinson's disease

PDD ..... Parkinson's disease dementia

PET ..... Position emission tomography

PFF ..... Preformed fibril

PRR ..... Pattern recognition receptor

ptau ..... Hyperphosphorylated tau

REM ..... Rapid eye movement

ROI ..... Region of interest

RNA ..... Ribonucleic acid

RORμt ..... Retinoic acid-related orphan receptor gamma t

RT-qPCR ..... Reverse transcription quantitative polymerase chain reaction

SPECT ..... Single-photon emission computed tomograph

SN ..... Substantia nigra

SWDBB ..... South West Dementia Brain Bank

Tbet ..... T-box transcription factor

TBS ..... Trisaminomethane buffered saline

Tc ..... T cytotoxic

TCM ..... Central memory T cell

TEM ..... Effector memory T cell

Th ..... T helper

TCR ..... T cell receptor

Thy-1 ..... Thymocyte differentiation antigen 1

TGF ..... Transforming growth factor

TNF ..... Tumour necrosis factor

TRM ..... Tissue-resident memory T cell

Treg ..... T regulatory

Ts ..... T suppressor

TSPO ..... Translocator protein

UHS ..... University Hospitals Southampton

UPDRS ..... Unified Parkinson's disease rating scale

vGLUT1 ..... Vesicular glutamate transporter 1

Chapter 1 Introduction

The prevalence of dementia worldwide is expected to almost triple by the year 2050 from an estimated 57.4 million in 2019 to 152.8 million (1). Dementia is associated with considerable societal and monetary costs with global spending reaching an approximated US$263 billion in 2019. The cost and prevalence of dementia are expected to rise exponentially due to continued population growth and ageing, further increasing the burden on healthcare systems (2).

Dementia is a progressive, irreversible clinical syndrome characterised by a range of cognitive and behavioural symptoms which cause a decline in functioning (3). Cognitive deficits in dementia should not be explained by any other psychiatric disorder and should not occur exclusively during episodes of delirium (4). The clinical presentation of dementia varies but symptoms can include impairments in memory, language, judgement and visuospatial ability. Cognitive impairment is often accompanied by deterioration in emotional control, social behaviour or motivation (5).

The most common cause of dementia is Alzheimer's disease (AD), comprising 60-80% of cases (6). Other major subtypes include vascular dementia, dementia with Lewy bodies (DLB), frontotemporal dementia and Parkinson's disease dementia (PDD). The onset and variable pattern of cognitive deficits can help attribute the cause of dementia to one or more of these diseases. It is often easiest to differentiate AD from other causes of dementia in the early stage of disease, as clinical features can appear similar in late stages (3).

1.1 Dementia with Lewy bodies

Lewy body diseases (LBD) are defined by the accumulation of aggregated forms of the synaptic protein alpha-synuclein (α-syn) in the brain, and include DLB, Parkinson's disease (PD) and PDD (7). DLB and PDD are typically associated with cognitive impairment, whereas PD involves early and prominent extrapyramidal motor features (8).

The motor signs of PD include bradykinesia, resting tremor and rigidity, in addition to changes in gait and posture. These movement disturbances are linked to striatal dopamine loss and nigral degeneration (9). Cognitive symptoms are common during PD progression and the prevalence of dementia is approximately 25%-30% (10), rising to over 80% 20 years after diagnosis (11).

PDD and DLB are clinically distinguishable by the timing of onset of motor symptoms compared to cognitive symptoms. DLB is diagnosed if dementia develops prior to parkinsonism or within one year after onset. PDD is diagnosed if dementia develops more than one year after the onset of parkinsonism (12). As both diseases progress, underlying pathological changes are often very

similar and they can be considered as a continuum rather than distinct entities (13). Together, PDD and DLB are commonly referred to as Lewy body dementia.

1.1.1 Epidemiology

DLB is the second most common neurodegenerative cause of dementia behind AD (14). Prevalence rates in the UK indicate that DLB accounts for 4.2% of dementia diagnoses in the community and 7.5% of dementia diagnoses in secondary care (15). DLB is more common in men than women (16) and most cases are seen between the ages of 70 and 85 (17).

There is significant disparity between the number of cases of DLB diagnosed clinically and those diagnosed via evaluation of neuropathology at *post-mortem*. In a study including 98 subjects with DLB confirmed at *post-mortem*, only 48% had been accurately diagnosed clinically with DLB (18). This suggests that clinical cases of DLB are under diagnosed and the prevalence of DLB is likely to be underestimated (19). Due to overlapping clinical features, DLB is commonly misdiagnosed as AD or PD (20).

1.1.2 Clinical features

The international consensus criteria for the diagnosis of DLB were updated in 2017 with the aim to increase suboptimal detection rates (12). Modifications to the international consensus criteria included differentiation between clinical features and diagnostic biomarkers, as well as guidance on how to assess and interpret these (19).

The essential feature of DLB is dementia, which can be defined as progressive cognitive decline interfering with social or occupational functioning (12). In early disease, patients may present with prominent impairment on tests of attention, visuospatial and executive functions (21). Probable DLB can be diagnosed with the presence of two or more core clinical features or with at least one core clinical feature plus at least one indicative biomarker (12).

The four core clinical features of DLB are fluctuating cognition, recurrent visual hallucinations, spontaneous features of Parkinsonism and rapid eye movement (REM) sleep behaviour disorder. Fluctuations occur as spontaneous alterations in cognition, attention and arousal, which vary in intensity and duration. Recurrent visual hallucinations, typically well-formed and detailed, occur in up to 80% of patients with DLB (12). During the early stages of DLB, REM sleep behaviour disorder is commonly observed and may precede the diagnosis by many years (21). Spontaneous features of Parkinsonism such as bradykinesia, rigidity and resting tremor eventually occur in over 85% of patients (12). Parkinsonism and orthostatic hypotension can be complicated by falls, which are associated with substantial morbidity and mortality (22). Core

clinical features, supportive clinical features, and indicative biomarkers of DLB are shown in **Table 1.1**.

The accurate clinical diagnosis of DLB is particularly important due to differences in treatment response and prognosis compared to AD. Individuals with DLB can experience increased sensitivity to antipsychotic medications, with associated extrapyramidal side effects and a higher risk of neuroleptic malignant syndrome (23). Prognostically, DLB is associated with more rapid disease progression, earlier loss of independence and greater neuropsychiatric burden (24, 25). Correct diagnosis of DLB can therefore guide safer prescribing and enable appropriate future care planning.

Table 1.1 Criteria for the diagnosis of DLB

Dementia	• Progressive cognitive decline that interferes with social or occupational functioning
Core Clinical Features	• Fluctuating cognition (experiencing variations in attention and alertness) • Repeated periodic visual hallucinations (well-formed typically featuring people or animals) • One or more spontaneous cardinal features of parkinsonism: bradykinesia, tremor at rest, rigidity • REM sleep behavioural disorder
Supportive clinical features	• Severe sensitivity to antipsychotics • Postural instability • Repeated falls • Syncope • Severe autonomic dysfunction (e.g., urinary incontinence, constipation, orthostatic hypotension) • Apathy, anxiety, depression
Indicative biomarkers	• Reduced dopamine transporter uptake in basal ganglia demonstrated by single-photon emission computed tomography (SPECT) or positron emission tomography (PET) • Reduced uptake on metaiodobenzylguanidine (MIBG) myocardial scintigraphy • Polysomnographic confirmation of REM sleep with atonia
Supportive biomarkers	• Relative preservation of medial temporal lobe structures on computerized tomography (CT)/ magnetic resonance imaging (MRI) • Generalised low uptake on SPECT/PET perfusion scan with reduced occipital activity +/- the cingulate island sign on fluorodeoxyglucose (FDG)-PET imaging • Prominent posterior slow-wave activity on electroencephalography (EEG) with periodic fluctuations in pre-alpha/theta range

Adapted from McKeith et al. 2017 (12).

1.1.3 Neuropathology

The neuropathology of DLB is defined by the presence of α-syn protein deposits in the form of Lewy-related pathology (LRP) consisting of intraneuronal Lewy bodies (LB) and Lewy neurites (LN), as illustrated in **Figure 1.1**. Associated pathological features include neuronal loss, synaptic loss and neurotransmitter deficits (26). α-syn is a presynaptic neuronal protein consisting of 140 amino acids and is normally expressed in the brain, comprising 1% of total cytosolic protein (27). The precise physiological function of α-syn is poorly defined but it is thought to play an essential role in synaptic vesicle trafficking and maintaining synaptic homeostasis (28).

Aggregated α-syn is the main constituent of LRP, which is not present in healthy individuals (29). The process of aggregation involves the formation of transient, soluble oligomers which eventually convert into insoluble fibrillar aggregates (30). There is growing evidence to suggest that α-syn oligomers are responsible for neurotoxicity in LBD (31). Indeed, progressive accumulation of oligomeric α-syn in the presynaptic terminal has been implicated in the alteration of synaptic functioning (31, 32). An imaging study using a PET ligand for synapses, [11C]UCB-J, demonstrated a significant reduction in cortical presynaptic terminal density in DLB/PDD, supporting synaptic dysfunction and loss (33).

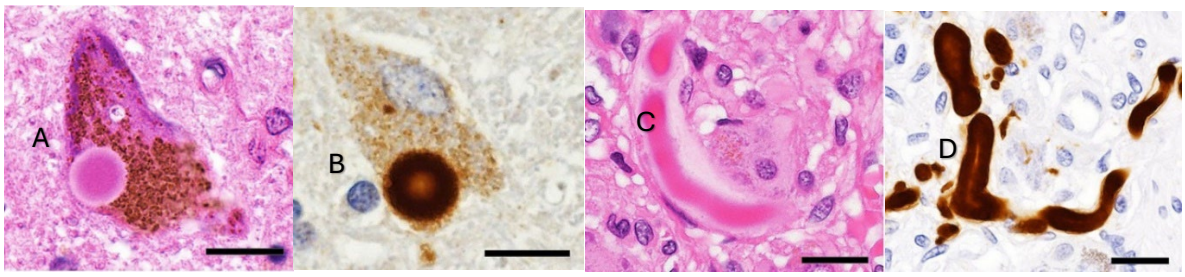

Figure 1.1 Lewy-related pathology
Images from substantia nigra (A,B) and sympathetic ganglia (C,D) in an individual with Parkinson's disease, immunostained for haematoxylin and eosin (A,C) and alpha-synuclein (B,D). Intracellular spherical Lewy body seen in (A) and (B). Lewy neurites as intra-axonal tubular structures seen in (C) and (D). Scale bar: 20μm. Images taken from Kon et al. 2020 (34).

It has been reported that α-syn fibrils may play a crucial role in the spread and progression of LBD through a prion-like mechanism (28). As LRP can occur in the peripheral nervous system, propagation of α-syn is unlikely to be confined to the brain. A large *post-mortem* study examining sections of spinal cord, sympathetic ganglia and organ tissue in LBD, AD and healthy controls, found that the presence of phosphorylated α-syn was most common in subjects with PD and DLB. The spinal cord was the most frequently affected area, followed by the sympathetic ganglia, vagus nerve and the gastrointestinal (GI) system. The submandibular gland

and lower oesophagus were the most common non-neural areas affected (35). This raises an important question as to whether α-syn pathology originates in the brain or peripheral nervous system, which has yet to be clarified. Earlier deposition of α-syn in the GI system and olfactory bulb may provide an explanation as to why symptoms of DLB such as constipation and hyposmia can precede motor and cognitive symptoms by many years. A route of α-syn transmission from the GI tract to the substantia nigra (SN) via the parasympathetic and vagus nerves has been identified in a mouse model of PD (36). Propagation of α-syn is also likely to occur in the opposite direction as supported by a further study that observed α-syn spreading from the midbrain to the gastric wall via the vagus nerve in rats (37).

LBDs share many neuropathological features which commonly include both LRP and AD-related pathologies such as amyloid-beta (Aβ) plaques and neurofibrillary tangles (NFTs) (26). Although a higher incidence of cortical Aβ and LRP deposition is observed in DLB compared to PDD, a combination of these pathologies contributes to the progression of both diseases (38). Comparisons between the neuropathological features of DLB and PDD are detailed in **Table 1.2**.

Table 1.2 Comparison of neuropathological features of dementia with Lewy bodies (DLB) and Parkinson's disease dementia (PDD)

Neuropathological feature	DLB	PDD
Cerebral cell loss	• Grey matter cortical atrophy more severe • Absence of cholinergic cell loss in pedunculopontine nucleus	• Substantia nigra cell loss more severe • Cholinergic cell loss in pedunculopontine nucleus (in hallucinating PDD)
Vascular changes	• Temporal lobe white matter hypointensities more severe	• Cerebral microbleeds less frequent
Lewy-related pathology	• Higher cortical load in temporal and parietal lobes, including hippocampus and amygdala	• Higher load in cingulate cortex • Diffuse or focal Lewy-related pathology
Amyloid-beta pathology	• Higher load in cortex and striatum	• Lower load in cortex and striatum
Tau pathology	• Higher load in cortex and striatum	• Lower load in cortex and striatum

Adapted from Jellinger KA. 2018 (39).

The presence of combined DLB and AD pathology has been associated with worsening cognitive decline in DLB (40). Aβ pathology arises from the abnormal cleavage of amyloid precursor

protein (APP) resulting in accumulation of oligomeric Aβ and amyloid fibrils that form extracellular plaques. NFTs are intracellular accumulations of hyperphosphorylated tau (ptau), a microtubule-associated protein that stabilises microtubules. The presence of Aβ peptides has been shown to enhance the fibrillisation and aggregation of α-syn (26), suggesting that the accumulation of one type of protein may promote abnormalities in the metabolism of other proteins.

DLB is characterised by relative preservation of cerebral grey matter on structural brain imaging (41) in comparison to AD, which is associated with a loss of neuron density within the medial temporal lobes (42). A recent imaging study revealed that patients with mild to moderate DLB had relatively preserved medial temporal structures, but similar frontal and parietal atrophy compared to AD patients. Atrophy of the medial temporal lobe and frontal lobe in severe DLB patients was consistent with that observed in severe AD patients, although parietal lobe atrophy was more prominent in AD patients (43). In patients with mixed AD and DLB pathology, higher rates of whole brain atrophy have been detected in comparison to DLB patients without coexisting AD pathology (44). Furthermore, a retrospective imaging study including patients with mixed AD and DLB pathology, reported an association between the presence of severe AD pathology and increased cerebral atrophy (45). These findings suggest that concomitant AD pathology contributes to increased cortical volume loss in DLB.

Staging systems such as the DLB international consensus criteria (12) are used in the neuropathological diagnosis of DLB. This system uses semi-quantitative scoring of LB and LN in defined brain regions to categorise LRP into stages ranging from mild to very severe, as shown in **Figure 1.2**.

Figure 1.2 Staging of Lewy-related pathology in dementia with Lewy bodies.
Immunostaining for alpha-synuclein in cerebral cortex demonstrating stages 1-4. Stage 1= sparse Lewy bodies (LB) or Lewy neurites (LN); Stage 2= >1 LB per high power field and sparse LNs; Stage 3= ≥4 LBs and scattered LNs in low power field; Stage 4= numerous LBs and LNs. Image taken from McKeith et al. 2005 (46).

The development of NFTs and neuropil threads is then categorised into Braak ptau stages ranging from stage I (lesions develop in the transentorhinal region) to stage 6 (pathology reaches the secondary and primary neocortical areas) (47). The extent of LRP and AD-type pathology are used to predict the likelihood that neuropathologic findings are associated with a typical DLB clinical syndrome. For example, distribution of LRP in the limbic region with a Braak ptau score of 1-2 has a 'high likelihood' of being associated with a DLB clinical syndrome. The same distribution of LRP with a Braak ptau score of 5-6 has a 'low likelihood' of being associated with a DLB clinical syndrome (12).

1.2 The innate and adaptive immune system

The immune system comprises a collection of cells, chemicals and processes which provide protection from foreign pathogens and promote repair following injury (48). Central to the immune system's response is the ability to discriminate self from non-self. Whilst eliminating pathogens, responses that induce damage to self-tissue need to be avoided. The immune system can be divided into two broad parts: innate and adaptive immunity. Although innate and adaptive responses have different mechanisms of action, synergy between them is essential for an effective immune response (49).

The innate immune system represents the body's first line of defence to intruding pathogens or tissue injury. Innate immunity is a non-specific defence mechanism that is usually activated immediately, or within hours, after encountering an antigen. Innate immune cells include phagocytes (macrophages and neutrophils), natural killer (NK) cells and dendritic cells. These rely on pattern recognition receptors (PRR) to detect pathogens that share common structures, known as pathogen associated molecular patterns (PAMPs) and damage associated molecular patterns (DAMPs) (48). Following trauma, the release of DAMPs from damaged cells stimulates an instant innate immune response, to clear damaged tissue and promote repair mechanisms (50).

Immune cells are rapidly recruited to sites of infection or injury and induce a process called inflammation through the co-ordinated production of cytokines and chemokines. These are small proteins which mediate cell communication and recruitment. Proinflammatory cytokines are released during the early response to infection or injury and include interleukin (IL)-1, IL-6 and tumour necrosis factor alpha (TNF-α). These cytokines induce cell recruitment and local inflammation which are essential for the clearance of pathogens. Macrophages engulf microbes and clear cell debris by the process of phagocytosis. Macrophages and dendritic cells can also activate the adaptive immune response by functioning as antigen presenting cells (APCs) (48).

The adaptive immune system provides a specific targeted immune response and comprises dendritic cells, antibodies and lymphocytes. Adaptive responses are based primarily on the antigen-specific receptors expressed on the surfaces of T lymphocytes (T cells) and B lymphocytes (B cells). These are known as T cell receptors (TCRs) and B cell receptors. T cells are activated to proliferate through the action of APCs, and B cells differentiate into plasma cells to produce antibodies. The primary role of antibodies is to mediate immune responses towards foreign pathogens. Whilst plasma cells produce antibodies specific for a pathogen, memory B cells remain to protect against subsequent attacks from the same pathogen. The development of an immunologic memory is an important function of adaptive immunity that enables a more rapid immune response upon subsequent exposure to an antigen (48).

1.2.1 Inflammaging

During ageing, alterations in the immune system result in chronic upregulation of the inflammatory response, termed inflammaging (51). This results in increased susceptibility to chronic conditions associated with ageing, including atherosclerosis, type 2 diabetes mellitus and macular degeneration (52). Inflammaging is characterised by increased levels of proinflammatory cytokines and is thought to develop as a consequence of lifetime exposure to antigen (53).

Both innate and adaptive immunity are affected during ageing, and the resultant remodelling of the immune response is named immunosenescence. The most prominent changes occur in the adaptive immune system, consisting of thymic involution and a reduced proportion of naïve T cells. There is instead a shift towards increased numbers of terminally differentiated cells which can produce high levels of proinflammatory cytokines (54). Immunosenescence related to the innate immune system involves a progressive decline of innate immune responses including reduced phagocytic activity. Innate immune cells contribute to inflammaging by acquiring a proinflammatory phenotype and prolonging the immune response (53).

A chronic upregulation of inflammation has been described in the ageing brain in a process known as ‘neuroinflammaging.’ This may predispose to the development and progression of neurodegenerative diseases (55).

1.2.2 Inflammation in AD

Inflammation is increasingly recognised as a key factor in the pathogenesis of neurodegenerative diseases and has been widely explored in AD. A persistent immune response in the brain has been associated with exacerbation of neuropathological changes in AD (56).

Microglia are the resident immune cells of the central nervous system (CNS) and provide the first line of immune defence during any insult to the brain (57). Deposition of Aβ can trigger the activation of microglia, promoting phagocytosis and clearance of Aβ (58). Activated microglia produce Aβ-degrading proteases, as well as clear fibrillar Aβ via phagocytosis (59, 60), suggesting a neuroprotective role. However, it has been proposed that overactivation or phagocytic dysfunction of microglia may result in Aβ accumulation and sustained release of proinflammatory cytokines (61). This response has been demonstrated in animal studies (62, 63) and infers a role for activated microglia in neuroinflammation and the progression of AD. A strong association between tau and microglial markers that promote phagocytic activity indicates that microglia are also responding to, and/or contributing to, tau accumulation in human AD (64, 65).

The involvement of neuroinflammation in AD pathology has been reinforced by human genome-wide association studies (GWAS), which have revealed polymorphisms in several genes associated with inflammation that increase the risk of late-onset AD. One such polymorphism is of the *CD33* gene, which is expressed by microglia and is associated with increased cognitive decline and Aβ plaque burden. GWAS have also reported a notable polymorphism in the *TREM2* gene, found to be associated with a higher risk of AD and increased severity of brain atrophy. *TREM2* is selectively expressed in myeloid cells and stimulates phagocytosis, suggesting a role in the clearance of Aβ (66).

Peripheral infections, including those that precede dementia onset by over ten years, have been shown to increase the risk of AD (67), indicating the involvement of systemic inflammatory mechanisms. This is supported by alterations in peripheral blood cell populations that include increased numbers of neutrophils and decreased numbers of T and B cells in AD (68). Neutrophils can increase in response to raised inflammatory cytokines, which have been implicated in the pathogenesis of AD (69). A decrease in peripheral T cells raises the possibility that a proportion or sub-population of T cells could be migrating into the brain. Indeed, pre-clinical and human *post-mortem* studies in AD have consistently demonstrated the presence of T cells in brain parenchyma (70-73). Reduced B cell counts in the periphery are associated with normal ageing, although a more prominent reduction is observed in AD (68).

1.2.3 Inflammation in PD

There is emerging evidence to suggest an important role for inflammation in the pathogenesis of PD. The most common genetic cause of sporadic and familial PD is a mutation in the *LRRK2* (*PARK8*) gene (74). Mutations in this gene have been identified in inflammatory diseases such as Crohn's disease and leprosy (75). This is supported by a GWAS that reported an association

between LRRK2 and autoimmune diseases including rheumatoid arthritis, ulcerative colitis and multiple sclerosis (76) .

Evidence of neuroinflammation in PD has been demonstrated by increased expression of the proinflammatory cytokines IL-1β, IL-2, IL-6 and TNF-α in the striatal regions of *post-mortem* human brain tissue (77). A further study reported an increased density of glial cells expressing IL-1β and TNF-α in the SN pars compacta of PD subjects compared to healthy controls (78). More recently, alterations in peripheral inflammatory responses have been investigated, showing increased levels of IL-1β, IL-6 and TNF-α in the serum of PD subjects (75).

Findings from studies using PD animal models suggest that infiltration of peripheral immune cells into the CNS may contribute to disease pathogenesis. Neuronal loss was found to be dependent on peripheral monocyte infiltration into the CNS in a viral mouse model overexpressing α-syn (79). Furthermore, aggregation of α-syn has been found to be associated with microglial activation and lymphocyte infiltration in PD (80).

1.2.4 Inflammation in DLB

The role of inflammation in DLB has been less extensively researched. The first large scale GWAS in DLB was conducted in 2017 and in contrast to AD, did not identify any polymorphisms associated with inflammation (81). A subsequent GWAS by Chia et al. in 2021 supported these findings, failing to reveal any significant associations at canonical immune or inflammatory genes (82). The largest GWAS meta-analysis to date including 4252 DLB cases and 189290 controls confirmed a lack of significant associations at immune loci (83). Collectively, these findings suggest that neuroinflammation in DLB may not represent a primary genetically driven process.

There is emerging evidence to suggest alterations in peripheral and cerebral immune responses in DLB. One study examining blood cytokines at both prodromal and established stages of DLB showed significantly higher concentrations of cytokines in the prodromal group, compared to the DLB and control groups. This finding suggests an early inflammatory response in the blood in DLB. Notably, higher levels of the plasma cytokines IL-6 and TNF-α were associated with greater severity of cognitive impairment and parkinsonism in DLB subjects (84). Increased serum concentrations of IL-6 have also been reported in subjects with delirium (85, 86), a complex neuropsychiatric condition characterised by an acute change in attention and cognitive function. These findings support a role for systemic inflammation in the development of these conditions which is of relevance, given that delirium and DLB share several clinical features including cognitive impairment, fluctuations in consciousness, and perceptual disturbances (87).

In vivo brain imaging using translocator protein (TSPO) PET ligands has been used to study microglial cells in DLB. Two studies have shown increased TSPO ligand binding using ^{11}C-PK11195 in DLB cases compared to controls (88, 89). The larger of these studies included 19 DLB subjects and grouped them into mild DLB (Addenbrooke's cognitive examination-revised (ACE-R) score >65/100) and moderate-severe DLB (ACE-R score ≤65/100). ^{11}C-PK11195 binding in mild DLB was increased but, in contrast, binding in moderate-severe DLB was lower than in controls (89). This suggests that increased microglial cell activity is prominent in early stages of disease, supporting the possibility of an early inflammatory response in DLB.

Several p*ost-mortem* human brain studies have examined the number of activated microglia in DLB with conflicting results. Two small studies have shown increased numbers of human leukocyte antigen – antigen D related (HLA-DR)+ activated microglia in DLB brains compared to controls (90, 91). In contrast, one study including eight DLB and 11 control cases failed to demonstrate upregulation of HLA-DR in DLB (92). Further studies investigating the expression of the microglial marker ionised calcium-binding adapter molecule 1 (Iba1) found Iba1 expression to be unchanged in the hippocampus of DLB cases compared to controls (93, 94). In support of this, a large study examining markers of microglial activation in the temporal lobe of 30 DLB and 29 control brains demonstrated no difference in the levels of Iba1, cluster of differentiation 68 (CD68) and HLA-DR+ protein load between groups (95). Furthermore, transcriptomic studies have reported a lack of microglial activation in *post-mortem* DLB brain tissue within the anterior cingulate, dorsolateral prefrontal cortex (96) and pulvinar (97). One study documented significant downregulation of several cytokine and chemokine genes in DLB brain tissue, supporting an absence of neuroinflammation (96). DLB may therefore be characterised by an absence of microglial activation, although it is possible that this is specific to brain region and stage of disease.

The increased presence of T cells observed in human *post-mortem* brain tissue from 30 DLB cases compared to 29 controls supports the possibility of interaction between the cerebral innate immune system and the peripheral adaptive immune system (95). T cell infiltration into the brain after initial microglia-mediated neuroinflammation may result in the spread and perpetuation of neuroinflammatory processes (98). Extracellular aggregates of α-syn have been shown to activate microglia and astrocytes via toll-like receptors, increasing both microglial phagocytic activity and the spread of α-syn in a prion-like manner (99). Microglia and astrocytes are able to directly activate T cells, supporting their antigen presenting capabilities (100). There have been no reports on microglia migrating outside of the brain for activation of T cells. T cells are instead activated by dendritic cells derived from monocytes in areas surrounding the brain such as the deep cervical lymph nodes. It is likely that microglia present antigen which can subsequently reactivate and modulate T cells that have infiltrated the brain (101).

1.3 The role of T cells

T cells derive from hematopoietic stem cells in bone marrow and migrate to the thymus where they mature. Most T cells express a single TCR variant on their cell surface membrane and require the action of APCs to recognise a specific antigen. APCs are usually dendritic cells but also include macrophages, B cells, fibroblasts and endothelial cells. These cells express a group of proteins on their surface known as major histocompatibility complex (MHC). MHC are classified into class I, which are found on all nucleated cells or class II, which are only found on APCs. The MHC protein displays fragments of antigen when a cell is infected with an intracellular pathogen or has phagocytosed foreign proteins (48).

T cells within the thymus differentiate into subsets which are defined by the selective expression of CD4 or CD8 on their surface. During development, they initially express neither CD4 or CD8 and then express both CD4 and CD8, known as double positive. These cells are tested by positive selection in the thymic cortex and those selected on class I MHC (MHCI) molecules become CD8+, and those selected on class II MHC (MHCII) molecules become CD4+. Following positive selection, the cells then move to the thymic medulla where they are exported to the periphery (49).

CD4+ T cells are known as T helper (Th) cells and have an important role in mediating and regulating immune responses. They are activated via recognition of antigen bound to MHCII. Upon antigen exposure, naïve CD4 T cells in lymphatic tissues undergo clonal expansion and differentiate into effector and memory Th subsets (102). The distinct cytokines produced by each Th cell subset determines the activity of many cell types including the APCs that activated them. There are several subsets of CD4+ T cells, the most common being Th1, Th2 and Th17 cells (48). These are involved in various immunological processes such as B cell maturation and macrophage activation (103). Regulatory T (Treg) cells act to suppress immune responses and may therefore have a role in limiting responses to self-antigen as well as the completion of immune responses once pathogens have been eliminated (48). Within the CNS, Th1 and Th17 are recognised to have a predominant role in neuroinflammation via proinflammatory cytokines. Other subsets such as Th2 and Treg are considered to facilitate neuronal protection (104). The range of CD4+ T cell subset functions and effector cytokines are summarised in **Table 1.3.**

Table 1.3 Overview of CD4+ T cell subsets

Subset	Effector cytokines produced	Functions
Th1	IFN-γ, Lymphotoxin, TNF-α	Cell-mediated immunity Delayed-type hypersensitivity responses Clearance of intracellular pathogens
Th2	IL-4, IL-5, IL-13, IL-10	Humoral immunity Clearance of extracellular worms and bacteria B cell switching to IgE Allergic responses
Th9	IL-9, IL-10	Protection against parasitic worms
Th17	IL-17, IL-17F, IL-6, IL-22, TNF-α, IL-10	Protection of mucosal surfaces Recruitment of neutrophils Clearance of *Mycobacterium tuberculosis* and *Klebsiella pneumonia*
Th22	IL-22, IL-13, FGF, CCL15, CCL17, TNF-α	Mucosal immunity Prevention of microbial translocation across epithelial surfaces Promotes wound repair
Th25	IL-25, IL-4, IL-5, IL-13	Mucosal immunity Stimulates nonlymphoid cells to produce IL-4 Limits Th1 and Th7 induced inflammation
ThFH	IL-21, TNFRSF4, ICOS	Helps B cells produce high affinity antibodies Trigger the formation and maintenance of germinal centres
Treg	TGF-β, IL-10	Suppression of existing immune responses Maintains tolerance against autoimmunity

Th (T helper), ThFH (T follicular helper cell), Treg (T regulatory cell), IFN-γ (Interferon-gamma), TNF-α (Tumour necrosis factor-alpha) IL (Interleukin), FGF (Fibroblast growth factor), CCL (Chemokine ligand), TNFRSF4 (Tumour necrosis factor receptor superfamily member 4), ICOS (Inducible T cell co-stimulator), TGF-β (Transforming growth factor-beta). Adapted from Caza et al. 2015 (103).

CD8+ T cells are known as cytotoxic T (Tc) cells and contribute to the clearance of intracellular pathogens and neoplastic cells that present antigen on MHCI molecules. Following activation by the recognition of antigen, they undergo differentiation and proliferation to generate an expanded population of effector and memory T cell types (48). APCs and CD4+ T cells can also mediate CD8+ T cell activation through co-stimulatory signals and the production of cytokines

(105). A subtype of CD8+ T cells known as T suppressor (Ts) cells function to down-regulate immune responses (49). Ts cells, similar to Treg cells, may reduce immune responses by releasing cytokines or by directly altering the function of other T cells or APCs (106). The characteristics of CD8+ T cell subtypes and their functions are shown in **Table 1.4**.

Table 1.4 Overview of CD8+ T cell subsets

Subset	Effector cytokines produced	Functions
Tc1	IFN-γ, TNF-α	Clearance of intracellular pathogens and tumours
Tc2	IL-4, IL-5, IL-13	Propagation of Th2-mediated allergy
Tc9	IL-9, IL-10	Inhibition of CD4+ T cell-mediated colitis Propagation of Th2-mediated allergy Anti-tumour response
Tc17	IL-17, IL-21	Promote autoimmune responses Immunity to viral infections Anti-tumour response
Tc22	IL-22, IL-2, TNF-α	Anti-tumour response
Ts	TGF-β, IL-10	Regulation of T cell-mediated responses

Tc (T cytotoxic), Ts (T suppressor cell), IFN-γ (Interferon-gamma), TNF-α (Tumour necrosis factor-alpha) IL (Interleukin), TGF-β (Transforming growth factor-beta). Adapted from Mittrucker et al. 2014 (105).

CD4+ and CD8+ T cells share signalling cytokines and lineage determining transcription factors that direct their differentiation into distinct T cell subsets. In addition, they have shared effector cytokine profiles that mediate the functions of each T cell subset. For example, Th1 and Tc1 cells can be differentiated under IL-12 conditions and produce interferon-gamma (IFN-γ) through the activation of T-box transcription factor (Tbet). Th2 and Tc2 cells can be differentiated under conditions involving IL-4 and produce IL-4, IL-5, IL-13 through activation of GATA binding protein 3 (GATA3). Differentiation of Th17 and Tc17 cells can occur under IL-6 and transforming growth factor-beta (TGF-β) conditions to produce IL-17A. This occurs through activation of retinoic acid-related orphan receptor gamma t (RORμt) and signal transducer and activator of transcription 3 (STAT3). Treg and Ts cells can differentiate under TGF-β conditions

and produce TGF-β and IL-10 through Forkhead box P3 (Foxp3) (107). A comparison of these T cell subsets is illustrated in **Figure 1.3**.

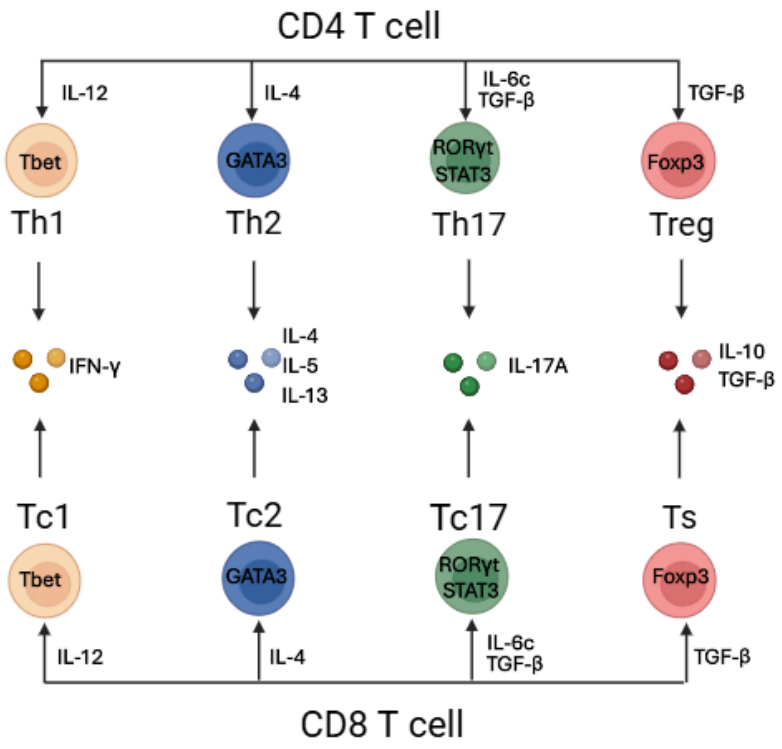

Figure 1.3 Comparison of CD4+ and CD8+ T cell subsets

CD4+ and CD8+ T cell subsets share signalling cytokines, transcription factors and effector cytokine profiles. Adapted from Koh et al. 2023 (107). Created by Biorender.com.

Following the resolution of immune responses, most effector T cells are cleared by apoptosis. A small population of memory cells remain which provide long-term immunity following re-exposure to the same antigen. There are three main subsets of memory T cells: central memory T cells (TCM), effector memory T cells (TEM) and tissue-resident memory T cells (TRM) (102). TCM cells patrol lymphoid organs and the blood providing immunosurveillance against their cognate antigen. TEM cells circulate through the blood and peripheral organs, where they can produce effector molecules to induce a more rapid response to antigen. TRM cells remain permanently in peripheral tissues and provide localised protection against re-encountered pathogens (108). T cells continue to replicate multiple times due to repeated exposure to pathogens but can eventually lose their ability to proliferate, reaching the stage of replicative senescence (109). Senescent T cells expressing elevated concentrations of inflammatory cytokines accumulate during ageing and have been implicated in age-related diseases such as AD (110).

1.4 T cells in healthy individuals

The profile of T cells in healthy individuals is summarised in the following sections on T cells in the brain, cerebrospinal fluid (CSF) and blood.

1.4.1 T cells in the brain

Infiltration of T cells into the brain parenchyma is restricted by the blood-brain barrier (BBB), which regulates the movement of cells and solutes between the blood compartment and the CNS. Migration of immune cells across the BBB appears to be controlled by the expression of adhesion molecules and chemokines, and their receptors (111). Reduced expression of cell adhesion molecules in CNS endothelia limits the entry of T cells and they are therefore only present sporadically in the brain parenchyma of healthy individuals (112). During periods of neuroinflammation, the BBB can lose its integrity becoming more permeable to solutes, innate immune cells and circulating leukocytes. This is a consequence of changes in the BBB epithelium which include increased expression of adhesion molecules, proinflammatory cytokines and chemokines (113).

The transmigration of T cells into the brain can activate endothelial cells through the release of cytokines which can increase the expression of adhesion molecules (114). The release of proinflammatory cytokines by activated glia, as well as cytokine presence in the blood can also lead to increased expression of adhesion molecules on microvascular endothelial cells (115). T cell infiltration can occur due to recognition of antigen or through bystander activation. Bystander activation refers to the cytokine-driven activation of non-specific T cells that happen to be present during an ongoing immune response (116). It is important to note that CD8+ T cell infiltration into the brain of CL4 transgenic mice has been shown to only occur when the cognate antigen is present in the parenchyma. Recognition of antigen presented by MHCI on the luminal surface of the cerebral endothelium provides a mechanism for CD8+ T cell recruitment across the BBB (117). Due to lack of expression of MHCII by cerebral endothelium, this mechanism does not apply to CD4+ T cells. Interestingly, animal studies investigating CD4+ T cells have observed that activated CD4+ T cells are able to infiltrate the brain regardless of antigen specificity (118-120), however, there remains uncertainty as to whether this is replicated in humans.

Another potential route of entry for peripheral immune cells into the brain parenchyma is at the choroid plexus which extends into the lumen of the ventricles. A single layer of endothelial cells surrounds the choroid plexus and forms the blood-CSF barrier (121). Molecules can diffuse across the endothelial cells through fenestrations and intracellular gaps, allowing T cell entry

into the subarachnoid space (122). It has been proposed that this is where immune surveillance primarily occurs and that any T cells in the CSF have migrated through the blood-CSF barrier (121). Once in the CSF, T cells can enter the brain parenchyma by breaching the ependymal layer of the ventricle (123). Studies in mice have demonstrated Th1 and Th17 cells using this pathway to infiltrate the brain parenchyma (124, 125). The lymphatic system of the meninges provides an opportunity for interaction between peripheral immune cells and immune cells within the meningeal compartment. Due to a lack of tight junctions between endothelial cells in the outer dura layer of the meninges, T cells are able to access and interact with CNS-derived APCs in the CSF, potentially providing another mechanism of entry into the brain parenchyma (126).

Human *post-mortem* studies have evidenced the presence of both CD4+ and CD8+ T cells in the brain. A study investigating the T cell profile in brain tissue from the corpus collosum of 20 donors (including 17 with a neurodegenerative disease), identified a predominant CD8+ T cell subtype. CD4+ T cells were noted to be present in lower numbers and both T cell subtypes were located around blood vessels (127). The same authors conducted a further study using brain sections of subcortical white matter. In this brain area, there were three times more CD8+ T cells detected when compared to CD4+ T cells. Once again, the majority of T cells were observed near to blood vessels and within the perivascular space (128). Another study has revealed insights into the role of ageing on the T cell profile by examining 19 brain tissue sections of white matter from the lateral geniculate nucleus of the thalamus. The cases were divided into three groups defined as young (36-58 years old), aged (65-87 years old) and neurodegenerative (diagnosis of AD). CD4+ and CD8+ T cells were detected in all groups and were mainly localised to perivascular areas, supporting the findings from previous studies. Interestingly, higher numbers of CD8+ T cells were detected in the aged and neurodegenerative groups in both parenchymal and perivascular regions. Overall, there were no significant differences between numbers of T cells in the neurodegenerative group compared to the aged group. On specific examination of the entorhinal cortex, lower numbers of CD4+ and CD8+ were detected in all groups and there remained similar numbers of T cells in both the aged and neurodegenerative groups (129).

Pre-clinical studies have indicated that infiltration of T cells into the brain can increase with advancing age. The presence of cerebral T cells has been examined in different ages of wild type mice by immunolabelling with the T cell marker CD3 (130), an antigen present on the surface of all T cells (131). Four age groups of mice were studied: 3-4 months, 6 months, 12 months and 24-30 months. T cells were identified in the brain parenchyma of mice aged 12 months and older and were predominantly located in white matter areas in close proximity to blood vessels. The number of T cells increased during ageing and also appeared in grey matter in mice aged 24 – 30

months old (130). T cells in the non-pathological brain were also studied in 34 rhesus macaques aged 5 -30 years old, equivalent to human ages of 15-90 years old (132). Rhesus monkeys do not develop neurodegenerative disease, and so confounding neuropathology is minimal in this model (133). Immunolabelling with CD3 was used to quantify T cell density in white matter and grey matter. Perivascular and parenchymal T cell density significantly increased with age in white matter areas. T cells were rarely present in grey matter and there was no significant difference with age. Interestingly, the percentage of parenchymal T cells correlated with age related impairments in cognitive function (132).

In summary, human *post-mortem* studies support a cerebral T cell profile with a predominant CD8+ T cell subtype and localisation to perivascular areas. Ageing appears to be associated with an increased infiltration of T cells, as has also been demonstrated in animal studies. It should be noted that the human studies examined regions of white matter and evidence is therefore lacking regarding the profile of T cells in grey matter. For example, the potential impact of protein deposition on T cell recruitment in grey matter is not represented. In animal studies, there were contrasting findings on the presence of T cells in grey matter which were only evident in older mice. This may have been due to the studies examining different areas of grey matter; notably the study on mice examined 29 brain areas compared to three areas in the study on rhesus macaques. T cell subsets were not determined in these studies and so it remains unclear whether the presence of T cells in ageing brains is likely to be detrimental or protective to neurons. The positive correlation found between increased T cells and cognitive impairment suggests that their presence may be detrimental. Further studies examining T cell infiltration in both grey and white matter would be beneficial to further define the cerebral profile of T cells in non-pathological brains.

1.4.2 T cells in the CSF

The CSF of healthy individuals contains stable populations of immune cells which carry out immune surveillance of the CNS and deep cervical nodes (134). These are predominantly CD4+ T cells, accounting for approximately 70% of immune cells in the CSF (135). CD8+ T cells are also present in the CSF but to a lesser extent (134). This was confirmed in a large study examining leukocyte subsets in the CSF of 84 healthy participants which detected the majority of T cells to be CD4+ T cells with a CM phenotype. The CM phenotype was defined to represent T cells that had been seen or primed by an antigen. Interestingly, comparison of T cell subsets in the blood and CSF of the 84 participants revealed that the percentage of naïve CD4+ and CD8+ T cells was significantly lower in CSF, compared to blood. The authors proposed that naïve T cells may require activation by antigen in perivascular spaces or CNS draining lymph nodes before they are able to enter the CSF (136).

1.4.3 T cells in the blood

The blood of healthy individuals comprises more CD4 T cells compared to CD8 T cells, and these are predominantly naïve T cells. Age-related changes occur in the peripheral T cell population which are associated with the natural process of thymic ageing and involution (104). Proportions of circulating CD8+ T cells are known to decrease with ageing (137) with a shift from naïve to more differentiated memory and senescent T cells, which is accompanied by reduced TCR diversity (104). This is supported by a recent systematic review on immunosenescence of T cells which included a meta-analysis of four studies, demonstrating a significant decrease in peripheral naïve T cells in older adults (>60 years) compared to young adults (18-44 years) (138). The decline in naïve T cells, combined with the accumulation of terminally differentiated memory T cells may contribute to increased susceptibility to new infections and a lower protective effect of vaccinations in older adults (139). In support of this, significant positive correlation has been demonstrated between the number of peripheral terminally differentiated ($CD28^-$) memory CD8+ T cells and the probability of non-response to a trivalent influenza vaccine in 153 individuals, aged between 65 and 98 years old (140).

Studies measuring T cell subsets in the blood of control participants have identified higher percentages of Tc1 cells compared to Th1 cells (141-143). Th2 and Tc2 cells are present in lower numbers (143), with Tc2 cells making up approximately 1% of CD8 T cells in the blood of healthy individuals (107). These studies included adult participants, aged matched to groups with an average age of 36 (141), 28 (142) and 48 years (143). The proportions of T cell subsets in these groups may therefore not reflect those found in older aged adults.

1.5 T cells in PD

Regarding the T cell profile associated with PD, previous studies have shown T cell infiltration into the brain, reduced numbers of T cells in the blood and an increase in proinflammatory T cell subsets (144). These findings are relevant to consider in relation to DLB, given that these LBDs share LRP as a key neuropathological feature. A summary of the PD profile of T cells in the brain, CSF and blood is provided below.

1.5.1 T cells in the brain in PD

T cell responses to the overexpression of α-syn in the brain have been investigated in a mouse model of PD. An adeno-associated viral model was used to express α-syn (AAV-SYN) in the SN of C57BL/6 mice. Immunofluorescent imaging showed increased CD3+ T cells in the ventral midbrain of AAV2-SYN mice compared to control mice. Immunohistochemistry performed on

the brain tissue revealed that the T cell population included both CD4+ and CD8+ T cells. Cytokine analysis identified an increase in interferon gamma (IFN-γ) and IL-10, expressed by Th1 and Treg cells. There was no increase in the Th2 and Th17 associated cytokines, IL-4 and IL-17a. This was supported by transcription factor staining which revealed an increase in the Th1 transcription factor, Tbet and the Treg transcription factor, Foxp3. CD4+ T cells producing IFN-γ were the most prominent cytokine producing cell, suggesting an increased Th1 proinflammatory response to α-syn overexpression (144).

Infiltration of CD4+ T cells and CD8+ T cells into the PD brain has been shown in a human *post-mortem* study. A significant increase in the number of CD4+ T cells in the SN was observed in 9 PD cases, compared to 7 controls. The number of CD8+ T cells in the SN was also found to be significantly increased in 14 PD cases, compared to four controls. Both subsets of T cell were observed adjacent to blood vessels or near to neuromelanin containing neurons (145). In PD, neurons containing neuromelanin preferentially degenerate (146). In contrast, a more recent study found no difference in the number of CD4+ T cells in the SN of 15 PD cases compared to seven control cases. However, CD8+ T cell density was significantly higher in the SN parenchyma in PD compared to controls. Interestingly, a higher density of CD8+ T cells was associated with a lower density of dopaminergic neurons, suggesting that CD8+ T cell infiltration contributes to neuronal cell death in PD (147). A further human *post-mortem* study demonstrated increased numbers of T cells in the SN of three subjects with sporadic PD, compared to two age and sex matched controls. CD3+ T cells were significantly increased in the PD group and were again located close to neuromelanin containing neurons (148). In summary, pre-clinical and human studies provide evidence of increased infiltration of T cells into the PD brain, which may involve a prominent Th1 response and contribute to neuronal degeneration.

1.5.2 T cells in the CSF in PD

Examination of CSF using flow cytometry in a study including 10 PD subjects and 14 healthy controls identified an increased percentage of total T cells in the PD group. The CD4+/CD8+ T cell ratio was unchanged, although there was a higher proportion of CD8+ T cells that were activated in PD CSF, as defined by HLA-DR expression. Increased levels of the proinflammatory cytokines, IL-2, IL-6, and TNF-α were detected in the CSF of PD subjects, however a specific Th subtype could not be identified (149). Higher concentrations of TNF-α have been detected in the CSF of PD subjects in an earlier study, however, T cell populations were not examined (77). Overall, studies examining the T cell profile of CSF in PD are lacking. Current evidence supports the possibility of increased T cells with a proinflammatory profile in the PD CSF, although further research is required in this area.

1.5.3 T cells in the blood in PD

One human study investigating the profile of T cells in the blood compared peripheral T cell subsets in 33 subjects with sporadic PD and 34 healthy controls. Compared to controls, the percentage of CD4+ T cells was significantly reduced and CD8+ T cells were significantly increased in PD subjects. Analysis of cytokines produced by T cells demonstrated an increased ratio of IFN-γ to IL-4, indicating a prominent Th1 response (150). A larger study, including 88 PD subjects and 77 control subjects showed numbers of peripheral CD4+ T cells were reduced by approximately 15-25% in PD subjects, compared to controls. In contrast to the previous study, there was no significant difference in CD8+ T cells between the groups (151). Further examination of the peripheral CD4+ T cell populations in 82 subjects with PD and 47 controls, has shown reduced numbers of Th2, Th17 and Treg cells, resulting in a relative increase in Th1 cells (152). This supports previous findings (150) and indicates that the peripheral immune system is shifted towards a Th1 cell response in PD.

Peripheral T cell responses to α-syn have been explored in a study investigating the relationship between T cell reactivity and PD pathogenesis. Cytokine responses against an α-syn epitope pool were measured to enable quantification of T cell response in 97 PD participants and 67 controls. Interestingly, T cell responses to α-syn were highest nearest to the time of PD diagnosis and declined over time, implicating increased T cell reactivity in early disease. Specific T cell subsets involved included CD4+ T cells producing IFN-γ and IL-4, and both CD4+ and CD8+ T cells producing IL-10. T cells producing IL-10 were distinct from T cells producing proinflammatory cytokines but were not found to express markers associated with Treg cells (153). These findings suggest a proinflammatory role for Th1 and Th2 subsets of α-syn-specific CD4+ T cells in PD progression, as well as a potential regulatory role for a T cell subset which is yet to be identified. Mapping and comparison of the TCR repertoire of α-syn-specific CD4+ T cells in PD patients has revealed a profile that was specific to each patient. There were no shared TCRs identified (154) and, therefore, no evidence of a public T cell response, in which individuals share identical TCRs in response to the same antigenic epitope (155).

Notably, peripheral CD4+ T cells were shown to specifically react to antigenic MHCII epitopes derived from α-syn in an earlier study including 67 PD subjects and 36 controls. T cell reactivity to α-syn was significantly higher in PD patients compared to healthy controls and the majority of T cell responses were associated with IL-5 production, further supporting a role for Th2 cells in mediating this response (156). Despite evidence of T cell co-localisation to α-syn in the PD brain, it remains unclear whether α-syn plays a fundamental role in T cell reactivity and proliferation. It is possible that α-syn-specific T cells exhibit the same or similar responses in other synucleinopathies, however, their recruitment into the brain has not yet been established.

1.6 T cells in DLB

The profile of T cells has been previously examined in DLB, providing a useful insight into neuroinflammatory processes involving the adaptive immune system. A literature review was carried out to identify relevant evidence on this topic. The electronic databases of MEDLINE, EMBASE, PsycINFO, PubMed, Scopus and Web of Science were searched using the terms dementia with Lewy bodies, Lewy body dementia, Lewy, synuclein*, Parkinson*, dementia, T cell, T lymphocyte, CD4, CD8, CD3, adaptive immun*, inflamm*. Searching syntax including Boolean, truncation, exact phrase searching and subject headings were utilised. The search included papers from 1947 to July 2025. References of relevant articles were searched to identify further studies. Papers on relevant clinical studies were selected for inclusion if they included a DLB or/and PDD group. A summary of evidence on the profile of T cells in *post-mortem* brain tissue, CSF, and the blood compartment is provided in the following sections.

1.6.1 T cells in the brain in DLB

The profile of T cells in the DLB brain has been examined in human *post-mortem* studies and pre-clinical studies using animal models of DLB, as summarised below.

1.6.1.1 Human studies

Post-mortem studies from as early as 1988 have consistently identified increased infiltration of CD4+ and CD8+ T cells into the brain parenchyma of AD patients (157). Fewer studies have evaluated the profile of T cells within the parenchyma of DLB brains, particularly in comparison to AD cohorts. One such study compared the number of CD3+ T cells within the hippocampus of *post-mortem* human brain tissue from 21 AD patients compared to ten patients with DLB associated with AD pathology and two DLB patients without AD pathology. A higher number of T cells was observed in AD cases compared to control cases but interestingly, the number of T cells in all DLB cases regardless of associated AD pathology was found to be similar to control cases (70). It is important to note that there are limitations in this study. Due to the inclusion of only two control cases and two DLB cases without AD pathology, it is difficult to draw comparisons using such small sample sizes. T cells were counted in a single section of grey matter from the hippocampus. This may not represent an area where T cells infiltrate the brain in DLB and limits any insight into T cell infiltration in areas of white matter.

Further studies have explored T cell populations in the brains of DLB subjects compared to controls. The largest human *post-mortem* study to date in this area analysed the middle temporal gyrus (Brodmann area 21) of 30 DLB cases and 29 control cases using CD3+ immunolabelling. CD3+ T cells were identified more frequently in grey and white matter in the

parenchyma of DLB cases. Infiltration of CD3+ T cells into perivascular areas appeared at similar levels in both control and DLB cases (95). It is noteworthy that in addition to the strength of a large sample size, cases were carefully selected using clinical records, *post-mortem* reports and Braak ptau stage (<IV) to minimise inclusion of cases with co-existing AD pathology. Control and DLB groups were matched for sex, *post-mortem* delay and age at death. However, the method of T cell quantification and the area of brain examined introduce potential limitations to the study. CD3+ T cells in each case were classified as either present or absent. The number and subset of T cells present in each case is therefore unknown and this limits more detailed analysis on the extent of T cell infiltration. Although examining a single neocortical area provided consistency of sampling, the presence or absence of T cells in this area may not be representative of other brain regions.

In contrast, a smaller *post-mortem* study by Iba *et al*. including eight DLB cases and eight controls found an increased number of CD3+ T cells around blood vessels in the neocortex and hippocampus in DLB cases compared to controls. T cells were further characterised into subsets of CD4+ and CD8+ T cells. Infiltration of CD4+ T cells was increased in the neocortex and hippocampus of DLB brains and correlated with CD3+ T cells. A small number of CD8+ T cells were detected in the DLB hippocampus but were absent in the neocortex of both DLB and control brains, suggesting that the majority of infiltrating T cells were CD4+ T cells. Increased numbers of CD8+ T cells were detected in the hippocampus in DLB compared to controls but differences did not reach statistical significance (158). The areas of brain examined in each case were described as samples from the frontal cortex and hippocampus. The number of T cells in each area were provided, however, despite noting their abundance around blood vessels, the distribution of T cells was not recorded. It is therefore unclear whether there were T cells present in the parenchyma. Details of case selection indicated that all DLB cases had a Braak stage ranging from III-V. Cases with a Braak stage of V would be categorised as having high AD neuropathic change according to the National Institute on Ageing-Alzheimer's Association (NIA-AA) (12). Co-existing AD pathology could therefore have contributed to the T cell populations identified in this study.

Infiltration of CD4+ T cells has been demonstrated in a *post-mortem* study examining seven brain regions from 17 PD patients with no dementia, 11 patients with PDD and 14 healthy controls. Increased numbers of CD4+ T cells were observed in the SN in PDD compared to control cases but there was no significant difference in the number of CD8+ T cells or Iba1+ microglia across the groups. Contrasting findings were observed in the amygdala where infiltration of CD4+ and CD8+ T cells was comparable between groups and microglial activation was significantly increased in PDD cases compared to controls. It is important to note that there was significant correlation between CD4+ T cells, α-syn and HLA-DR-activated microglia in the

amygdala (159), implicating the involvement of α-syn in driving neuroinflammatory responses. Although no significant difference was detected in the number of CD8+ T cells between groups, these cells were more abundant in the PDD group compared to controls in both the SN and amygdala (159). Strengths of this study are the inclusion of control, PD and PDD groups that were matched for age, sex and *post-mortem* interval and the examination of different regions of the brain. Although quantification of microglia activation was performed in seven different brain regions, T cells were only counted in sections of the SN and the amygdala. Another limitation was that CD4+ and CD8+ T cells were counted in the parenchyma but not in perivascular areas. Given that T cells have been observed in perivascular areas as previously described (158), the T cell counts may not be truly representative of the total number of T cells present in each case.

The potential association between α-syn aggregation and T cell recruitment into the brain in DLB has been previously explored. Widespread immunoreactivity for CD3 was observed in a *post-mortem* study of six DLB brains compared to an absence of CD3 expression in four control subjects. Immunoreactivity was discovered to precisely positively correlate with α-syn pathology in the brainstem and with neocortical LRP (160). In a further study by Gate *et al*., higher numbers of CD3+ T cells were observed in the SN of two DLB and four PDD brains compared to five controls, with a higher percentage localising to α-syn deposits and Iba1+ microglia. Increased immunoreactivity for the proinflammatory cytokine IL-17A was also detected, implying that Th17 cells that express this cytokine may contribute to neuronal damage. This was further supported by the presence of CD4+ IL-17+ T cells in the SN in PDD cases. Interestingly, CD3+ T cells were identified in the hippocampus, near LB and the excitatory presynaptic marker, vesicular glutamate transporter 1 (vGLUT1) (161). Co-localisation of α-syn and vGLUT1+ neurons has been previously demonstrated in the hippocampus of C57BL/6N mice (162, 163) and it has been proposed that vGLUT1+ neurons are vulnerable to α-syn pathology, resulting in detrimental effects on synaptic transmission (164).

It is important to consider the mechanisms by which T cells can infiltrate the brain parenchyma. Immunohistochemistry on PDD meninges revealed T cells expressing the chemokine receptor, C-X-C motif chemokine receptor 4 (CXCR4), in response to the presence of its ligand, C-X-C motif chemokine ligand 12 (CXCL12). This was supported by examination of the SN in two DLB and four PDD cases, which detected T cells located in the perivascular spaces next to blood vessels expressing CXCL12 (161). CXCL12 and CXCR4 are known to be involved in the migration of T cells from perivascular spaces into the parenchyma, following their passage through post capillary venules (165). In experimental autoimmune encephalomyelitis, T cells that express CXCR4 have been shown to accumulate in perivascular spaces surrounded by endothelial cells expressing CXCL12 (166). In the presence of inflammation, CXCL12 expression is reduced due to the upregulation of atypical chemokine receptor 3 (ACKR3), a specific scavenger for CXCL12,

and results in the migration of T cells out of the perivascular space into the parenchyma (167). CXCL12 may therefore play a role in limiting the parenchymal infiltration of T cells in the absence of inflammation, although it is unknown if this is replicated in DLB.

1.6.1.2 Pre-clinical studies

A study by Iba *et al.* evaluated T cell populations in brain sections from 12 transgenic mice over expressing wild type human α-syn and 12 non-transgenic littermates (158). This animal model reproduces similar neuropathological changes to those observed in LBD (168, 169). There were significantly higher numbers of CD4+ T cells in the neocortex, hippocampus and striatum of α-syn transgenic mice compared to non-transgenic mice and minimal differences in CD8+ T cells between the two groups. Lymphoid cells isolated from the α-syn transgenic mice and non-transgenic mice brains were analysed using flow cytometry and revealed an increased frequency of NK cells in α-syn transgenic mice. Further analysis of cytokines demonstrated higher expression of IFN-Y and tumour necrosis factor (TNF-α) messenger ribonucleic acid (mRNA) in the brains of α-syn transgenic mice compared to non-transgenic mice. IFN-Y is a potent inducer of the proinflammatory phenotype of macrophage and is predominantly produced by CD4+ T cells, particularly Th1 cells (158). TNF-α has been identified as a major regulator of inflammatory responses and is produced by Th1 cells in addition to Th17 cells, activated macrophages and NK cells (170). The presence of IFN-Y and TNF-α therefore supports an infiltration of proinflammatory CD4+ T cells and NK cells into the brains of α-syn transgenic mice.

The same animal model was used to investigate interactions between T cells and cerebral innate immune cells using immunohistochemistry with the microglia marker, Iba1, and the astrocyte marker, glial fibrillary acidic protein (GFAP). CD3+ T cells were more frequently detected near to Iba1+ microglia and GFAP+ astrocytic processes in the neocortex, hippocampus, and striatum of α-syn transgenic mice compared to non-transgenic mice (158). It has been proposed that α-syn induces MHCII expression in microglia and enhances presentation of antigen, leading to proliferation of CD4+ T cells. This was demonstrated in a pre-clinical study using a co-culture of CD4 T cells and microglia from C57BL/6 wild type mice, isolated and pretreated with recombinant full-length aggregated α-syn (171).

Increased activation of microglia and astrocytes in the SN has been demonstrated in non-transgenic C57BL/6J mice inoculated with preformed fibril (PFF) α-syn, compared with monomer controls. This was determined by increased expression of Iba1 and MHCII on microglia and GFAP on astrocytes. The relative percentage of CD4+ and CD8+ T cells within the brain parenchyma of PFF inoculated mice was significantly higher than in monomer controls. Analysis was conducted five months after intrastriatal PFF α-syn injection when synuclein

pathology was prevalent but dopaminergic neurodegeneration had not occurred. Therefore, infiltration of T cells was not regarded to have been induced by neuronal degeneration (172). The PFF α-syn model has been primarily utilised as an animal model of PD because this induces dopaminergic cell loss, LRP and impaired motor coordination (173). However, changes in the human DLB brain may not be accurately represented by the PFF α-syn model. Extrapolation of findings is challenging as despite similarities in neuropathology between PD and DLB, the immunophenotype of these diseases likely differ.

In summary, there is evidence of increased parenchymal infiltration of T cells in DLB. Interaction between infiltrating peripheral T cells and brain resident immune cells, as well as the ability of α-syn to induce inflammatory changes may play a role in neuroinflammation and neurodegeneration in DLB. Infiltration of T cells into the brain in DLB may be influenced by CXCL12, although the mechanism and consequences of this remains unknown. The potential role of T cells contributing to neuroinflammation in DLB is summarised in **Figure 1.4**.

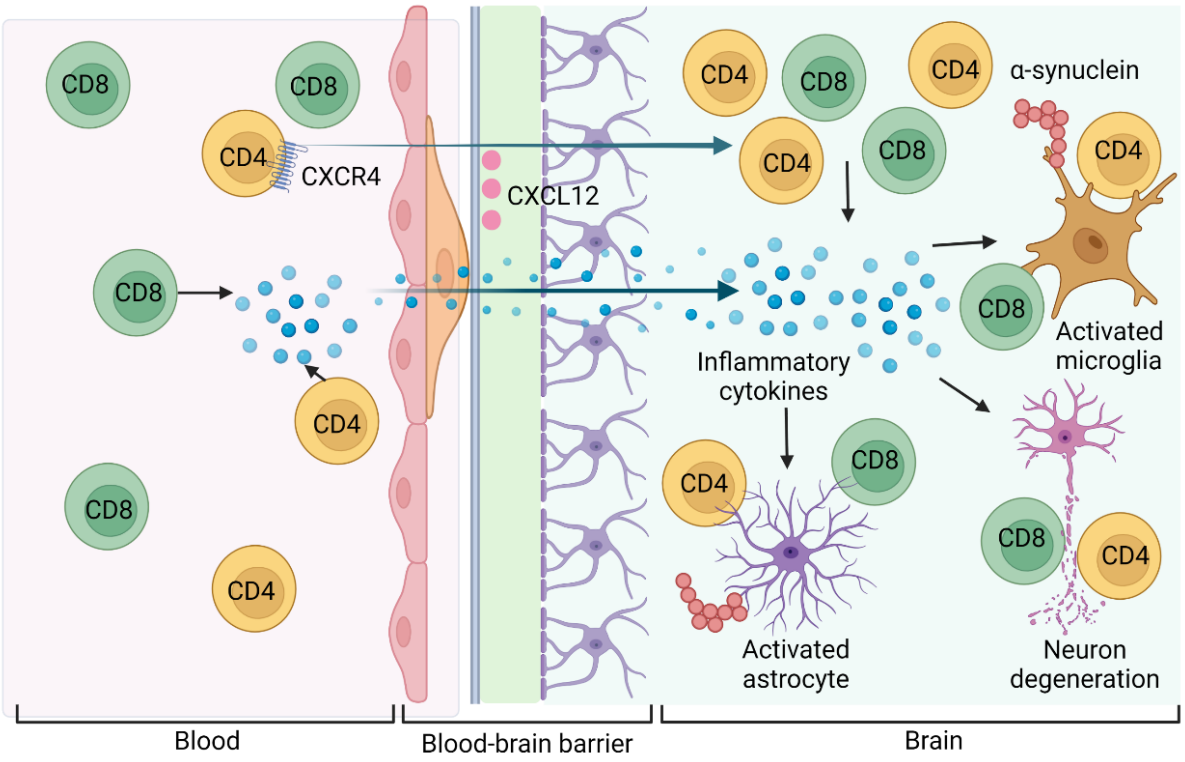

Figure 1.4 The potential role of T cells contributing to neuroinflammation in DLB
Extracellular aggregates of α-syn activate microglia and astrocytes, inducing an inflammatory response involving T cell activation and infiltration into the parenchyma. T cells expressing CXCR4 localise to CXCL12 which may play a role in the migration of T cells across the BBB. Created by Biorender.com.

1.6.2 T cells in the CSF in DLB

Examination of CSF in AD and PD subjects has shown increased numbers of activated T cells (149, 174). The frequency of immune cell populations in the CSF of DLB subjects has been previously reported, providing valuable insight into peripheral neuroinflammatory mechanisms.

In a recent study by Gate *et al*. CD4+ T cells in the CSF of 11 PD/DLB subjects were found to have a transcriptionally altered immune cell subtype compared to 11 control subjects. Analysis of differentially expressed genes revealed higher expression of CD69, an early activation marker on T cells, and of the chemokine receptor CXCR4. It is important to note that the cohorts were matched for age and sex, however there were only two DLB cases in the PD/DLB group (161).

CXCL12 levels in the CSF of 79 PD/PDD subjects and 84 controls were compared, revealing higher levels in PD/PDD subjects. CXCL12 levels were found to positively correlate with neurodegenerative markers, including the neurofilament light chain (161) which reflects neuronal damage (175). As previously discussed, CXCL12 has been implicated in the infiltration of T cells from perivascular spaces into the parenchyma in DLB. Furthermore, studies examining CSF in subjects with neuroinflammatory diseases have demonstrated positive correlation between levels of CXCL12 and evidence of BBB disruption (176, 177). The presence of CXCL12 in the CSF may therefore play a role in T cell migration across the BBB in PD/PDD. Although this study supports an important role for CXCL12 in the pathogenesis of PD/PDD, caution should be applied as to whether the findings are applicable to a DLB population. Further studies are required in this area using larger cohorts of DLB subjects to establish the profile of T cells in CSF.

1.6.3 T cells in the blood in DLB

There is growing evidence of alterations in the peripheral immune system in neurodegenerative disease. A recent meta-analysis including nine studies involving 1,696 subjects found significantly lower peripheral lymphocyte counts in AD subjects compared to aged matched healthy controls. CD8+ T cell subsets were significantly reduced and AD subjects had a higher CD4:CD8 ratio (68). Numerous studies have shown alterations in cytokine concentrations in DLB (30), but very few have examined T cell subsets within the blood.

1.6.3.1 Human studies

One study examined T cell subsets in blood using flow cytometry, comparing 31 DLB subjects, 31 AD subjects and 31 healthy controls. There were significantly reduced proportions of CD4+ T cells and HLA–DR+ activated B cells in DLB subjects and although numbers of CD8+ T cells

were increased, this difference was not statistically significant. CD8+ terminal effector cells were increased and naïve CD8+ T cells were reduced in DLB subjects compared to controls, however, differences did not reach statistical significance (178). Terminal effector cells are known to express markers of senescence. They have limited proliferative capacity but tend to produce a wider range of cytokines following activation (179). Analysis of peripheral cytokines in this study showed significantly higher IL-1β and IL-6 in DLB compared to controls (178). IL-6 induces the development of Th17 cells and inhibits Treg cell differentiation, therefore acting as a proinflammatory cytokine in T cells (180). IL-1β is known to be a potent inducer of IL-6 (181) and in addition to its presence in the periphery, has been shown to be upregulated in the SN and frontal cortex of PD/PDD brains (159). In addition, increased peripheral levels of IL-1β and IL-6 can disrupt BBB integrity (182), providing a mechanism for T cell infiltration into the brain. Strengths of this study include a large cohort of subjects and the use of consensus diagnostic criteria. Although the control group was significantly younger, statistical correction was carried out to account for this. Cell populations were measured as a percentage of parent populations rather than quantified as absolute cell counts. This limits further analysis of the T cell population such as the CD4+:CD8+ T cell ratio.

1.6.3.2 Pre-clinical studies

An animal model compared T cell subsets in the blood of transgenic mice overexpressing wild type human α-syn, driven by the thymocyte differentiation antigen 1 (Thy-1) promoter, and non-transgenic wild type mice using flow cytometry. Increased numbers of CD4+ and CD8+ T cells were detected in the blood of α-syn transgenic mice and interestingly this finding was only observed in mice at 22 months of age, implicating late involvement of the adaptive immune system. No differences in CD4+ and CD8+ T cell percentages were found between younger α-syn transgenic mice and wild type mice aged 1 month, 5-6 months and 14 months (183). A further animal model comparing peripheral lymphocyte populations in PFF α-syn inoculated non-transgenic mice and non-transgenic mice aged 5 months found no significant changes in the total number of T cells (172).

The literature to date suggests an altered peripheral immune profile in DLB but there are conflicting findings from human and animal studies which may reflect difficulty in the production of an accurate animal model of DLB. Peripheral CD4+ T cells were reduced in human DLB cases and in contrast, overexpression of α-syn replicating LBD in older mice resulted in higher proportions of peripheral T cells. Reduced numbers of peripheral CD4+ T cells in human DLB subjects may represent impaired proliferation or reduced activation of CD4+ T cells in DLB and the trend towards increased peripheral CD8+ T cells differs from the reduction in CD8+ T cells associated with normal ageing. A potential shift from naïve to terminal effector cells in DLB

subjects raises the possibility of increased senescence of CD8+ T cells, as has been reported previously in AD (184). This immune profile may result in the preferential expression of proinflammatory cytokines, potentially contributing to BBB disruption and T cell infiltration into the DLB brain. Overall, studies examining the T cell profile of blood in DLB subjects are lacking, with no longitudinal studies that quantify absolute T cell counts.

1.7 Scope for this project

Over recent years, there has been increasing evidence to support that altered immune responses can exacerbate and facilitate neuropathological changes in dementia. Although the role of inflammation in DLB has been less extensively researched compared to AD, a review of the relevant literature to date has revealed evidence of alterations in adaptive immune responses involving T cells. A proposed profile of T cells in the brain, CSF and blood in DLB is summarised in **Figure 1.5**.

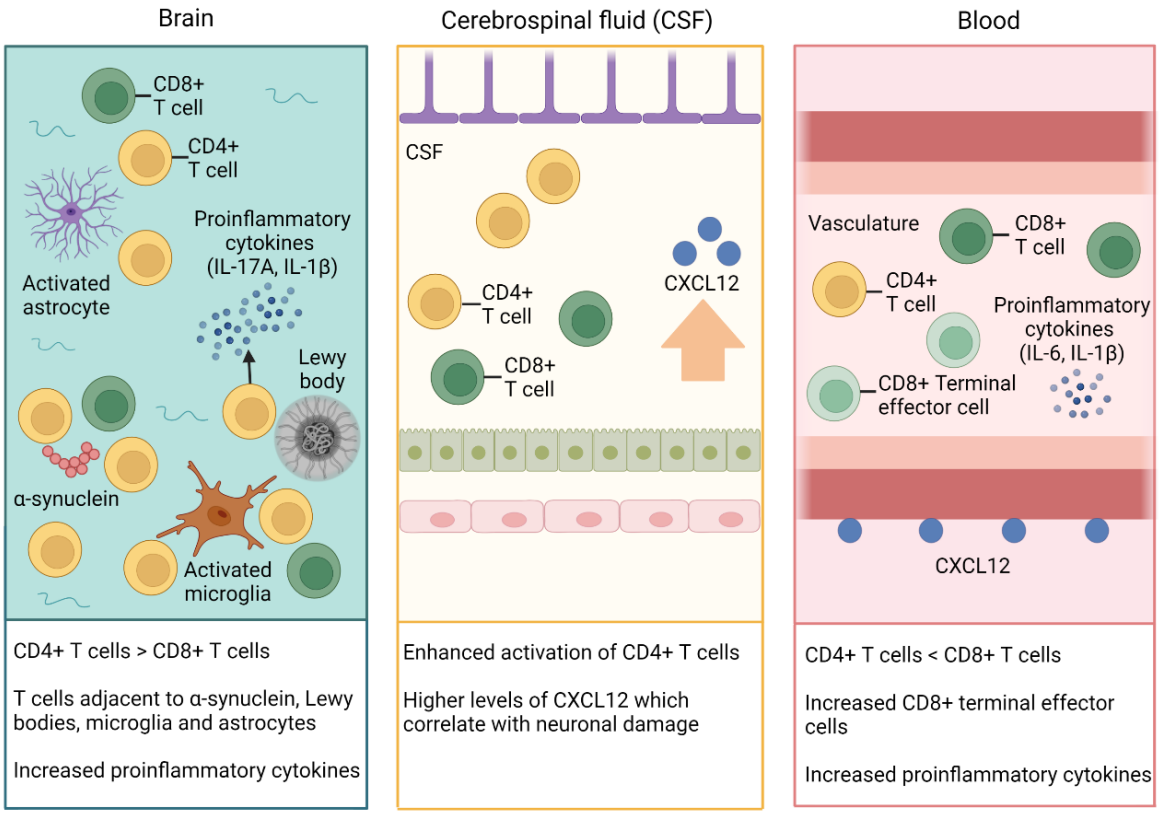

Figure 1.5 Alterations in the profile of T cells in the brain, CSF and blood in DLB
Increased numbers of T cells adjacent to α-syn and microglia in the brain, enhanced CD4+ T cell activation in the CSF, and reduced numbers of CD4+ T cells in the blood have been demonstrated in DLB. The presence of CXCL12 in perivascular spaces and increased levels of CXCL12 in the CSF may contribute to disruption of the BBB and infiltration of T cells into the parenchyma. Created with Biorender.com.

This suggested profile of T cells in DLB was derived from a small number of studies, the majority of which included small sample sizes which may have been underpowered to show significant

differences. There is certainly a gap in evidence exploring the distribution of T cells in the DLB brain. Only one study examined the presence of T cells in white matter compared to grey matter, and parenchymal compared to perivascular areas of the brain (95) . There are few studies which differentiated the subset of T cells in the DLB brain (61, 105, 121). Two of the three studies to do so included animal models of PD/DLB (61, 121) and one *post-mortem* study included PDD cases (159). The different methods used to quantify T cells, for example via absolute cell counts, relative percentages or identifying presence or absence, as well examination of different brain regions, limits comparisons between studies.

An interesting finding from the review was the observation of increased T cell infiltration into the brain prior to neurodegeneration in mice overexpressing α-syn (172). In contrast to this, changes in peripheral T cell subsets only occurred as disease progressed (183). This implicates an adaptive immune response occurring during prodromal or early stages of DLB in the brain, and a peripheral response occurring later with progressing disease. This conflicts with the presence of an early peripheral inflammatory response inferred from increased peripheral cytokines during the prodromal stage of DLB (30). It is important to consider that animal models may not accurately represent DLB in humans and human *post-mortem* studies tend to examine later stage disease. Given that longitudinal analysis of T cell profiles has not yet been investigated in humans with DLB, there is currently a lack of evidence relating to how inflammatory responses change with disease progression.

The presence of α-syn in DLB brains appears to play a role in promoting inflammatory changes through interaction with microglia and T cells, suggested by their co-localisation. However, the mechanism and consequences of these interactions remain unclear. The higher expression of proinflammatory cytokines such as IL-17A in DLB brain tissue supports that infiltrating T cells may have pathogenic rather than neuroprotective properties. Overall, there are a lack of studies examining different T cell subsets and their roles in DLB.

My project aims to further investigate the cerebral T cell profile in DLB using a large cohort of *post-mortem* brain tissue. Analysis of the number, distribution and subset of T cells will be performed to provide new information on the role of T cells in DLB. The expected outcome of this work is to improve our understanding of disease mechanisms underpinning DLB and how inflammation may contribute to the pathogenesis of DLB. Developing a greater understanding of T cell subsets in DLB may help to guide the development of potential therapeutic strategies such as T cell modulation.

Chapter 2 Hypothesis and aims

2.1 Hypothesis and aims

Hypothesis: The profile of cerebral T cells will be altered in DLB compared with aged controls and will be associated with microglial activation and/or neuropathological features of DLB.

This hypothesis will be investigated by exploring the following **aims**:

1. To define the profile of cerebral T cells in the parenchyma and perivascular regions of grey and white matter in DLB and controls.

2. To determine if the number of cerebral T cells is associated with markers of inflammation and/or neuropathological features of DLB.

Chapter 3 Materials and Methods

A *post-mortem* study will be carried out using immunohistochemistry to detect subsets of CD4+ T cells (Treg, Th1 and Th2) and CD8+ T cells (Ts, Tc1 and Tc2) in human brain tissue. The presence of CXCR4 and CXCL12 in human brain tissue will also be investigated using immunohistochemistry.

Post-mortem brain tissue will be obtained from an existing cohort of 30 cases of DLB and 29 non-neurological controls. Protein loads for microglial and neuropathological markers have already been quantified and published by Dr Jay Amin (95). This data will be correlated with T cell markers.

Power calculations were previously generated for the existing cohort and identified that a sample size of 30 in each group, with a power of 80% and a significance level of 5% would detect effect sizes greater than 0.516 (95). Using the same sample size in this study should allow adequate power to detect at least moderate effect sizes.

3.1.1 Ethics approval

Post-mortem brain tissue from 30 DLB cases and 29 control cases was sourced from the London Neurodegenerative Brain Bank (LNDBB) and the South West Dementia Brain Bank (SWDBB). Blanket ethical approval was provided by both brain banks: LNDBB reference 08/MRE09/38+5 from the National Research Ethics Committee (NREC) Wales and SWDBB reference 08/H0106/28+5 from NREC South West Central Bristol. The project is registered with University of Southampton Ethics and Research Governance Online (ERGOII ref: 13170).

3.1.2 Case selection

The existing cohort of DLB cases were previously selected by Dr Jay Amin and Prof Delphine Boche. Clinical details and neuropathology reports were reviewed prior to selection to ensure cases were consistent with a diagnosis of probable DLB. Control cases were selected by Dr Jay Amin after review of *post-mortem* reports. Inclusion criteria for selection into DLB and control groups were as follows; aged 60 or over at death, *post-mortem* delay less than 72 hours, no co-existing severe vascular disease or cerebral amyloid angiopathy and Braak ptau stage less than or equal to 3. In addition to these criteria, inclusion to the DLB group required a diagnosis of DLB on *post-mortem* report. Inclusion to the control group required cases to be neuropathologically 'normal' or have 'appearances consistent with ageing' with a Braak ptau stage less than or equal to 3 on *post-mortem* report. Clinical information at time of death was reviewed for all

cases, however, no information relating to cognitive function was available. Group-level matching for age, sex and *post-mortem* delay was performed, without individual case-control pairing. Baseline characteristics for DLB and control cases are documented in **Table 3.1** and **Table 3.2**, respectively.

Table 3.1 Characteristics of DLB cases

Case ID	Sex	Age (years)	*Post-mortem* delay (hours)	Braak ptau stage	Disease duration (years)	*APOE* genotype	Clinical information at time of death
A025/98	M	75	24	N/A	5	N/A	Unknown
A028/10	M	81	57	3	7	3,3	Pneumonia
A036/10	M	81	24	3	5	N/A	Unknown
A040/10	F	87	9	2	2	3,3	Unknown
A056/01	F	80	17	0	16	N/A	Unknown
A076/99	M	59	30	N/A	4	N/A	Unknown
A109/01	M	65	5	0	11	N/A	Unknown
A175/09	M	73	6	1	9	N/A	Prostate cancer
A190/03	M	83	38	3	6	N/A	Pneumonia
A204/07	M	74	18	2	12	3,3	Unknown
A225/03	M	70	8	1	6	N/A	Unknown
A231/09	M	66	35	2	7	N/A	Unknown
A241/11	M	82	32	1	8	N/A	Unknown
A242/04	M	72	22	1	9	N/A	Myelodysplasia
A245/09	M	78	46	3	4	N/A	Pneumonia
A263/05	M	78	41	2	8	N/A	Unknown
A273/05	M	86	8	0	5	3,3	Unknown
A273/07	M	71	19	2	10	N/A	Intestinal perforation
A304/06	F	92	55	3	9	N/A	Unknown
A339/96	M	86	48	N/A	2	N/A	Unknown
701	M	73	8	3	7	3,4	Unknown
738	F	76	33	3	13	3,3	Pneumonia
743	M	86	15	3	N/A	3,3	Pulmonary Embolism
756	M	69	38	0	5	3,3	Septicaemia
776	F	79	26	2	1	3,3	Frailty of old age
817	M	89	40	2	1	3,4	Unknown
823	M	80	38	2	4	3,4	Unknown
832	M	76	26	0	7	3,3	Unknown
846	F	67	20	0	5	3,3	Pneumonia
901	M	94	32	3	N/A	3,3	Unknown

Table 3.2 Characteristics of control cases

Case ID	Sex	Age (years)	*Post-mortem* delay (hours)	Braak ptau stage	Disease duration (years)	*APOE* genotype	Clinical information at time of death
A002/13	M	90	45	0	N/A	2,3	Myocardial infarction
A033/11	M	82	47	1	N/A	3,4	Heart failure
A049/03	M	79	24	0	N/A	2,3	Septicaemia
A051/14	F	76	22	2	N/A	N/A	Lung cancer
A053/11	M	77	11	0	N/A	3,3	Prostate cancer
A114/12	M	82	24	2	N/A	3,3	Lung cancer
A127/11	M	73	23	0	N/A	3,3	Bile duct cancer
A130/12	F	89	43	2	N/A	2,3	Cancer
A133/12	F	88	39	3	N/A	3,3	Unknown
A134/00	M	86	6	N/A	N/A	3,3	Myocardial infarction
A213/12	M	78	24	3	N/A	3,3	Prostate cancer
A261/12	M	63	23	0	N/A	3,3	Colon cancer
A265/08	M	79	47	2	N/A	2,3	Myocardial infarction
A273/12	M	67	25	1	N/A	3,3	Prostate cancer
A310/09	F	84	35	2	N/A	N/A	Unknown
A346/10	F	84	34	2	N/A	2,3	Sepsis
A359/08	F	80	3	1	N/A	3,3	Adenocarcinoma
A388/12	M	65	26	1	N/A	3,3	Prostate cancer
A407/13	F	80	22	2	N/A	3,4	Unknown
786	M	85	31	2	N/A	3,3	Myocardial infarction
803	M	77	42	1	N/A	3,3	Pneumonia
818	F	87	47	3	N/A	2,3	Septicaemia
851	F	68	39	0	N/A	2,3	Ovarian cancer
870	F	90	41	2	N/A	3,3	Unknown
877	M	82	67	2	N/A	3,3	Prostate cancer
894	M	74	58	0	N/A	3,3	Metastatic cancer
887	F	74	40	1	N/A	3,3	Unknown
940	M	94	64	2	N/A	2,4	Unknown
943	F	70	33	2	N/A	3,3	Cancer of larynx

3.1.3 Immunohistochemistry

The middle temporal gyrus (Brodmann area 21) was selected for examination as LRP is typically present in this area in DLB (31). Brain banks provided formalin fixed and paraffin embedded (FFPE) mounted sections at a thickness of 4µm.

Immunohistochemistry experiments were performed in the Clinical Pathology Department, University Hospitals Southampton (UHS) and the Histochemistry Research Unit (HRU), University of Southampton. I conducted immunohistochemistry experiments for GATA3. Tbet and Foxp3 staining was performed by Dr Jin Wang, and CD4 and CD8 T cell markers were immunolabelled by UHS staff in the Clinical Pathology Department. A positive control of tonsil tissue was used in each run to confirm successful immunostaining. A total of 8 tissue slides were immunolabelled for CXCL12, using a positive control of breast tumour tissue and for CXCR4, using a positive control of tonsil.

An automated slide stainer was used to immunolabel for CD4 and CD8. All immunohistochemistry experiments for the other T cell markers were performed manually. The protocol for immunohistochemistry is summarised below and a copy of the full lab protocol is included in **Appendix A**. An ImmPRESS detection kit was used for Foxp3, Tbet, GATA3 and CXCR4 immunostaining and the protocol for this method is provided in **Appendix B**.

FFPE brain sections were rehydrated by immersing in alcohol solutions and water followed by a rinse with trisaminomethane buffered saline (TBS). Endogenous peroxidase was blocked with 3% hydrogen peroxide in methanol. The tissue slides were then rinsed with TBS. Antigen retrieval was performed by heating the tissue slides in an ethylenediaminetetraacetic acid (EDTA) or citrate buffer. The tissue slides were then rinsed with TBS again. A blocking solution was applied to minimise non-specific staining. The primary antibody was added and left to incubate. Following incubation, the tissue slides were washed with TBS. The secondary antibody was applied and washed with TBS prior to the application of avidin-biotin complex (ABC) which amplifies the target antigen signal. Following a wash with TBS, 3,3'-diaminobenzidine (DAB) was used to produce a chromogenic reaction. The reaction was stopped by thoroughly washing with TBS and then distilled water. The tissue slides were counterstained with haematoxylin and the reaction was subsequently stopped by washing with water. The slides were dehydrated using alcohol solutions prior to mounting and finally left to dry.

3.1.4 Primary antibodies

Immunohistochemistry was performed using primary antibodies listed in **Table 3.3**. Five T cell markers were selected to identify different T cell subsets, details of which are listed below.

- **CD4** is a membrane glycoprotein and specific marker of Th cells (185).
- **CD8** is a membrane glycoprotein and specific marker of Tc cells (185).
- **Foxp3** is an X-linked transcription factor and is highly and specifically expressed in Treg cells. Although CD4+Foxp3+ cells are the most prominent regulatory T cells, a subtype of CD8+ T cells also express Foxp3 (107). These are very low in frequency, comprising approximately 0.3% of peripheral blood T cells in humans (186).
- **Tbet** is a transcription factor expressed by Th1 and Tc1 cells and is recognised as the master regulator of these cells (107).
- **GATA3** is a transcription factor, and marker of Th2 and Tc2 cells. Tc2 cells express GATA3 at lower levels than Th2 cells (105).

Immunohistochemistry using a CXCL12 antibody was trialled on a small sample of 8 DLB cases from the cohort. CXCL12 is expressed by astrocytes, microglia, neurons and endothelial cells in the brain (187). Expression of CXCL12 plays an important role in the trafficking of T cells expressing the CXCR4 receptor (188, 189).

As CXCL12 functions as the ligand for CXCR4, immunohistochemistry was performed using a CXCR4 antibody in the same sample of DLB cases. CXCR4 is expressed on the cell surface of most leukocytes including T cells, B cells and monocytes, as well as endothelial cells, epithelial cells and adult stem cells (190, 191).

Table 3.3 Details of primary antibodies used in immunohistochemistry

Primary antibody	Species	Clone	Manufacturer	Concentration	Experimental conditions
CD4	Mouse	4B12	Dako (IR649)	RTU	Automated slide stainer
CD8	Mouse	C8/144B	Dako (M7103)	RTU	Automated slide stainer
Foxp3	Mouse	236A/E7	Abcam (ab20034)	1:500	Citrate buffer in microwave, room temperature, ImmPRESS kit, DAB 7 minutes
Tbet	Rabbit	EPR27094-16	Abcam (ab307193)	1:500	EDTA buffer in microwave, room temperature, ImmPRESS kit, DAB 5 minutes
GATA3	Rabbit	ERP16651	Abcam (ab199428)	1:750	EDTA buffer in microwave, room temperature, ImmPRESS kit, DAB 3 minutes
CXCL12	Rabbit	#97958	Cell Signalling	1:100	Citrate buffer in microwave, room temperature, DAB 8 minutes
CXCR4	Mouse	MAB172-SP	R&D systems	1:10000	Citrate buffer in microwave, room temperature, ImmPRESS kit, DAB 5 minutes

RTU (ready-to-use concentration supplied by manufacturer, Dako)

3.1.5 Image acquisition and T cell quantification

In order to quantify numbers of T cells in the parenchymal and perivascular compartments in the grey and white matter, tissue slides were digitally scanned at 20x magnification using an automated Olympus VS110 slide scanning microscope at the Biomedical Imaging Unit (BIU). Scan settings were consistent for each T cell marker: Brightfield batch scan, magnification 20x, one Z plane, high sample detection sensitivity. T cell quantification for CD4, CD8, Foxp3, Tbet and GATA3 was carried out using QuPath v0.3.0, an open source bioimage analysis software (192). A recent *post-mortem* brain study used QuPath for CD4+ and CD8+ T cell quantification in the middle frontal gyrus, validating this as a method for T cell detection in brain tissue (193).

Prior to running T cell detections on QuPath, the entire section of brain tissue on each slide image was circumscribed to create a region of interest (ROI) that excluded imaging artefacts and meningeal tissue. Grey and white matter regions were also circumscribed to allow analysis of T cell distribution and calculation of area. An example digital slide image showing circumscribed brain tissue is provided in **Figure 3.1**. The areas of grey and white matter within the ROI for control and DLB cases are shown in **Table 3.4** and **Table 3.5,** respectively.

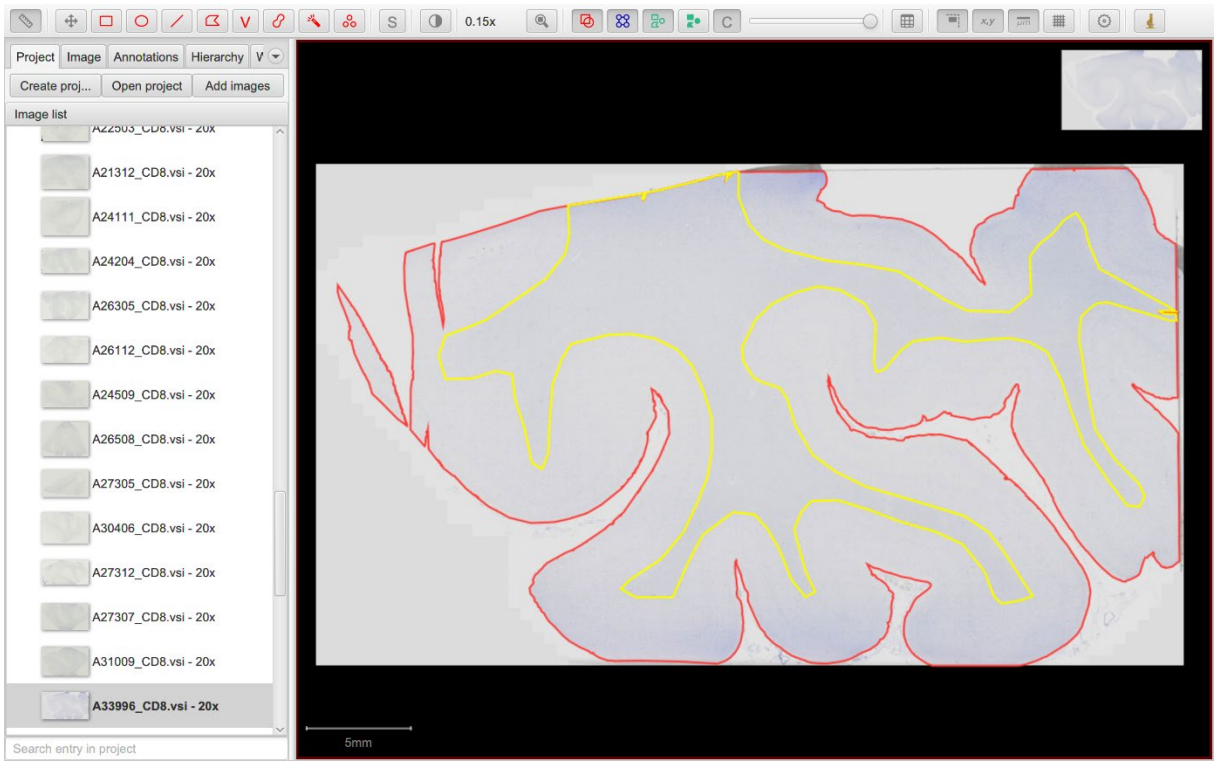

Figure 3.1 Example digital image taken from QuPath showing annotated brain tissue
Whole section of brain tissue is annotated in red and white matter is annotated in yellow (x20 magnification, scale bar =5µm).

Table 3.4 Total area of brain tissue, grey matter and white matter for control cases

Case ID	Total area (mm^2)	Grey matter (mm^2)	White matter (mm^2)
A002/13	719.99	476.47	243.52
A033/11	502.70	354.24	148.46
A049/03	544.63	394.31	150.33
A051/14	306.19	246.64	59.56
A053/11	501.90	389.96	111.94
A114/12	726.24	485.45	240.79
A127/11	506.64	410.94	95.70
A130/12	713.38	487.06	226.32
A133/12	740.00	518.54	221.45
A134/00	589.72	445.23	144.49
A213/12	585.68	381.33	204.35
A261/12	714.76	414.96	299.80
A265/08	452.97	323.51	129.46
A273/12	760.46	502.05	258.41
A310/09	581.50	377.83	203.68
A346/10	549.75	388.17	161.58
A359/08	658.56	492.68	165.88
A388/12	903.22	621.78	281.44
A407/13	448.15	305.82	142.33
786	478.42	358.91	119.50
803	505.77	401.21	104.56
818	541.32	428.55	112.77
851	658.20	419.59	238.61
870	410.72	353.97	56.74
877	389.66	316.21	73.44
894	399.80	377.90	21.90
887	249.46	231.23	18.23
940	612.17	421.14	191.03
943	91.53	91.53	0.00

Table 3.5 Total area of brain tissue, grey matter and white matter for DLB cases

Case ID	Total area (mm^2)	Grey matter (mm^2)	White matter (mm^2)
A025/98	801.28	565.89	235.38
A028/10	633.67	440.63	193.05
A036/10	672.82	491.70	181.12
A040/10	632.82	443.69	189.13
A056/01	636.20	430.12	206.08
A076/99	414.62	244.35	170.27
A109/01	665.75	377.23	288.52
A175/09	736.37	426.20	310.17
A190/03	689.06	471.95	217.10
A204/07	396.08	286.18	109.90
A225/03	610.80	251.65	359.15
A231/09	432.03	313.96	118.07
A241/11	320.55	217.51	103.04
A242/04	643.06	453.21	189.85
A245/09	622.09	430.97	191.12
A263/05	694.56	467.66	226.91
A273/05	163.57	121.98	41.58
A273/07	657.25	428.56	228.69
A304/06	549.75	388.17	161.58
A339/96	701.30	494.25	207.04
701	137.80	137.80	0.00
738	292.79	292.79	0.00
743	406.52	336.89	69.63
756	250.29	250.29	0.00
776	508.99	378.17	130.82
817	554.11	376.92	177.19
823	366.99	332.80	34.19
832	647.11	539.95	107.16
846	595.05	346.78	248.27
901	504.27	399.00	105.27

Positive staining was detected within the ROI on all digital slide images, using the 'fast cell counts' function on QuPath. Threshold and cell detection parameters were optimised to detect each T cell marker and remained consistent. The cell detection parameters set for CD4, CD8, Foxp3, Tbet and GATA3 are shown in **Table 3.6**. All T cell quantification was performed blinded to groups.

Table 3.6 Detection parameters for CD4 and CD8

	CD4	CD8	Foxp3	Tbet	GATA3
Cell detection channel *(Channel to be thresholded to detect cells)*	Haematoxylin & DAB	Haematoxylin & DAB	Haematoxylin & DAB	Haematoxylin & DAB	Haematoxylin & DAB
Gaussian sigma *(Smoothing filter)*	3µm	3µm	1.5µm	1.5µm	3µm
Background radius *(Filter size to estimate background, should be > nucleus radius)*	25µm	25µm	15µm	15µm	25µm
Cell detection threshold *(Haematoxylin intensity threshold)*	0.15	0.05	0.1	0.1	0.3
DAB threshold *(DAB intensity threshold)*	0.15	0.2	0.2	0.2	0.2
Detection object diameter *(Size of detection object around each peak)*	25 pixels	25 pixels	25 pixels	25 pixels	25 pixels

Every positive detection identified by QuPath was manually checked and categorised by location (grey matter or white matter) and compartment (parenchyma or perivascular). Any detection that was not deemed to be a T cell, such as non-specific staining or artefact, was excluded. An example digital slide image showing positive cell detections is shown in **Figure 3.2**.

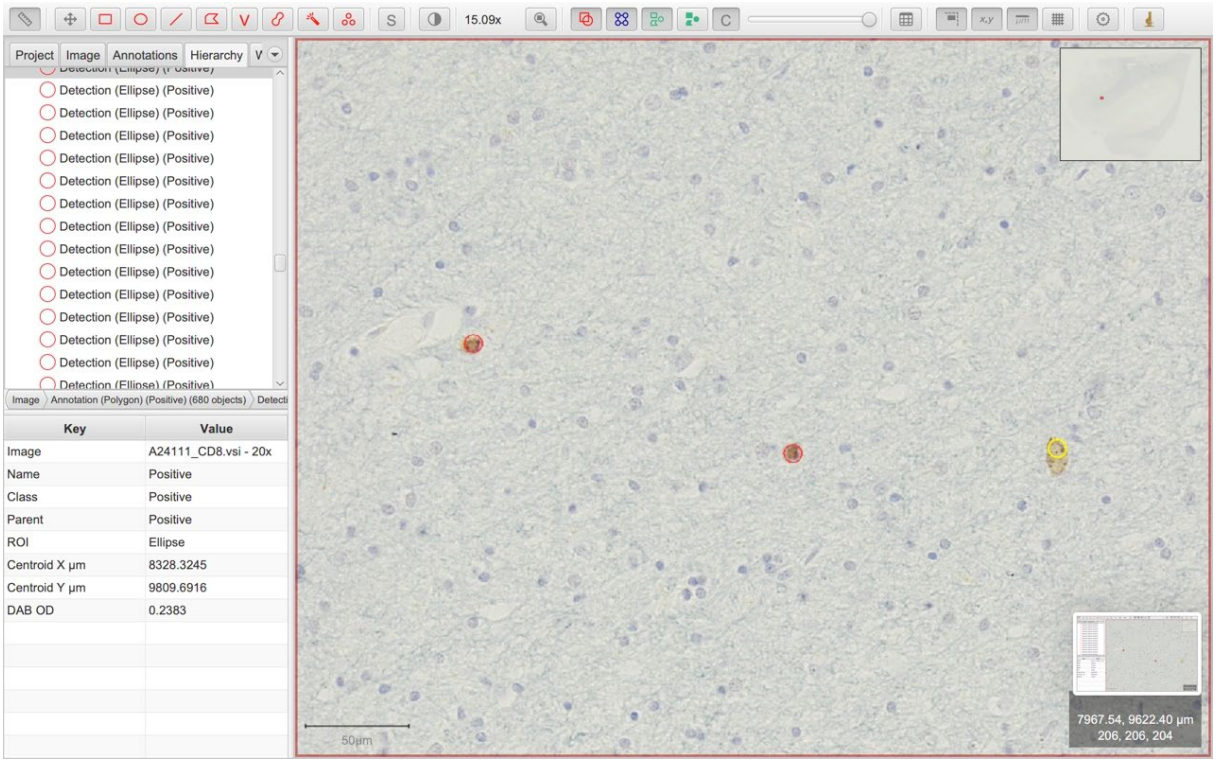

Figure 3.2 An example digital image taken from QuPath showing cell detections
Parenchymal T cells in grey matter are marked in red and an excluded positive detection is marked in yellow (x20 magnification, scale bar =50µm).

T cells were classified as perivascular if any part was located adjacent (within 20µm) to the abluminal surface of a blood vessel or within a perivascular space. Perivascular spaces are compartments between the endothelial basement membrane of blood vessels and the parenchymal basement membrane (165). Although the basement membrane structures were not visible in the scanned images, the perivascular spaces could still be clearly identified. Perivascular T cells have not been previously defined in studies examining brain tissue in DLB, however, have been defined in the dermis as T cells located <15µm from a blood vessel (194). For the purposes of this study, perivascular T cells were defined as T cells less than or equal to 20µm from the abluminal surface of a blood vessel. This allowed the inclusion of all T cells

which were regarded to be perivascular following review of CD4 and CD8 images. Example digital images of perivascular T cells are shown in **Figure 3.3**.

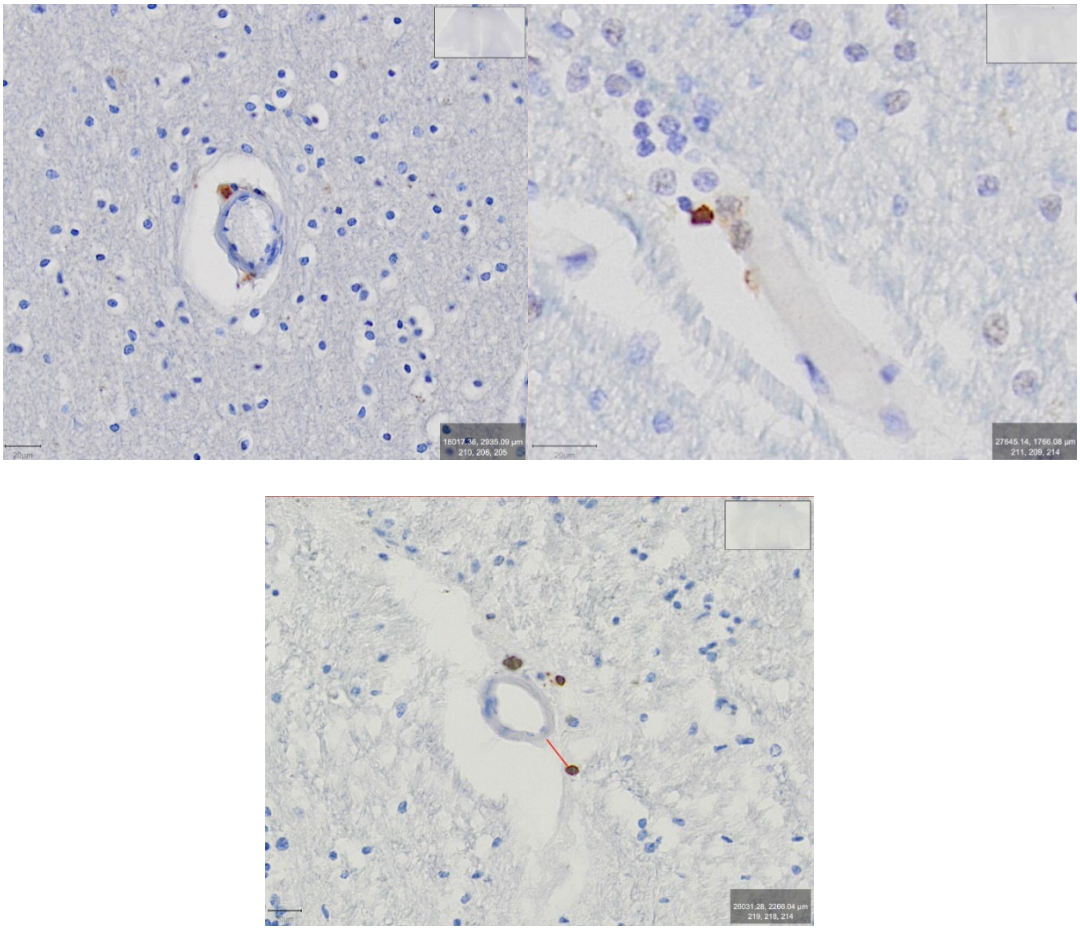

Figure 3.3 Perivascular T cells
Example digital images or perivascular T cells. T cell adjacent to a blood vessel (top left). T cell within the perivascular space (top right). T cells within 20µm of blood vessel, red line measures 20.0µm (bottom) (x20 magnification, scale bar =20µm).

3.1.6 Markers of neuropathology

The neuropathological markers, α-syn, ptau and Aβ had been quantified by Dr Jay Amin as part of a previous study using the same cohort of DLB and control cases (95). Grey matter within the superior temporal sulcus of the middle temporal gyrus (Brodmann area 21) was identified in each case as the ROI. Results for the markers ptau and Aβ were expressed as percentage protein loads. For each case, 30 images were captured from the ROI, creating a sample size of 15mm^2. ImageJ software (195) was used to quantify the immunostaining present in each image. The overall protein load in each case was defined as the mean percentage protein load of the 30 images captured in each case.

To assess the extent of α-syn pathology, the ROI was examined using a light microscope with low magnification (x4). A semi-quantitative analysis of LRP was used to attribute a score to each

case ranging from 0 to 4, as recommended by the international consensus criteria (12). The criteria for scoring LRP are listed below.

0 = None

1 = Mild (sparse LB or LN)

2 = Moderate (one or more LB in high power field and sparse LN)

3 = Severe (four or more LB and scattered LN in low power field)

4 = Very severe (numerous LB and LN)

3.1.7 Markers of inflammation

Protein loads for the inflammatory markers Iba1, HLA-DR, CD68, CD64, CD32a, CD32b, CD16, chitinase-3-like-1 (CHI3L1) and IL4R had been quantified for each DLB and control case by Dr Jay Amin as part of a previous study (95). The markers are associated with specific microglial functions as described below.

- **Iba1** is a marker of homeostatic microglia/macrophages associated with motility and is upregulated upon microglial activation (196).
- **HLA-DR** is a MHCII cell surface receptor expressed on the surface of APCs. HLA-DR is widely used as a marker of activated microglia (197).
- **CD68** a lysosomal protein localised to microglia and perivascular macrophages. It is used as marker of phagocytic activity (198).
- **CD64** is a high affinity cell surface receptor known as immunoglobulin Fcγ receptor 1 (FcγRI). FcγRs bind to IgG and are expressed at low levels on microglia. Activation of microglia through CD64 results in phagocytosis and the release of proinflammatory cytokines (199). CD64 is therefore used as a marker of antibody dependent phagocytic activity.
- **CD32a** (FcγRIIa) has a low affinity to IgG and high affinity for immune complexes and is used as a marker of phagocytic and anti-inflammatory microglia (200).
- **CD32b** (FcγRIIb) is a low affinity receptor that activates inhibitory signalling in microglia, suppressing phagocytic capabilities (197).
- **CD16** (FcγRIII) is a low affinity receptor that activates proinflammatory signalling and is a marker of activated microglia (197).
- **IL4R** is a cell surface receptor for IL-4, a cytokine with anti-inflammatory properties that induces alternative activation of microglia (201).
- **CHI3L1** is a secreted glycoprotein with anti-inflammatory properties (202), expressed by activated microglia and astrocytes (203).

Image J software (195) was used to quantify the percentage protein loads for each marker on 30 images of both grey and white matter taken from the ROI in each case. The images were obtained in a zigzag sequence to ensure sampling of all cortical layers. The mean value was calculated to provide the overall protein load for each marker.

3.1.8 Statistical analysis

Results were recorded as number of T cells per 100mm^2 in the parenchyma and perivascular areas for grey and white matter. Data was entered into IBM SPSS Statistics for Windows, version 28 (IBM Corp., Armonk, N.Y., USA). Baseline comparisons for age at death, sex, *post-mortem* delay, Braak ptau stage, disease duration and apolipoprotein E *(APOE)* genotype were performed to check for significant differences between DLB and control cases.

The number of T cells per 100mm^2 in each case was assessed for normality using quantile-quantile (Q-Q) plots and Shapiro-Wilk tests. For all T cell markers, the data was non-parametric, and the Mann-Whitney U test was used to compare the number of T cells between DLB and control groups. P values of less than 0.05 were deemed to be statistically significant. Scatter plot graphs were then prepared using GraphPad Prism version 10.1.0 for Windows (GraphPad Software, Boston, Massachusetts, USA, www.graphpad.com).

Spearman's rank correlations were used to test for associations between number of T cells and markers of neuropathology, and between number of T cells and inflammatory markers. P values were adjusted using the Bonferroni correction, to account for multiple testing. P values of less than 0.002 were deemed to be significant for associations between T cells and neuropathological markers. P values of less than 0.001 were deemed to be significant for associations between T cells and inflammatory markers.

Chapter 4 Results

Data were obtained from 30 DLB and 29 control cases for the analysis of CD4+ and CD8+ T cells. For analysis of further T cell markers there were insufficient numbers of tissue sections to include all cases. Data were collected from 28 DLB cases and 25 control cases for the analysis of Foxp3+ T cells. The analysis of Tbet+ T cells included data obtained from 26 DLB cases and 23 control cases. There were 22 DLB cases and 20 control cases remaining for the analysis of GATA3+ T cells. No data for analysis was collected for CXCL12 and CXCR4 markers due to methodological limitations which are discussed in section 4.14.

4.1 Baseline characteristics

Baseline characteristics were assessed for differences between the DLB and control groups.

- **Age at death:** An independent samples T test showed no significance difference between groups (DLB: mean 77.6 years, SD 8.3; Control: mean 79.4 years, SD 8.0; p=0.397).
- **Sex:** There were more males than females in both groups (DLB: 24 males, 6 females; Control: 17 males, 12 females). No significant difference in sex was identified using a Pearson Chi-squared test ($\chi^2(1)=3.179$, p=0.075).
- ***Post-mortem* delay:** An independent samples T test showed no significant difference between groups (DLB: mean 27.3hours, SD 14.6; Control: mean 33.9 hours, SD 15.5; p= 0.096).
- **Braak ptau stage:** A Pearson Chi-squared test showed no significance difference between groups ($\chi^2(3)=4.360$, p=0.235). Data were missing for 3 DLB cases and 1 control case.
- ***APOE* genotype:** No significant difference was found between groups using a Fisher's Exact Test (p=0.393). Data were missing for 16 DLB cases and 2 control cases.
- **Disease duration:** Duration of disease in the DLB group was found to be normally distributed (mean 6.7, SD 3.6). Data were missing for 2 cases.
- **Clinical information at time of death:** Clinical information was limited and it was not possible to accurately confirm the presence or absence of systemic infection or inflammation at the time of death. Clinical data were unavailable for 19 DLB cases and 10 control cases; therefore, no comparative analysis was performed.

4.2 CD4+ T cell data

The number of CD4+ T cells per 100mm^2 detected in the parenchymal and perivascular compartments of grey and white matter was assessed for differences between the DLB and control groups. The localisation of CD4 staining was observed to be cytoplasmic and detected T cells measured between 5-8µm in diameter.

Example images of CD4+ T cells acquired during T cell detection are shown in **Figure 4.1**.

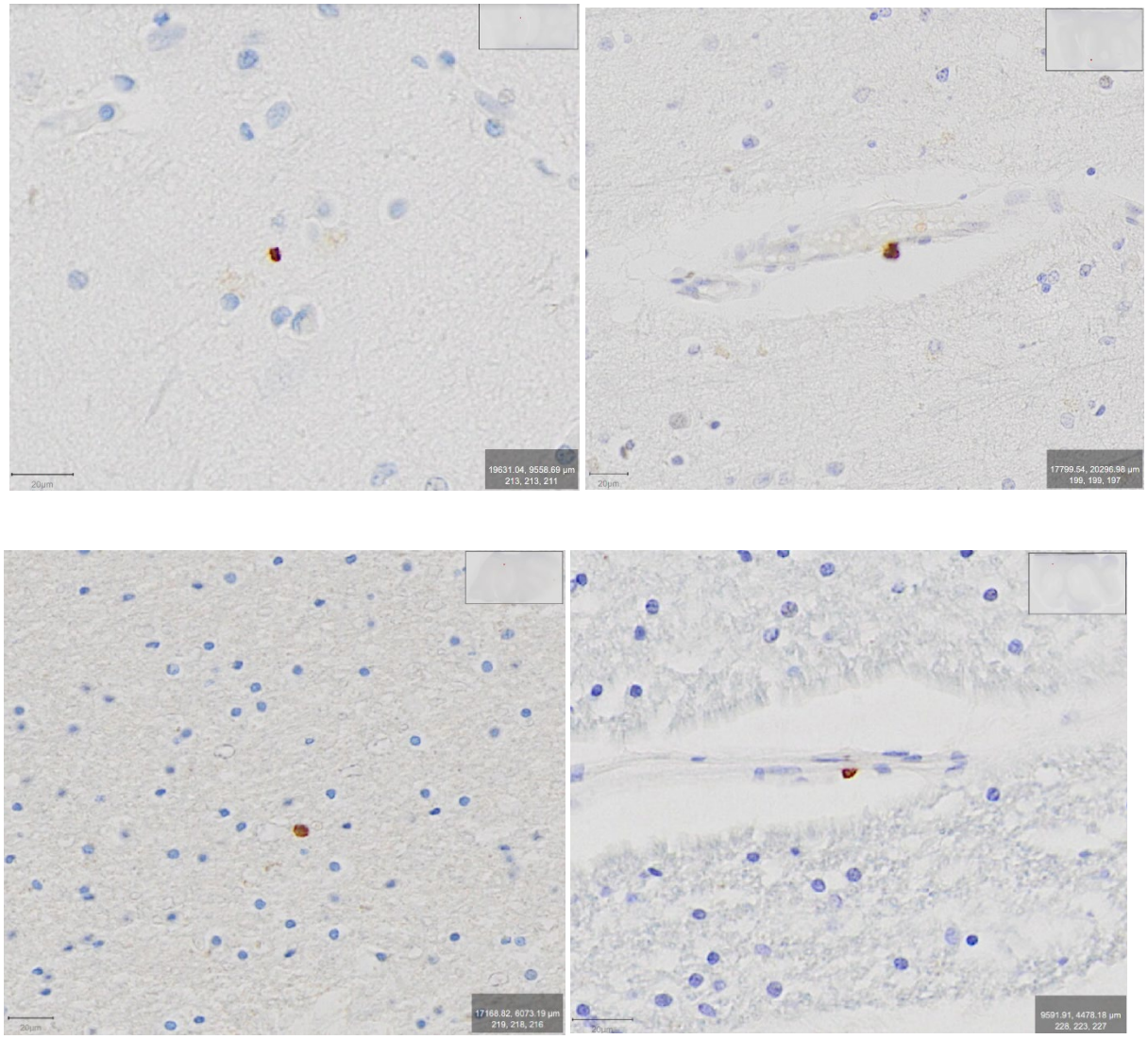

Figure 4.1 CD4 immunostaining
Example digital images of CD4 immunostaining. CD4+ T cell in the grey matter parenchyma (top left). Perivascular CD4+ T cell in the grey matter (top right). CD4+ T cell in the white matter parenchyma (bottom left). Perivascular CD4+ T cell in the white matter (bottom right) (x20 magnification, scale bar =20µm).

A Mann-Whitney U test was used to test for significant differences between the groups. A summary of the data is presented in **Table 4.1**.

Table 4.1 Parenchymal and perivascular CD4+ T cells (per 100mm^2) in grey and white matter

	Control (n=29)	DLB (n=30)	Mann-Whitney U test statistic	p value
Total CD4+ T cells	1.290 (0.73-1.55)	1.615 (0.92-2.72)	305	**p=0.049***
CD4+ T cells in grey matter	1.246 (0.57-1.80)	1.676 (1.05-2.45)	323	p=0.089
Parenchymal CD4+ T cells in grey matter	1.118 (0.50-1.56)	1.584 (1.02-2.19)	302	**p=0.044***
Perivascular CD4+ T cells in grey matter	0.182 (0.00-0.40)	0.000 (0.00-0.42)	428	p=0.910
CD4+ T cells in white matter	0.426 (0.00-1.00)	0.800 (0.00-2.10)	327	p=0.091
Parenchymal CD4+ T cells in white matter	0.000 (0.00-0.99)	0.647 (0.00-1.43)	332	p=0.101
Perivascular CD4+ T cells in white matter	0.000 (0.00-0.00)	0.000 (0.00-0.55)	371	p=0.193

Data presented as median (IQR) based on non-parametric distribution.
*p<0.05

The number of total CD4+ T cells/100mm^2 was significantly increased in the DLB group compared to the control group (DLB: median 1.615 [IQR 1.802], Control: median 1.290 [IQR 0.817], p=0.049). There were significantly more parenchymal CD4+ T cells in grey matter/100mm^2 in the DLB group compared to the control group (DLB: median 1.584 [IQR 1.099], Control: median 1.118 [IQR 1.064], p=0.044).

Between DLB and control groups, there was no significant difference in the number of CD4+ T cells/100mm^2 in grey matter, number of perivascular CD4+ T cells/100mm^2 in grey matter, number of CD4+ T cells/100mm^2 in white matter, number of parenchymal CD4+ T cells/100mm^2 in white matter and the number of perivascular CD4+ T cells/100mm^2 in white matter. These data are presented graphically in composite **Figure 4.2.**

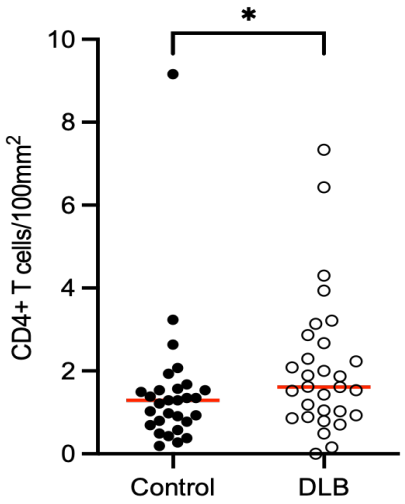

Scatter plot of total CD4+ T cells in brain (grey and white) matter
The total number of CD4+ T cells in brain matter was significantly higher in DLB compared to controls. *p=0.049. Red line represents median.

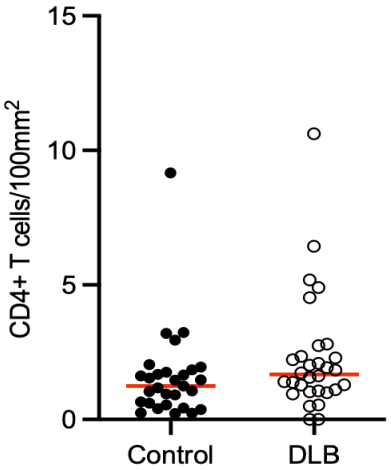

Scatter plot of total CD4+ T cells in grey matter
No significant difference in number of CD4+ T cells in grey matter between control and DLB groups. p=0.089. Red line represents median.

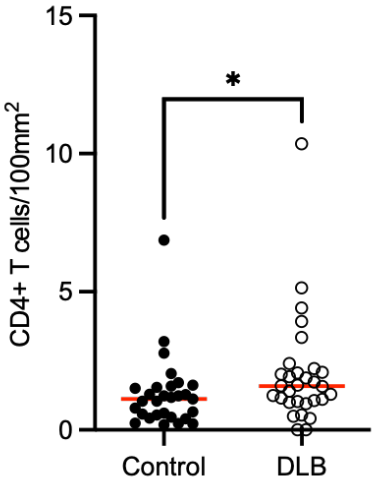

Scatter plot of parenchymal CD4+ T cells in grey matter
The number of parenchymal CD4+ T cells in grey matter was significantly higher in DLB compared to controls. *p=0.044. Red line represents median.

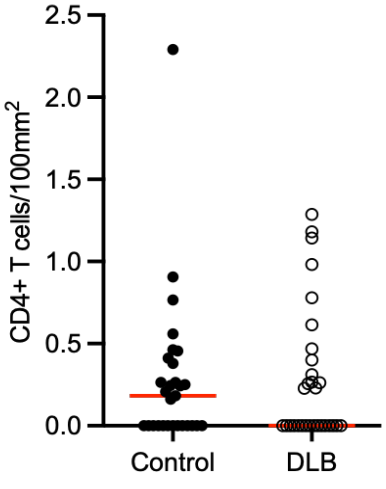

Scatter plot of perivascular CD4+ T cells in grey matter
No significant difference in number of perivascular CD4+ T cells in grey matter between control and DLB groups. p=0.910. Red line represents median.

Figure 4.2 Scatter plot graphs of total, parenchymal and perivascular CD4+ T cells/100mm^2 in grey and white matter

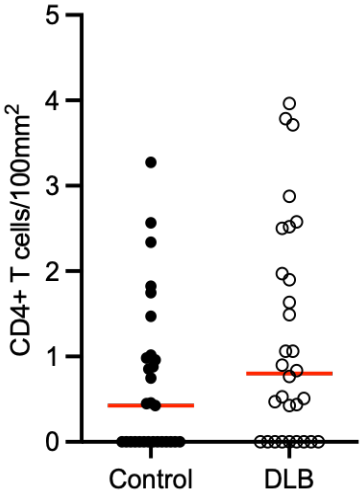

Scatter plot of total CD4+ T cells in white matter
No significant difference in number of CD4+ T cells in white matter between control and DLB groups. p=0.091. Red line represents median.

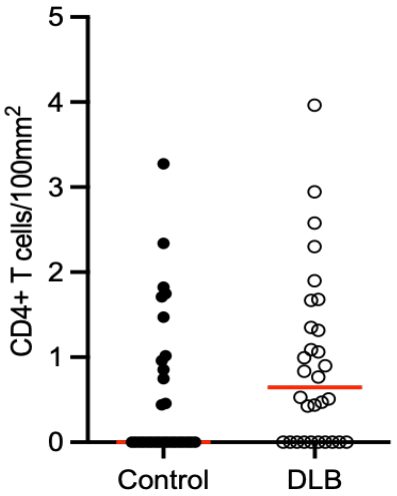

Scatter plot of parenchymal CD4+ T cells in white matter
No significant difference in number of parenchymal CD4+ T cells in white matter between control and DLB groups. p=0.101. Red line represents median.

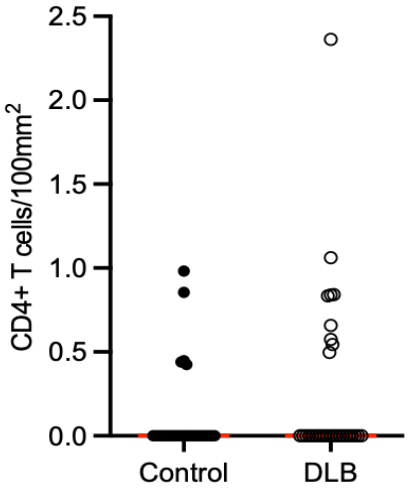

Scatter plot of perivascular CD4+ T cells in white matter
No significant difference in number of perivascular CD4+ T cells in white matter between control and DLB groups. p=0.193. Red line represents median.

Figure 4.2 (continued) Scatter plot graphs of total, parenchymal and perivascular CD4+ T cells/100mm^2 in grey and white matter

4.3 CD8+ T cell data

The number of CD8+ T cells per 100mm^2 detected in the parenchymal and perivascular compartments of grey and white matter was assessed for differences between the DLB and control groups. The localisation of CD8 staining was observed to be cytoplasmic and detected T cells measured between 5-8µm in diameter.

Example images of brain tissue immunostained for CD8 are provided below in **Figure 4.3.**

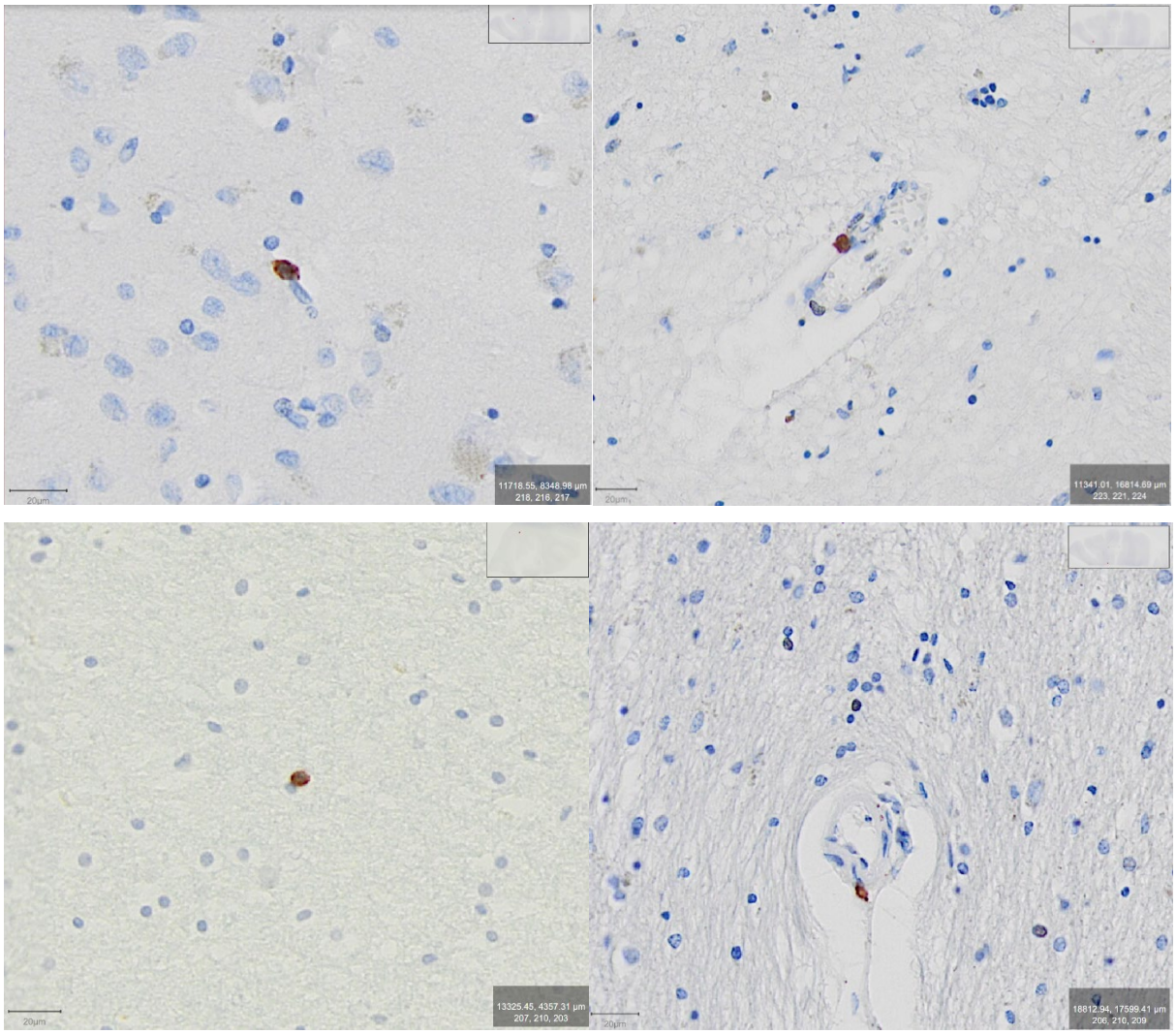

Figure 4.3 CD8 immunostaining
Example digital images of CD8 immunostaining. CD8+ T cell in the grey matter parenchyma (top left). Perivascular CD8+ T cell in the grey matter (top right). CD8+ T cell in the white matter parenchyma (bottom left). Perivascular CD8+ T cell in the white matter (bottom right) (x20 magnification, scale bar =20µm).

The number of CD8+ T cells per 100mm^2 detected in the parenchymal and perivascular compartments of grey and white matter was deemed to be nonparametric in distribution. A Mann-Whitney U test was used to assess for significant differences between the DLB and control groups and a summary of the data is presented in **Table 4.2**.

Table 4.2 Parenchymal and perivascular CD8+ T cells (per 100mm^2) in grey and white matter

	Control (n=29)	DLB (n=30)	Mann-Whitney U test statistic	p value
Total CD8+ T cells	4.002 (1.10-17.01)	10.123 (3.28-23.40)	330	p=0.111
CD8+ T cells in grey matter	1.836 (0.33-10.64)	3.544 (0.89-10.18)	362	p=0.268
Parenchymal CD8+ T cells in grey matter	0.405 (0.00-3.06)	1.264 (0.39-4.90)	348	p=0.184
Perivascular CD8+ T cells in grey matter	1.573 (0.20-3.79)	2.398 (0.40-5.69)	372	p=0.338
CD8+ T cells in white matter	8.359 (2.53-35.68)	15.600 (2.17-41.67)	411.5	p=0.721
Parenchymal CD8+ T cells in white matter	2.108 (0.56-6.63)	2.416 (0.42-10.86)	418	p=0.796
Perivascular CD8+ T cells in white matter	6.966 (1.18-22.53)	11.702 (0.54-33.98)	404	p=0.638

Data presented as median (IQR) based on non-parametric distribution.
*p<0.05

Between DLB and control groups, there was no significant difference in the total number of CD8+ T cells/100mm^2, number of CD8+ T cells/100mm^2 in grey matter, number of parenchymal CD8+ T cells/100mm^2 in grey matter, number of perivascular CD8+ T cells/100mm^2 in grey matter, number of CD8+ T cells/100mm^2 in white matter, number of parenchymal CD8+ T cells/100mm^2 in white matter and the number of perivascular CD8+ T cells/100mm^2 in white matter. These data are presented graphically in composite **Figure 4.4**.

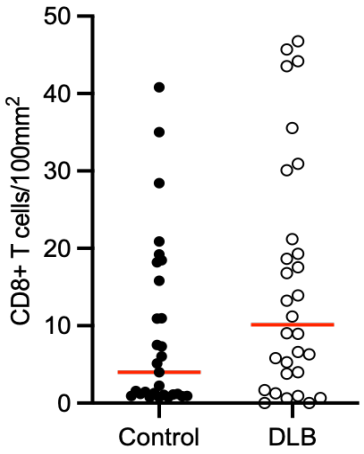

Scatter plot of total CD8+ T cells in brain (grey and white) matter
No significant difference in total number of CD8+ T cells in brain matter between control and DLB groups. p=0111. Red line represents median.

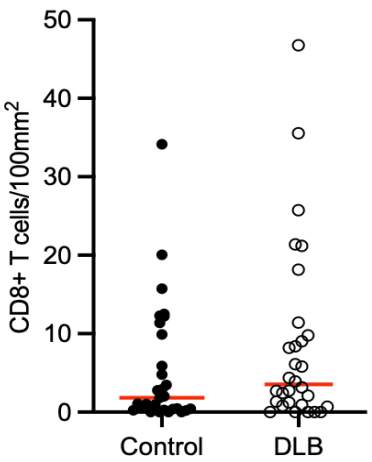

Scatter plot of total CD8+ T cells in grey matter
No significant difference in number of CD8+ T cells in grey matter between control and DLB groups. p=0.268. Red line represents median.

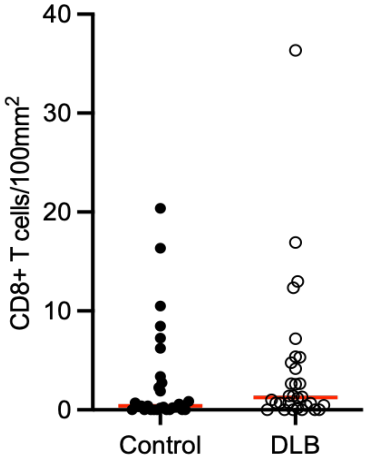

Scatter plot of parenchymal CD8+ T cells in grey matter
No significant difference in number of parenchymal CD8+ T cells in grey matter between control and DLB groups. p=0.184. Red line represents median.

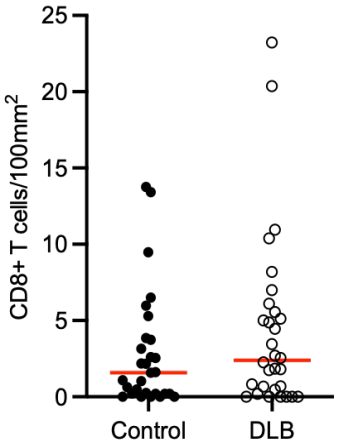

Scatter plot of perivascular CD8+ T cells in grey matter
No significant difference in number of perivascular CD8+ T cells in grey matter between control and DLB groups. p=0.338. Red line represents median.

Figure 4.4 Scatter plot graphs of total, parenchymal and perivascular CD8+ T cells/100mm^2 in grey and white matter

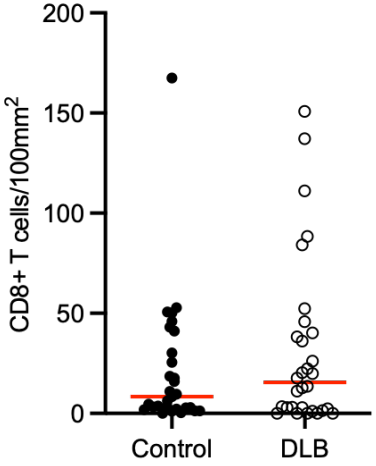

Scatter plot of total CD8+ T cells in white matter
No significant difference in number of CD8+ T cells in white matter between control and DLB groups. p=0.721. Red line represents median.

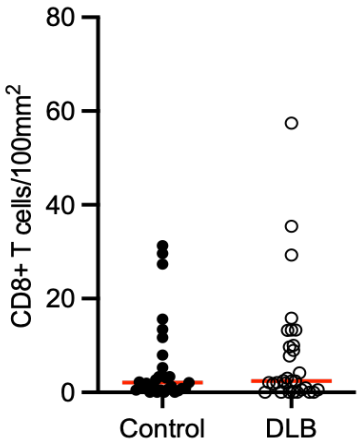

Scatter plot of parenchymal CD8+ T cells in white matter
No significant difference in number of parenchymal CD8+ T cells in white matter between control and DLB groups. p=0796. Red line represents median.

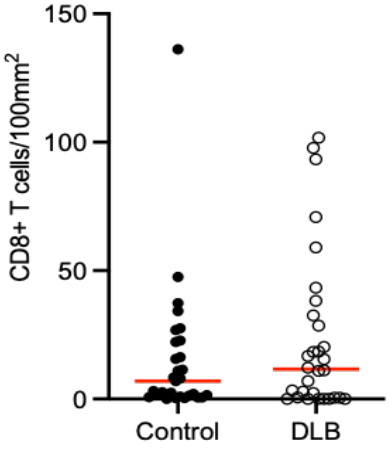

Scatter plot of perivascular CD8+ T cells in white matter
No significant difference in number of perivascular CD8+ T cells in white matter between control and DLB groups. p=0638. Red line represents median.

Figure 4.4 (continued) Scatter plot graphs of total, parenchymal and perivascular CD8+ T cells/100mm^2 in grey and white matter

4.4 Outliers in T cell data

On review of the scatter plot graphs presenting CD4+ T cell and CD8+ T cell data, potential outliers were identified and then confirmed using the interquartile range (IQR) method. Mild outliers were defined as data points more than 1.5 IQR above the third quartile or 1.5 IQR below the first quartile. Extreme outliers were defined as data points more than 3 IQR above the third quartile or 3 IQR below the first quartile. Following the identification of extreme outliers, clinical and *port-mortem* reports for related cases were obtained and reviewed.

4.4.1 Extreme outliers in CD4+ T cell data

Control case 943 was identified as an extreme outlier in the following data sets: total number of CD4+ T cells/100mm^2 in brain (grey and white) matter, number of CD4+ T cells/100mm^2 in grey matter, number of parenchymal CD4+ T cells/100mm^2 in grey matter and number of perivascular CD4+ T cells/100mm^2 in grey matter. The *post-mortem* report for control case 943 was reviewed and revealed a neuropathological diagnosis of argyrophilic grain disease. Cause of death was metastatic squamous cell carcinoma of the larynx. Inclusion to the study required control cases to be neuropathologically normal on *post-mortem* report and it was therefore deemed not to be eligible for inclusion in this study. Statistical analysis was repeated following exclusion of data for case 943.

DLB case A304/06 was identified as an extreme outlier in the following data sets: number of CD4+ T cells/100mm^2 in grey matter and number of parenchymal CD4+ T cells/100mm^2 in grey matter. The *post-mortem* information available for this case revealed a neuropathological diagnosis of diffuse neocortical LBD and co-morbid argyrophilic grain disease. Duration of DLB was reported to be 9 years and cause of death was unavailable. Data points for case A304/06 were excluded from repeat statistical analysis due to the presence of argyrophilic grain disease as a possible confounder.

DLB case A175/09 was identified as an extreme outlier in the data set: number of perivascular CD4+ T cells/100mm^2 in white matter. The *post-mortem* report indicated a neuropathological diagnosis of mild neocortical LBD. Duration of DLB was reported to be 4 years and cause of death was due to prostate cancer and atrial fibrillation. Data points for case A175/09 were deemed to be legitimate observations reflecting a DLB group population and were not excluded from repeat analysis.

4.4.2 Extreme outliers in CD8+ T cell data

Control case 877 was identified as an extreme outlier in the following data sets: number of CD8+ T cells/100mm^2 in white matter, number of parenchymal CD8+ T cells/100mm^2 in white matter and number of perivascular CD8+ T cells/100mm^2 in white matter. The *post-mortem* report stated, 'very mild arteriosclerotic small vessel disease' and cause of death was cerebrovascular event, metastatic prostate cancer and end-stage renal failure. Data points for control case 877 were deemed to be legitimate observations reflecting a control group population and were not excluded from repeat analysis.

Control case 818 was identified as an extreme outlier in the data set: number of parenchymal CD8+ T cells in grey matter. A neuropathological diagnosis of mild small vessel disease was documented on the *post-mortem* report. Cause of death was septicaemia, urinary tract infection, bronchial pneumonia and chronic obstructive pulmonary disease. Data points for control case 818 were deemed to be legitimate observations reflecting a control group population and were not excluded from repeat analysis.

Control case 894 was identified as an extreme outlier in the following data sets: number of parenchymal CD8+ T cells/100mm^2 in grey matter and number of parenchymal CD8+ T cells/100mm^2 in white matter. The *post-mortem* report indicated a neuropathological diagnosis of argyrophilic grain disease and cause of death was disseminated metastatic cancer. Data points for control case 894 were excluded from statistical analysis due to a neuropathological diagnosis of argyrophilic grain disease.

Control case 803 was identified as an extreme outlier in the data set: number of parenchymal CD8+ T cells in white matter. A neuropathological diagnosis of 'mild to moderate cerebral amyloid angiopathy, no AD' was reported on *post-mortem*. Cause of death was bronchopneumonia, left cerebrovascular event, atrial fibrillation, hypertension and myocardial infarction. Data points for control case 803 were excluded from statistical analysis due to the neuropathological diagnosis of cerebral amyloid angiopathy not meeting the inclusion criteria for control cases.

DLB case 756 was identified as an extreme outlier in the following data sets: number of CD8+ T cells/100mm^2 in grey matter and number of parenchymal CD8+ T cells/100mm^2 in grey matter. The *post-mortem* report indicated a neuropathological diagnosis of DLB and cause of death was septicaemia, pneumonia and DLB. DLB case 701 was identified as an extreme outlier in the following data set: number of perivascular CD8+ T cells/100mm^2 in grey matter. The *post-mortem* report stated a neuropathological diagnosis of DLB and cause of death was not provided. DLB case 743 was identified as an extreme outlier in the following data set: number of

parenchymal CD8+ T cells/100mm^2 in white matter. Information from *post-mortem* revealed a neuropathological diagnosis of mild LBD with cortical involvement and cause of death was pulmonary embolism. Data points for cases 756, 701 and 743 were deemed to be legitimate observations reflecting a DLB group population and were therefore not excluded from repeat statistical analysis.

4.5 CD4+ T cell data (excluding selected outliers)

A Mann-Whitney U test was used to test for significant differences between the DLB and control group, following exclusion of control cases 803, 894, 943 and DLB case A304/06. A summary of the data is presented in **Table 4.3**.

Table 4.3 Parenchymal and perivascular CD4+ T cells (per 100mm^2) in grey and white matter (excluding outliers)

	Control (n=26)	DLB (n=29)	Mann-Whitney U test statistic	p value
Total CD4+ T cells	1.251 (0.67-1.53)	1.609 (0.91-2.48)	249	**p=0.031***
CD4+ T cells in grey matter	1.210 (0.51-1.69)	1.615 (1.04-2.32)	268	p=0.066
Parenchymal CD4+ T cells in grey matter	1.078 (0.45-1.55)	1.568 (1.01-2.07)	256	**p=0.041***
Perivascular CD4+ T cells in grey matter	0.081 (0.00-0.29)	0.000 (0.00-0.44)	361	p=0.770
CD4+ T cells in white matter	0.451 (0.00-1.13)	0.834 (0.00-2.23)	293	p=0.148
Parenchymal CD4+ T cells in white matter	0.000 (0.00-1.13)	0.767 (0.00-1.51)	298	p=0.167
Perivascular CD4+ T cells in white matter	0.000 (0.00-0.00)	0.000 (0.00-0.56)	324	p=0.243

Data presented as median (IQR) based on non-parametric distribution.
*p<0.05

Following exclusion of control cases 943, 803, 894 and DLB case A304/06, there remained a significant increase in the total number of CD4+ T cells/100mm^2 in the DLB group compared to the control group (DLB: median 1.609 [IQR 1.575], Control: median 1.251 [IQR 0.821], p=0.031). There were significantly more parenchymal CD4+ T cells/100mm^2 in grey matter in the DLB

group compared to the control group (DLB: median 1.568 [IQR 1.060], Control: median 1.078 [IQR 1.101], p=0.041).

Between DLB and control groups, there remained no significant difference in the number of CD4+ T cells in grey matter/100mm^2, number of perivascular CD4+ T cells/100mm^2 in grey matter, number of CD4+ T cells in white matter/100mm^2, number of parenchymal CD4+ T cells/100mm^2 in white matter and the number of perivascular CD4+ T cells/100mm^2 in white matter. These data are presented graphically in composite **Figure 4.5.**

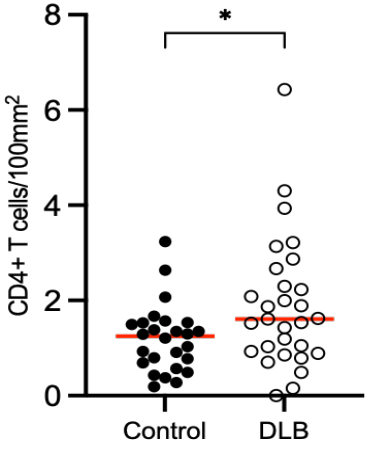

Scatter plot of total CD4+ T cells in brain (grey and white) matter
The total number of CD4+ T cells in brain matter was significantly higher in DLB compared to controls. *p=0.031. Red line represents median.

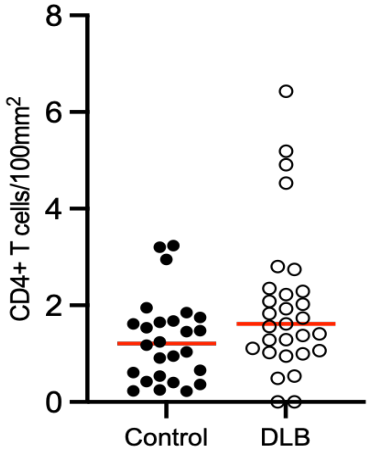

Scatter plot of total CD4+ T cells in grey matter
No significant difference in number of CD4+ T cells in grey matter between control and DLB groups. p=0.066. Red line represents median.

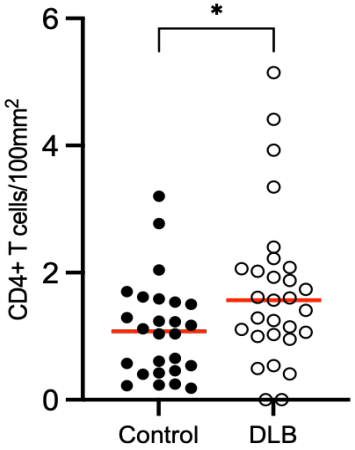

Scatter plot of parenchymal CD4+ T cells in grey matter
The number of parenchymal CD4+ T cells in grey matter was significantly higher in DLB compared to controls. *p=0.041. Red line represents median.

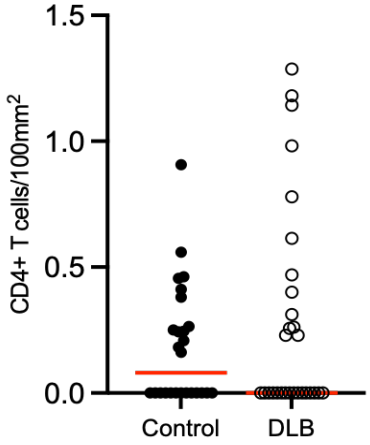

Scatter plot of perivascular CD4+ T cells in grey matter
No significant difference in number of perivascular CD4+ T cells in grey matter between control and DLB groups. p=0.770. Red line represents median.

Figure 4.5 Scatter plot graphs of total, parenchymal and perivascular CD4+ T cells/100mm² in grey and white matter excluding outliers

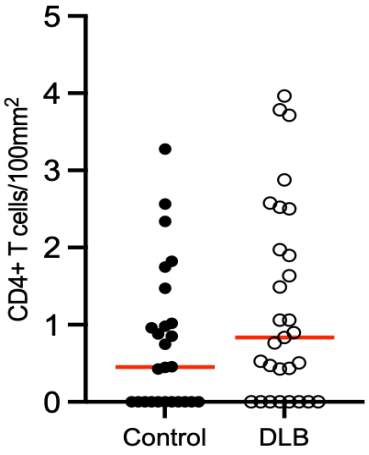

Scatter plot of total CD4+ T cells in white matter
No significant difference in number of CD4+ T cells in white matter between control and DLB groups. p=0.148.
Red line represents median.

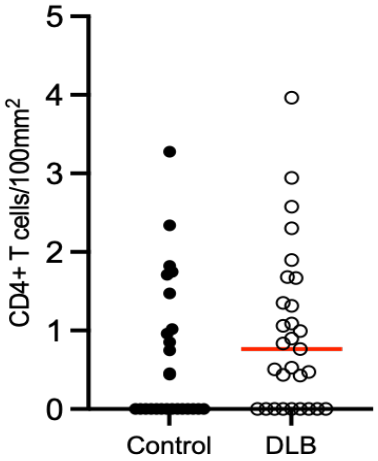

Scatter plot of parenchymal CD4+ T cells in white matter
No significant difference in number of parenchymal CD4+ T cells in white matter between control and DLB groups. p=0.167.
Red line represents median.

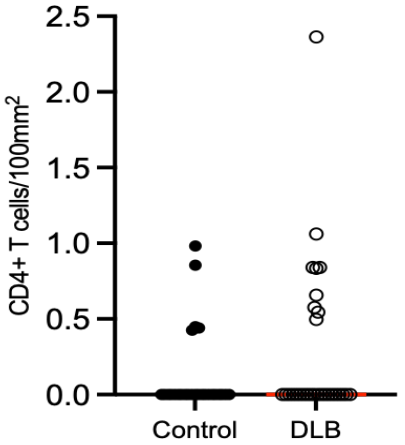

Scatter plot of perivascular CD4+ T cells in white matter
No significant difference in number of perivascular CD4+ T cells in white matter between control and DLB groups. p=0.243.
Red line represents median.

Figure 4.5 (continued) Scatter plot graphs of total, parenchymal and perivascular CD4+ T cells/100mm^2 in grey and white matter excluding outliers

4.6 CD8+ T cell data (excluding selected outliers)

A Mann-Whitney U test was used to test for significant differences between the DLB and control group, following exclusion of control cases 803, 894, 943 and DLB case A304/06. A summary of the data is presented in **Table 4.4**.

Table 4.4 Parenchymal and perivascular CD8+ T cells (per 100mm^2) in grey and white matter

	Control (n=26)	DLB (n=29)	Mann-Whitney U test statistic	p value
Total CD8+ T cells	3.124 (1.06-12.18)	11.199 (2.75-25.63)	267	p=0.064
CD8+ T cells in grey matter	1.433 (0.28-6.88)	3.181 (0.87-10.59)	294	p=0.161
Parenchymal CD8+ T cells in grey matter	0.364 (0.00-2.38)	1.202 (0.33-5.03)	285	p=0.118
Perivascular CD8+ T cells in grey matter	1.302 (0.20-3.29)	2.543 (0.33-5.83)	299	p=0.187
CD8+ T cells in white matter	7.306 (2.67-26.75)	17.612 (1.93-43.06)	344	p=0.578
Parenchymal CD8+ T cells in white matter	2.033 (0.58-4.00)	2.405 (0.28-11.65)	348.5	p=0.630
Perivascular CD8+ T cells in white matter	5.053 (1.27-23.39)	12.244 (0.52-35.39)	342	p=0.555

Data presented as median (IQR) based on non-parametric distribution.
*p<0.05

Following exclusion of control cases 943, 803, 894 and DLB case A304/06, there was no significant difference between DLB and control groups in the total number of CD8+ T cells/100mm^2, number of CD8+ T cells/100mm^2 in grey matter, number of parenchymal CD8+ T cells/100mm^2 in grey matter, number of perivascular CD8+ T cells/100mm^2 in grey matter, number of CD8+ T cells/100mm^2 in white matter, number of parenchymal CD8+ T cells/100mm^2

in white matter and the number of perivascular CD8+ T cells/100mm^2 in white matter. These data are presented graphically in composite **Figure 4.6.**

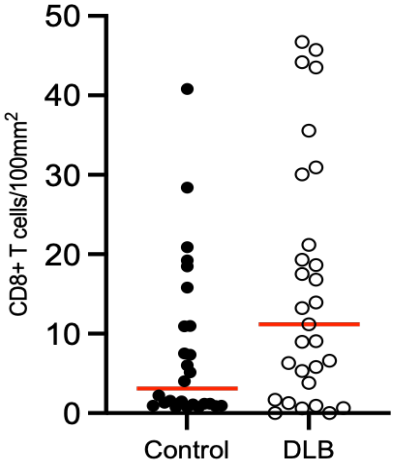

Scatter plot of total CD8+ T cells in brain (grey and white) matter
No significant difference in total number of CD8+ T cells in brain matter between control and DLB groups. p=0.064. Red line represents median.

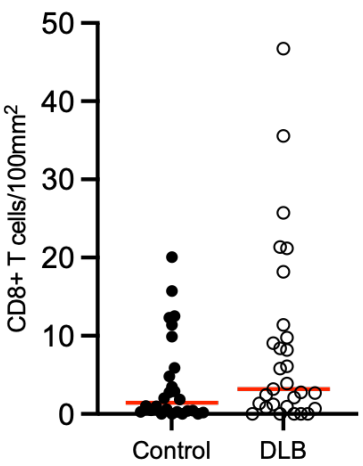

Scatter plot of total CD8+ T cells in grey matter
No significant difference in number of CD8+ T cells in grey matter between control and DLB groups. p=0.161. Red line represents median.

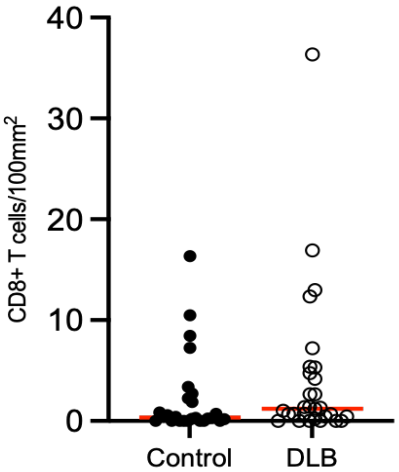

Scatter plot of parenchymal CD8+ T cells in grey matter
No significant difference in number of parenchymal CD8+ T cells in grey matter between control and DLB groups. p=0.118. Red line represents median.

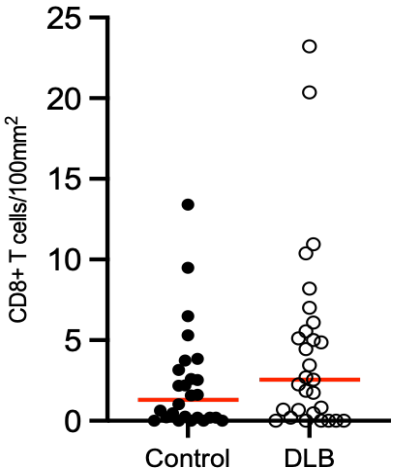

Scatter plot of perivascular CD8+ T cells in grey matter
No significant difference in number of perivascular CD8+ T cells in grey matter between control and DLB groups. p=0.187. Red line represents median.

Figure 4.6 Scatter plot graphs of total, parenchymal and perivascular CD8+ T cells/100mm^2 in grey and white matter excluding outliers

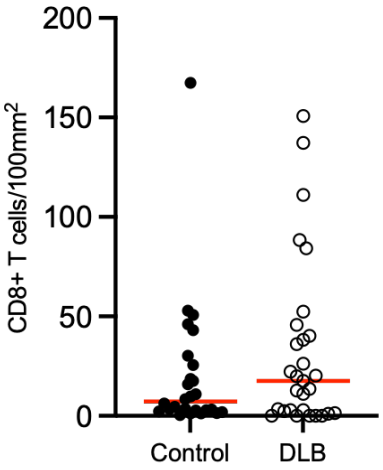

Scatter plot of total CD8+ T cells in white matter
No significant difference in number of CD8+ T cells in white matter between control and DLB groups. p=0.578.
Red line represents median.

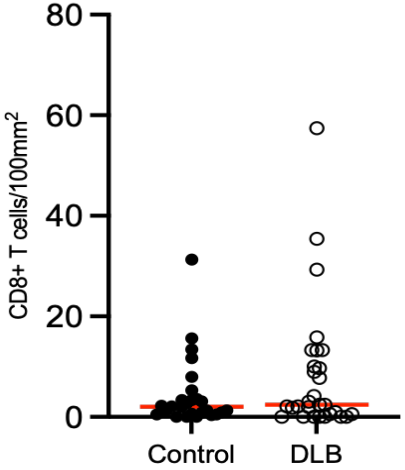

Scatter plot of parenchymal CD8+ T cells in white matter
No significant difference in number of parenchymal CD8+ T cells in white matter between control and DLB groups. p=0.630.
Red line represents median.

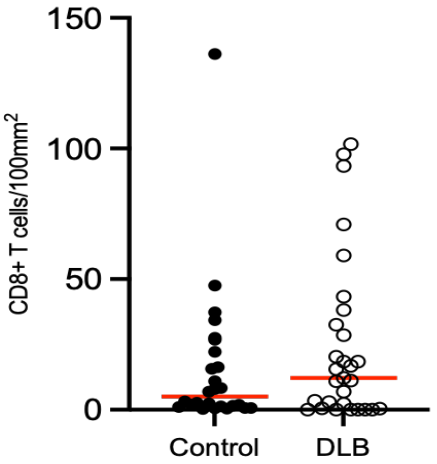

Scatter plot of perivascular CD8+ T cells in white matter
No significant difference in number of perivascular CD8+ T cells in white matter between control and DLB groups. p=0.555.
Red line represents median.

Figure 4.6 (continued) Scatter plot graphs of total, parenchymal and perivascular CD8+ T cells/100mm^2 in grey and white matter excluding outliers

4.7 Profile of CD4+ versus CD8+ T cells in control cases

A Mann-Whitney U test was used to test for significant differences between the number of CD4+ and CD8+ T cells/100mm^2 in total, parenchymal and perivascular compartments of grey and white matter in the control group. Cases 803, 894, 943 were excluded from analysis due to being previously identified as outliers not meeting inclusion criteria. A summary of the data is presented in **Table 4.5**.

Table 4.5 CD4+ and CD8+ T cells (per 100mm^2) in control group (n=26)

	CD4+	CD8+	Mann-Whitney U test statistic	p value
Total T cells	1.251 (0.67–1.53)	3.124 (1.06-12.18)	171	**0.002***
T cells in grey matter	1.210 (0.51-1.69)	1.433 (0.28-6.88)	300	0.487
Parenchymal T cells in grey matter	1.078 (0.45-1.55)	0.364 (0.00-2.38)	257	0.138
Perivascular T cells in grey matter	0.081 (0.00 – 0.29)	1.302 (0.20-3.29)	149.5	**<0.001***
T cells in white matter	0.451 (0.00-1.13)	7.306 (2.67-26.75)	41	**<0.001***
Parenchymal T cells in white matter	0.000 (0.00-1.13)	2.033 (0.58-4.00)	142	**<0.001***
Perivascular T cells in white matter	0.000 (0.00-0.00)	5.053 (1.27-23.39)	16	**<0.001***

Data presented as median (IQR) based on non-parametric distribution.
*p<0.05

The number of CD8+ T cells/100mm^2 was significantly higher compared to CD4+ T cells/100mm^2 in total brain matter (CD4: median 1.251 [IQR 0.873], CD8: median 3.124 [IQR 11.113], p=0.002) and in white matter (CD4: median 0.451 [IQR 1.132], CD8: median 7.306 [IQR 24.081], p=<0.001). The number of parenchymal CD8+ T cells/100mm^2 was significantly higher compared to parenchymal CD4+ T cells/100mm^2 in white matter (CD4: median 0.000 [IQR

1.132], CD8: median 2.033 [IQR 3.419], p=<0.001). The number of perivascular CD8+ T cells/100mm^2 was significantly higher compared to perivascular CD4+ T cells/100mm^2 in grey matter (CD4: median 0.081 [IQR 0.293], CD8: median 1.302 [IQR 3.094], p=<0.001) and in white matter (CD4: median 0.000 [IQR 0.000], CD8: median 5.053 [IQR 22.121], p=<0.001).

No significant differences were found between the number of CD4+ and CD8+ T cells/100mm^2 in grey matter (CD4: median 1.210 [IQR 1.185], CD8: median 1.433 [IQR 6.600], p=0.487) or between the number of parenchymal CD4 and CD8+ T cells/100mm^2 in grey matter (CD4: median 1.078 [IQR 1.101], CD8: median 0.364 [IQR 2.376], p=0.138). These data are presented graphically in composite **Figure 4.7**.

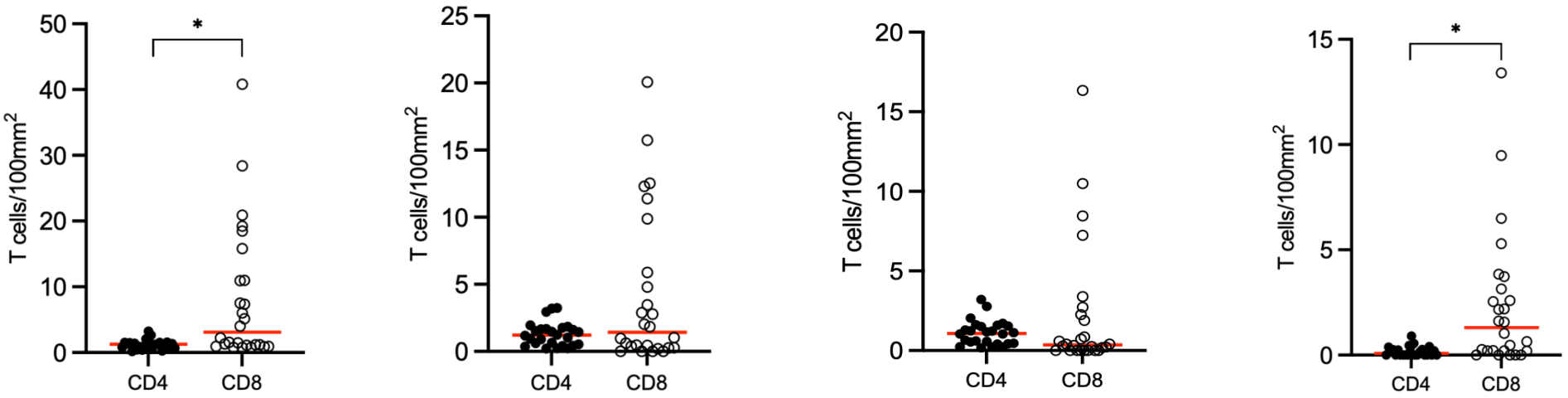

Scatter plot of total CD4+ and CD8+ cells in brain (grey and white) matter
The number of CD8+ T cells was significantly higher than the number of CD4+ T cells. *p=0.002. Red line represents median.

Scatter plot of total CD4+ and CD8+ T cells in grey matter
No significant difference in number of CD4+ compared to CD8+ T cells in grey matter. p=0.487. Red line represents median.

Scatter plot of parenchymal CD4+ and CD8+ T cells in grey matter
No significant difference in number of parenchymal CD4+ compared to CD8+ T cells. p=0.138 Red line represents median.

Scatter plot of perivascular CD4+ and CD8+ T cells in grey matter
The number of perivascular CD8+ T cells was significantly higher than the number of CD4+ T cells in grey matter. *p=<0.001. Red line represents median.

Figure 4.7 Scatter plot graphs of CD4+ and CD8+ T cells/100mm^2 in total, parenchymal and perivascular compartments of grey and white matter in the control group

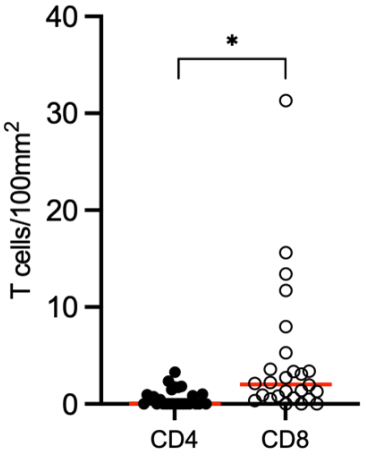

Scatter plot of total CD4+ and CD8+ T cells in white matter
The number of CD8+ T cells was significantly higher than the number of CD4+ T cells in white matter. *p=<0.001. Red line represents median.

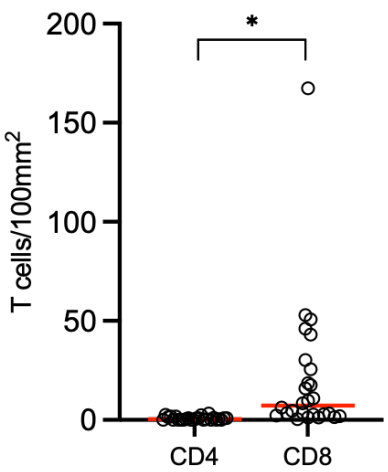

Scatter plot of parenchymal CD4+ and CD8+ T cells in white matter
The number of parenchymal CD8+ T cells was significantly higher than the number of CD4+ T cells in white matter. *p=<0.001. Red line represents median.

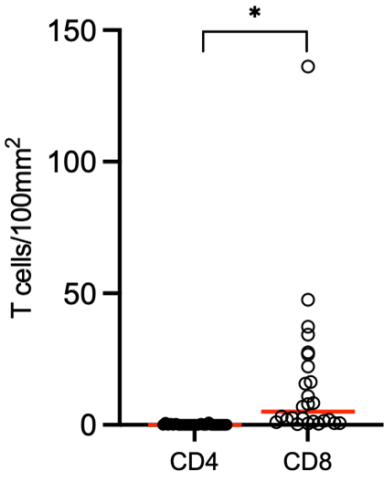

Scatter plot of perivascular CD4+ and CD8+ T cells in white matter
The number of perivascular CD8+ T cells was significantly higher than the number of CD4+ T cells in white matter. *p=<0.001. Red line represents median.

Figure 4.7 (continued) Scatter plot graphs of CD4+ and CD8+ T cells/100mm^2 in total, parenchymal and perivascular compartments of grey and white matter in the control group

4.8 Profile of CD4+ versus CD8+ T cells in DLB cases

A Mann-Whitney U test was used to test for significant differences between the number of CD4+ and CD8+ T cells/100mm^2 in total, parenchymal and perivascular compartments of grey and white matter in the DLB group. Case A304/06 was excluded from analysis due to being previously identified as an outlier. A summary of the data is presented in **Table 4.6.**

Table 4.6 CD4+ and CD8+ T cells (per 100mm^2) in DLB group (n=29)

	CD4+	CD8+	Mann-Whitney U test statistic	p value
Total T cells	1.609 (0.91-2.48)	11.199 (2.75-25.63)	168	**<0.001**
T cells in grey matter	1.615 (1.04-2.32)	3.181 (0.87-10.59)	289	**0.041**
Parenchymal T cells in grey matter	1.568 (1.01-2.07)	1.202 (0.33-5.03)	399	0.738
Perivascular T cells in grey matter	0.000 (0.00-0.44)	2.543 (0.33-5.83)	160	**<0.001**
T cells in white matter	0.834 (0.00-2.24)	17.612 (1.93-43.06)	163	**<0.001**
Parenchymal T cells in white matter	0.767 (0.00-1.51)	2.405 (0.28-11.65)	237.5	**0.004**
Perivascular T cells in white matter	0.000 (0.00-0.56)	12.244 (0.52-35.39)	131	**<0.001**

Data presented as median (IQR) based on non-parametric distribution.
*p<0.05

The number of CD8+ T cells/100mm^2 was significantly higher compared to CD4+ T cells/100mm^2 in total brain matter (CD4: median 1.609 [IQR 1.575], CD8: median 11.199 [IQR 22.875], p=<0.001), in grey matter (CD4: median 1.615 [IQR 1.274], CD8: median 3.181 [IQR 9.722], p=0.041) and in white matter (CD4: median 0.834 [IQR 2.237], CD8: median 17.612 [IQR 41.130], p=<0.001).

The number of parenchymal CD8+ T cells/100mm^2 was significantly higher than the number of parenchymal CD4+ T cells/100mm^2 in white matter (CD4: median 0.767 [IQR 1.509], CD8: median 2.405 [IQR 11.376], p=0.004). There was a significant increase in the number of perivascular CD8+ T cells/100mm^2 compared to perivascular CD4+ T cells in grey matter (CD4: median 0.000 [IQR 0.435], CD8: median 2.543 [IQR 5.496], p=<0.001) and white matter (CD4: median 0.000 [IQR 0.560], CD8: median 12.244 [IQR 34.865], p=<0.001).

No significant differences were found between the number of parenchymal CD4 and CD8+ T cells/100mm^2 in grey matter (CD4: median 1.568 [IQR 1.060], CD8: median 1.202 [IQR 4.703], p=0.738). These data are presented graphically in composite **Figure 4.8**.

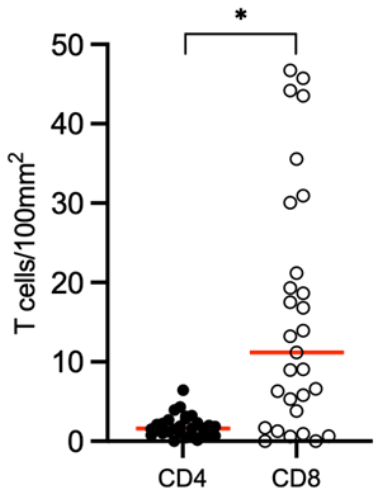

Scatter plot of total CD4+ and CD8+ cells in brain (grey and white) matter
The number of CD8+ T cells was significantly higher than the number of CD4+ T cells. *p=<0.001. Red line represents median.

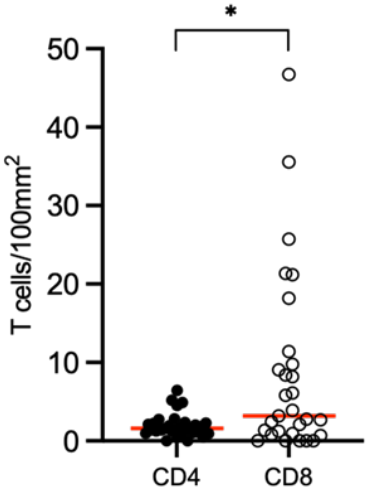

Scatter plot of total CD4+ and CD8+ cells in grey matter
The number of CD8+ T cells was significantly higher than the number of CD4+ T cells in grey matter. *p=0.041. Red line represents median.

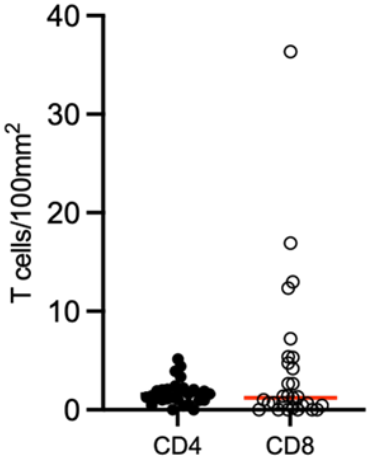

Scatter plot of parenchymal CD4+ and CD8+ T cells in grey matter
No significant difference in number of parenchymal CD4+ compared to CD8+ T cells. p=0.738 Red line represents median.

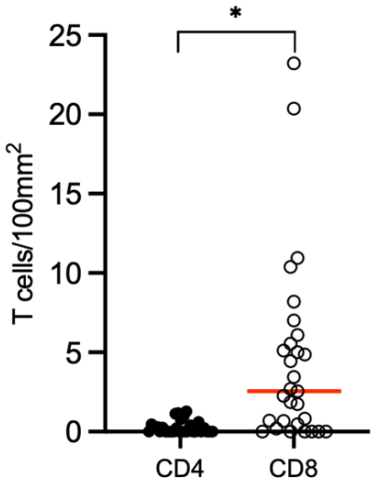

Scatter plot of perivascular CD4+ and CD8+ T cells in grey matter
The number of perivascular CD8+ T cells was significantly higher than the number of CD4+ T cells in grey matter. *p=<0.001. Red line represents median.

Figure 4.8 Scatter plot graphs of CD4+ and CD8+ T cells/100mm^2 in total, parenchymal and perivascular compartments of grey and white matter in the DLB group

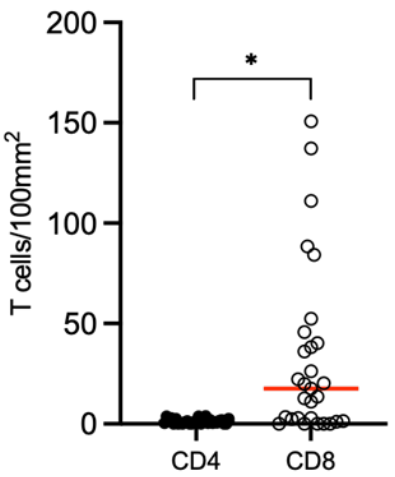

Scatter plot of total CD4+ and CD8+ T cells in white matter
The number of CD8+ T cells was significantly higher than the number of CD4+ T cells in white matter. *p=<0.001. Red line represents median.

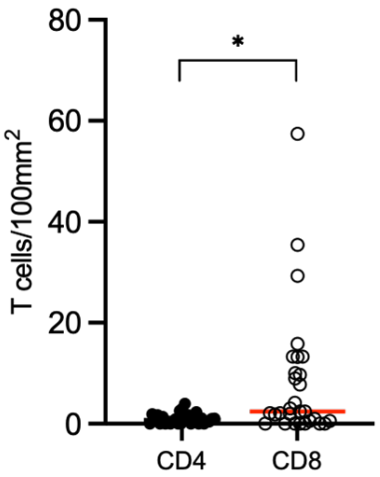

Scatter plot of parenchymal CD4+ and CD8+ T cells in white matter
The number of parenchymal CD8+ T cells was significantly higher than the number of CD4+ T cells in white matter. *p=0.004. Red line represents median.

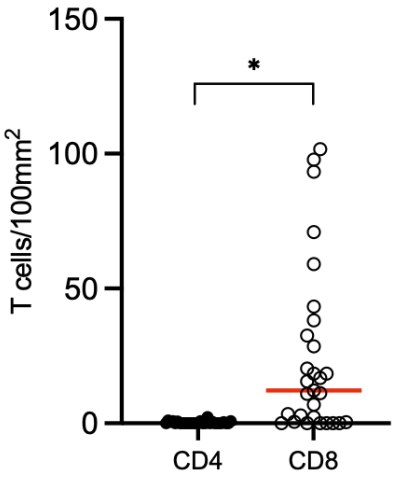

Scatter plot of perivascular CD4+ and CD8+ T cells in white matter
The number of perivascular CD8+ T cells was significantly higher than the number of CD4+ T cells in white matter. *p=<0.001. Red line represents median.

Figure 4.8 (continued) Scatter plot graphs of CD4+ and CD8+ T cells/100mm^2 in total, parenchymal and perivascular compartments of grey and white matter in the DLB group

4.9 Foxp3+ T cell data

The number of Foxp3+ T cells per 100mm^2 detected in the parenchymal and perivascular compartments of grey and white matter were assessed for differences between the DLB and control groups. Foxp3 staining was localised to the nucleus and cytoplasm. Detected T cells measured between 2-8μm in diameter. A positive control of tonsil tissue used during the Foxp3 run confirmed successful immunostaining, as shown in **Figure 4.9.**

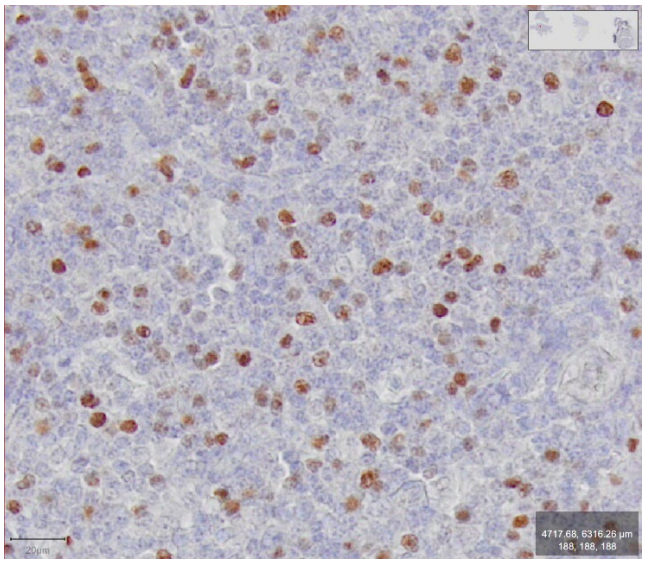

Figure 4.9 Foxp3 immunostaining in tonsil

Example digital image of Foxp3 immunostaining in section of tonsil (x20 magnification, scale bar =20μm).

Example images of Foxp3+ T cells in brain tissue acquired during T cell detection are shown in **Figure 4.10**.

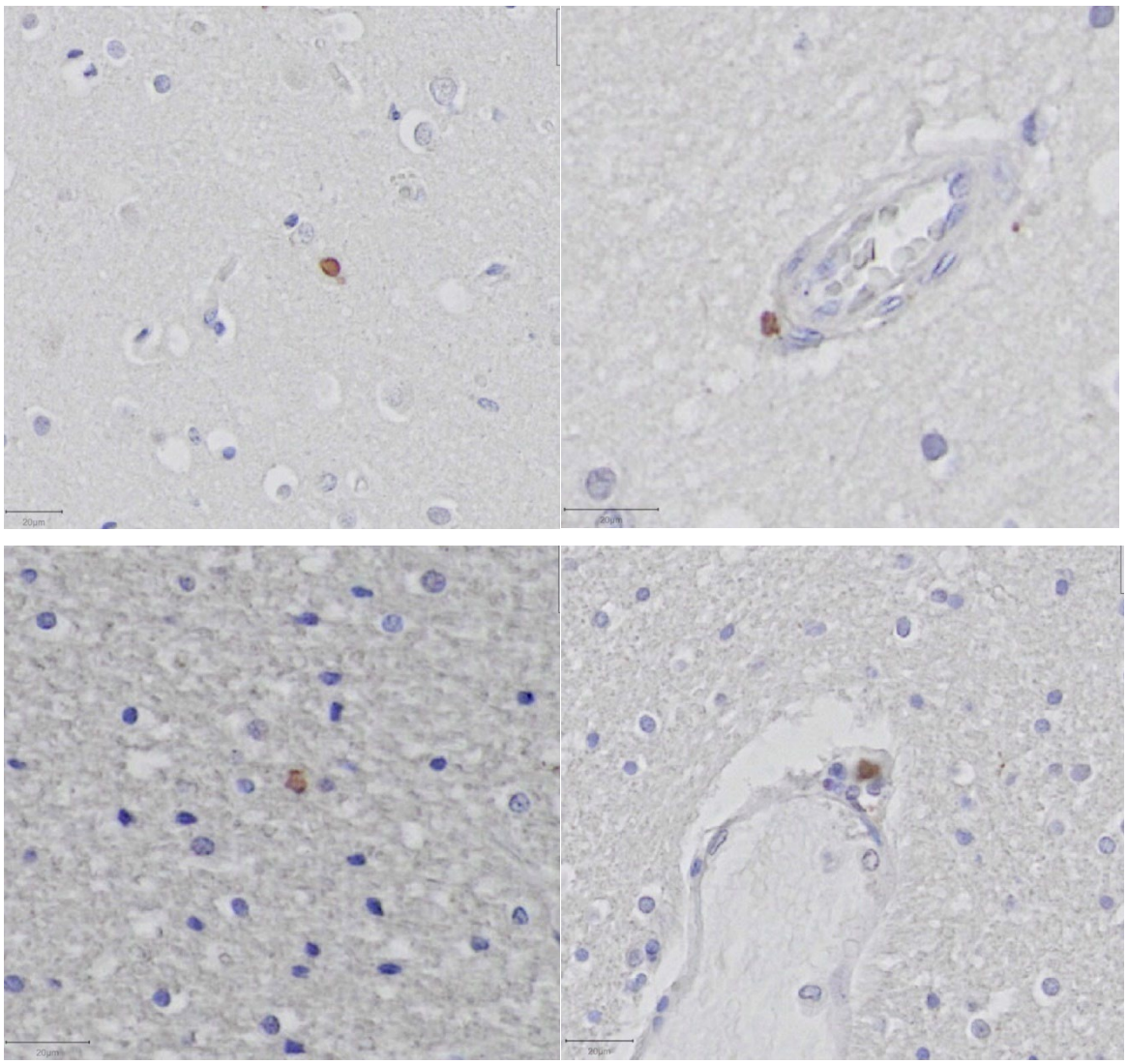

Figure 4.10 Foxp3 immunostaining in brain tissue

Example digital images of Foxp3 immunostaining. Foxp3+ T cell in the grey matter parenchyma (top left). Perivascular Foxp3+ T cell in the grey matter (top right). Foxp3+ T cell in the white matter parenchyma (bottom left). Perivascular Foxp3+ T cell in the white matter (bottom right) (x20 magnification, scale bar =20µm).

A Mann-Whitney U test was used to test for significant differences between the groups. The cases previously selected as outliers were excluded from analysis. A summary of the data is presented in **Table 4.7.**

Table 4.7 Parenchymal and perivascular Foxp3+ T cells (per 100mm^2) in grey and white matter

	Control (n=25)	DLB (n=28)	Mann-Whitney U test statistic	p value
Total Foxp3+ T cells	0.688 (0.49-1.03)	0.904 (0.52-2.56)	249	p=0.072
Foxp3+ T cells in grey matter	0.603 (0.42-0.93)	0.922 (0.45-2.21)	250	p=0.075
Parenchymal Foxp3+ T cells in grey matter	0.331 (0.00-0.82)	0.615 (0.36-1.37)	245.5	p=0.062
Perivascular Foxp3+ T cells in grey matter	0.000 (0.00-0.40)	0.207 (0.00-0.86)	302	p=0.359
Foxp3+ T cells in white matter	0.636 (0.00-1.21)	0.872 (0.01-1.65)	298.5	p=0.352
Parenchymal Foxp3+ T cells in white matter	0.000 (0.00-0.67)	0.000 (0.00-0.51)	299.5	p=0.308
Perivascular Foxp3+ T cells in white matter	0.000 (0.00-0.91)	0.544 (0.00-1.31)	262	p=0.092

Data presented as median (IQR) based on non-parametric distribution.
*p<0.05

Between DLB and control groups, there was no significant difference in the total number of Foxp3+ T cells/100mm^2, number of Foxp3+ T cells/100mm^2 in grey matter, number of parenchymal Foxp3+ T cells/100mm^2 in grey matter, number of perivascular Foxp3+ T cells/100mm^2 in grey matter, number of FoxP3+ T cells/100mm^2 in white matter, number of parenchymal Foxp3+ T cells/100mm^2 in white matter and the number of perivascular Foxp3+ T cells/100mm^2 in white matter. These data are presented graphically in composite **Figure 4.11**.

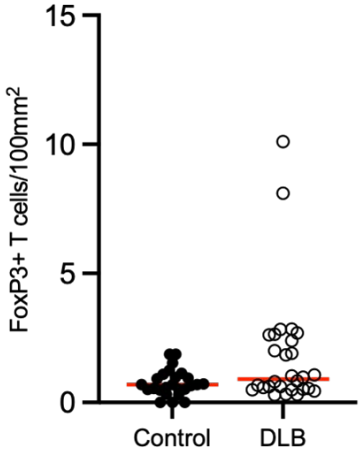

Scatter plot of total Foxp3+ T cells in brain (grey and white) matter
No significant difference in total number of Foxp3+ T cells in brain matter between control and DLB groups. p=0.072. Red line represents median.

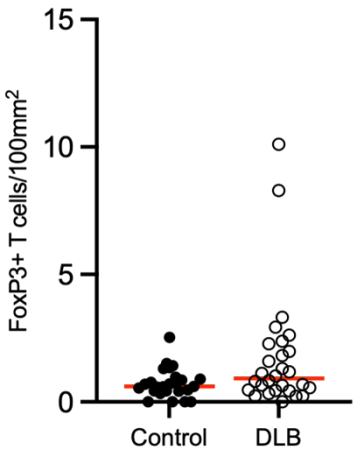

Scatter plot of total Foxp3+ T cells in grey matter
No significant difference in number of Foxp3+ T cells in grey matter between control and DLB groups. p=0.075. Red line represents median.

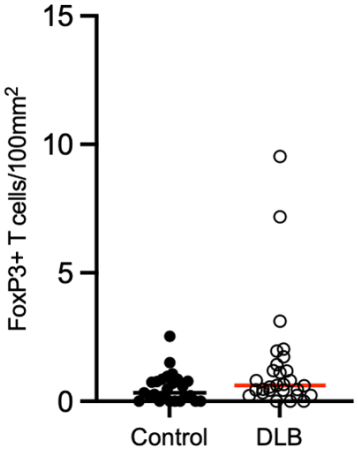

Scatter plot of parenchymal Foxp3+ T cells in grey matter
No significant difference in number of parenchymal Foxp3+ T cells in grey matter between control and DLB groups. p=0.062. Red line represents median.

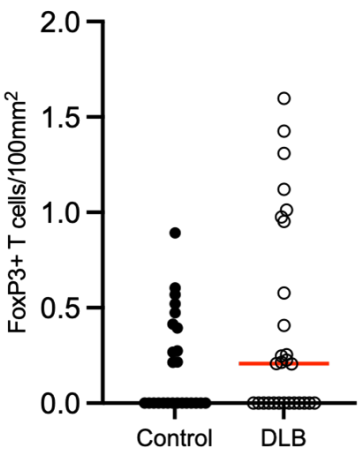

Scatter plot of perivascular Foxp3+ T cells in grey matter
No significant difference in number of perivascular Foxp3+ T cells in grey matter between control and DLB groups. p=0.359. Red line represents median.

Figure 4.11 Scatter plot graphs of total, parenchymal and perivascular Foxp3+ T cells/100mm^2 in grey and white matter

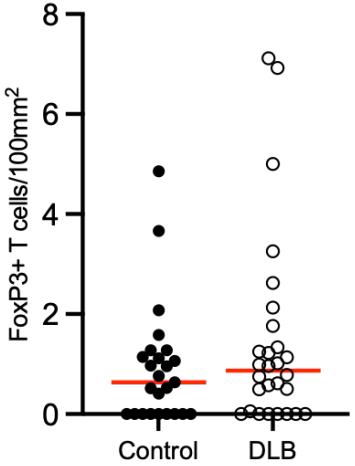

Scatter plot of total Foxp3+ T cells in white matter
No significant difference in number of Foxp3+ T cells in white matter between control and DLB groups. p=0.352. Red line represents median.

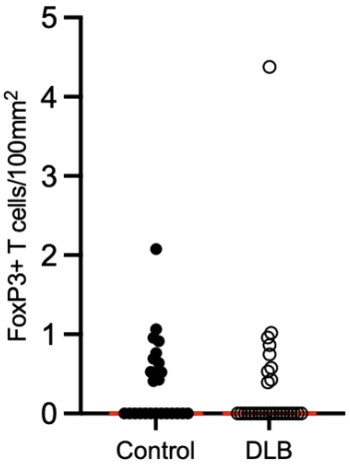

Scatter plot of parenchymal Foxp3+ T cells in white matter
No significant difference in number of parenchymal Foxp3+ T cells in white matter between control and DLB groups. p=0.308. Red line represents median.

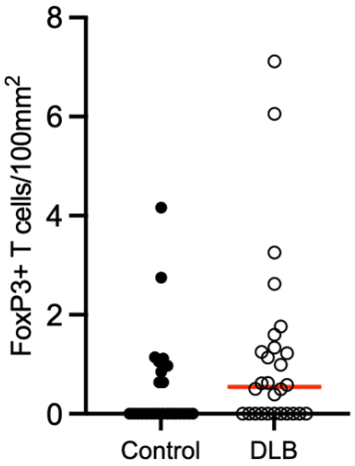

Scatter plot of perivascular Foxp3+ T cells in white matter
No significant difference in number of perivascular CD8+ T cells in white matter between control and DLB groups. p=0.092. Red line represents median.

Figure 4.11 (continued) **Scatter plot graphs of total, parenchymal and perivascular Foxp3+ T cells/100mm^2 in grey and white matter**

4.10 Tbet+ T cell data

The number of Tbet+ T cells per 100mm^2 detected in the parenchymal and perivascular compartments of grey and white matter were assessed for differences between the DLB and control groups. Tbet staining was predominantly localised to the cytoplasm. Detected T cells measured between 3-8μm in diameter. A positive control of tonsil tissue was used to confirm successful immunostaining, as shown in **Figure 4.12**.

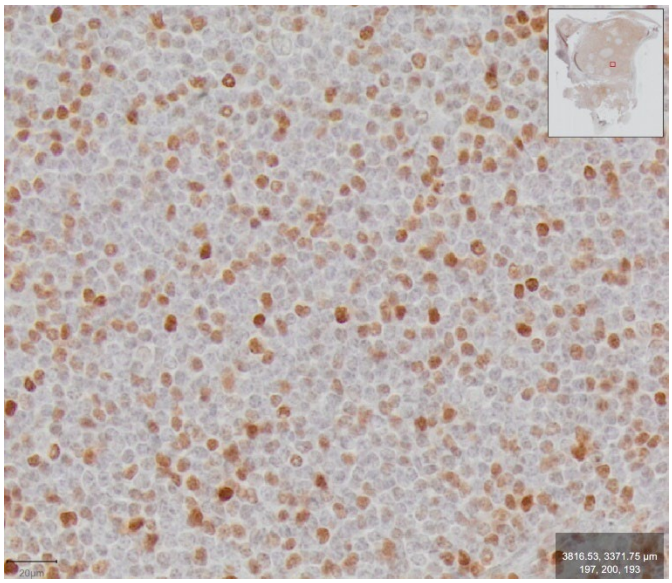

Figure 4.12 Tbet immunostaining in tonsil

Example digital image of Tbet immunostaining in section of tonsil (x20 magnification, scale bar =20μm).

Example images of Tbet+ T cells acquired during T cell detection are shown in **Figure 4.13**.

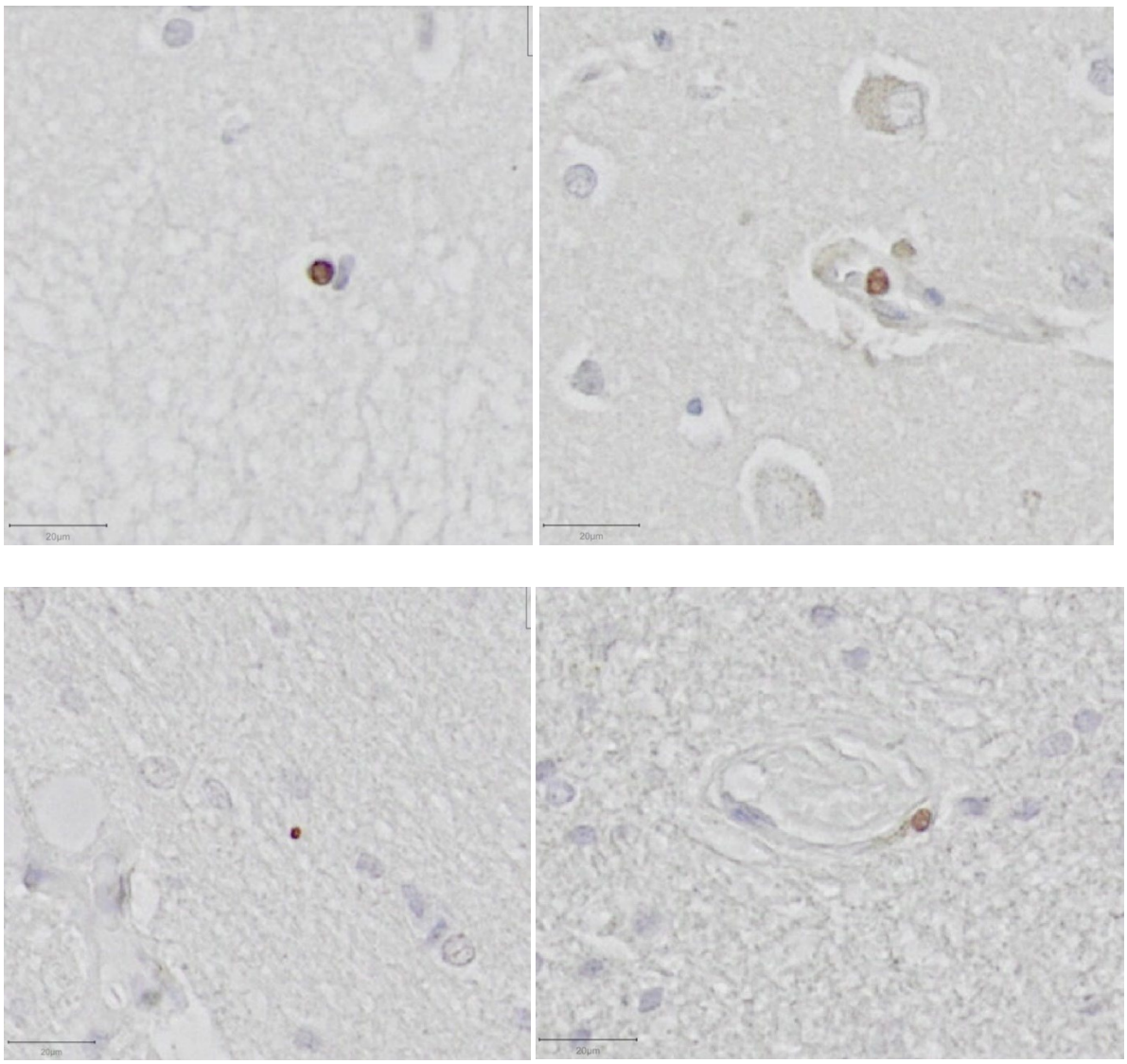

Figure 4.13 Tbet immunostaining in brain tissue
Example digital images of Tbet immunostaining. Tbet+ T cell in the grey matter parenchyma (top left). Perivascular Tbet+ T cell in the grey matter (top right). Tbet+ T cell in the white matter parenchyma (bottom left). Perivascular Tbet+ T cell in the white matter (bottom right) (x20 magnification, scale bar =20µm).

A Mann-Whitney U test was used to test for significant differences between the groups. The cases previously identified as outliers were excluded from analysis. A summary of the data is presented in **Table 4.8.**

Table 4.8 Parenchymal and perivascular Tbet+ T cells (per 100mm^2) in grey and white matter

	Control (n=23)	DLB (n=26)	Mann-Whitney U test statistic	p value
Total Tbet+ T cells	2.767 (0.89-4.00)	3.974 (1.62-14.31)	200.5	**p=0.048***
Tbet+ T cells in grey matter	1.713 (0.51-2.95)	1.814 (0.90-10.35)	221.5	p=0.120
Parenchymal Tbet+ T cells in grey matter	1.105 (0.32-2.78)	1.462 (0.85-8.64)	200.5	**p=0.048***
Perivascular Tbet+ T cells in grey matter	0.249 (0.00-0.75)	0.444 (0.00-1.94)	272.5	p=0.584
Tbet+ T cells in white matter	4.608 (1.85-7.92)	7.019 (1.51-20.14)	254	p=0.367
Parenchymal Tbet+ T cells in white matter	1.896 (1.18-5.03)	4.090 (1.20-16.48)	235.5	p=0.202
Perivascular Tbet+ T cells in white matter	1.437 (0.38-4.03)	1.235 (0.00-5.87)	289.5	p=0.848

Data presented as median (IQR) based on non-parametric distribution.
*p<0.05

There was a significant increase in the total number of Tbet+ T cells/100mm^2 in the DLB group compared to the control group (DLB: median 3.974 [IQR 12.690], Control: median 2.767 [IQR 3.119], p=0.048). The number of parenchymal Tbet+ T cells in grey matter/100mm^2 was significantly higher in the DLB group compared to the control group (DLB: median 1.814 [IQR 9.457], Control: median 1.713 [IQR 2.449], p=0.048).

Between DLB and control groups, there was no significant difference in the number of Tbet+ T cells/100mm^2 in grey matter, number of perivascular Tbet+ T cells/100mm^2 in grey matter, number of Tbet+ T cells/100mm^2 in white matter, number of parenchymal Tbet+ T cells/100mm^2 in white matter and the number of perivascular Tbet+ T cells/100mm^2 in white matter. These data are presented graphically in composite **Figure 4.14**.

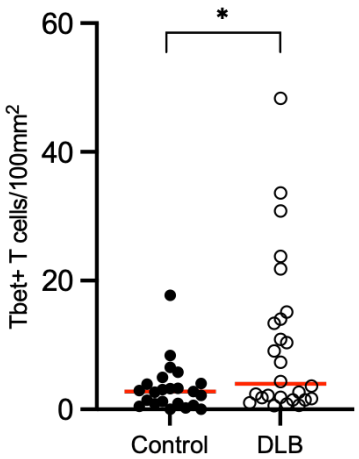

Scatter plot of total Tbet+ T cells in brain (grey and white) matter
The total number of Tbet+ T cells in brain matter was significantly higher in DLB compared to controls. *p=0.048. Red line represents median.

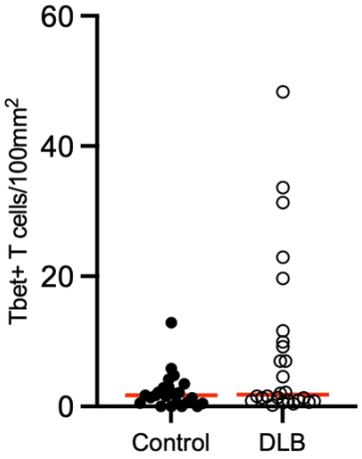

Scatter plot of total Tbet+ T cells in grey matter
No significant difference in number of Tbet+ T cells in grey matter between control and DLB groups. p=0.120. Red line represents median.

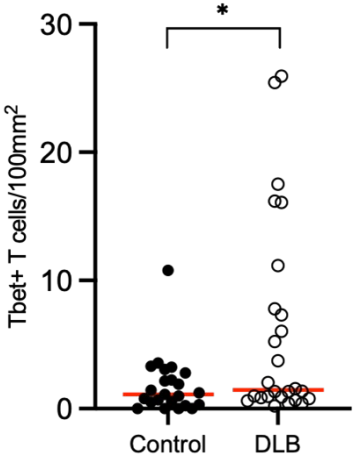

Scatter plot of parenchymal Tbet+ T cells in grey matter
The number of parenchymal Tbet+ T cells in grey matter was significantly higher in DLB compared to controls. p=*0.048. Red line represents median.

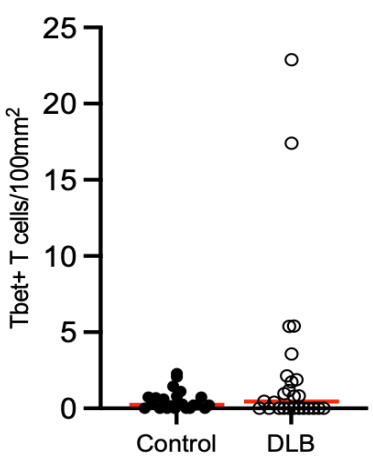

Scatter plot of perivascular Tbet+ T cells in grey matter
No significant difference in number of perivascular Tbet+ T cells in grey matter between control and DLB groups. p=0.584. Red line represents median.

Figure 4.14 Scatter plot graphs of total, parenchymal and perivascular Tbet+ T cells/100mm^2 in grey and white matter

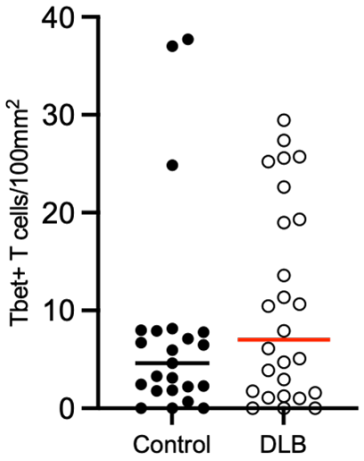

Scatter plot of total Tbet+ T cells in white matter
No significant difference in number of Tbet+ T cells in white matter between control and DLB groups. p=0.367. Red line represents median.

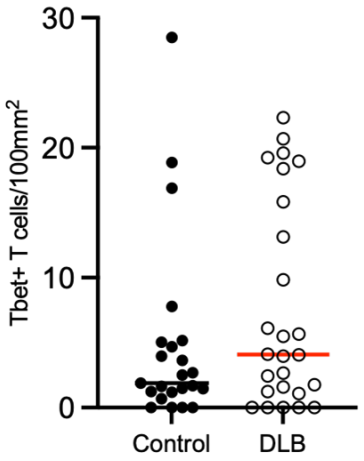

Scatter plot of parenchymal Tbet+ T cells in white matter
No significant difference in number of parenchymal Tbet+ T cells in white matter between control and DLB groups. p=0.202. Red line represents median.

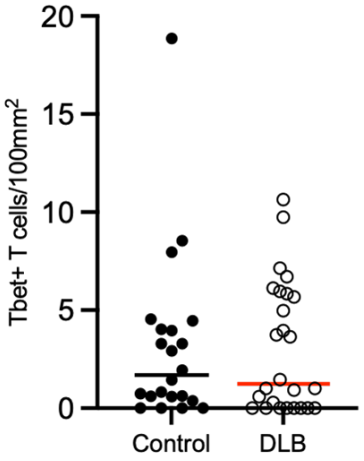

Scatter plot of perivascular Tbet+ T cells in white matter
No significant difference in number of perivascular Tbet+ T cells in white matter between control and DLB groups. p=0.848. Red line represents median.

Figure 4.14 (continued) **Scatter plot graphs of total, parenchymal and perivascular Tbet+ T cells/100mm^2 in grey and white matter**

4.11 GATA3+ T cell data

The number of GATA3+ T cells per 100mm^2 detected in the parenchymal and perivascular compartments of grey and white matter were assessed for differences between the DLB and control groups. T cells measured between 3-8μm in diameter and staining was localised to the cytoplasm. A positive control of tonsil tissue used during the GATA3+ run confirmed successful immunostaining, as shown in **Figure 4.15**.

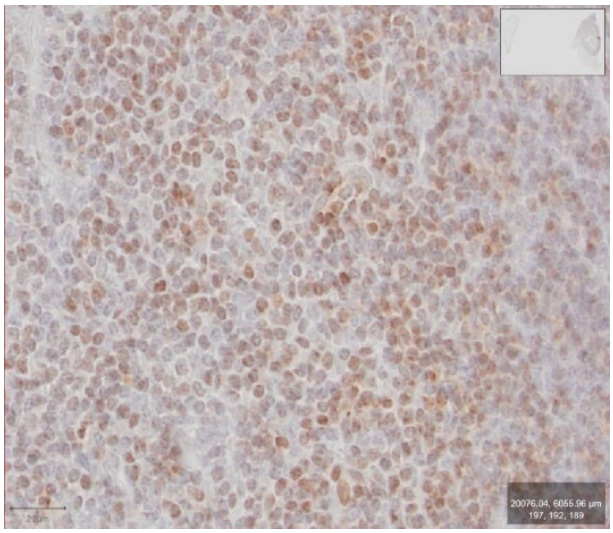

Figure 4.15 GATA3 immunostaining in tonsil

Example digital image of GATA3 immunostaining in section of tonsil (x20 magnification, scale bar =20μm).

Example images of GATA3+ T cells acquired during T cell detection are shown in **Figure 4.16**.

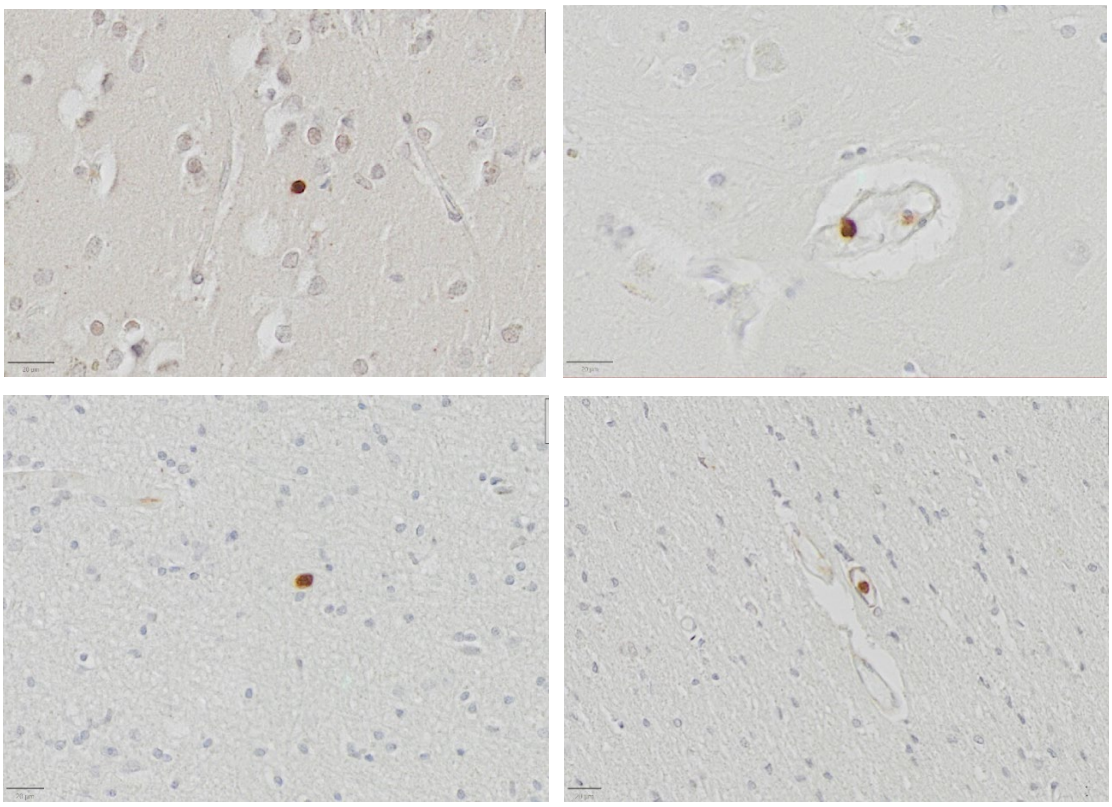

Figure 4.16 GATA3 immunostaining in brain tissue

Example digital images of GATA3 immunostaining. GATA3+ T cell in the grey matter parenchyma (top left). Perivascular GATA3+ T cell in the grey matter (top right). GATA3+ T cell in the white matter parenchyma (bottom left). Perivascular GATA3+ T cell in the white matter (bottom right) (x20 magnification, scale bar =20µm).

A Mann-Whitney U test was used to test for significant differences between the groups. The cases previously selected as outliers were excluded from analysis. A summary of the data is presented in **Table 4.9.**

Table 4.9 Parenchymal and perivascular GATA3+ T cells (per 100mm^2) in grey and white matter

	Control (n=20)	DLB (n=22)	Mann-Whitney U test statistic	p value
Total GATA3+ T cells	0.038 (0.004-0.098)	0.112 (0.041-0.303)	125	**p=0.017***
GATA3+ T cells in grey matter	0.016 (0.003-0.067)	0.133 (0.040-0.236)	108	**p=0.005***
Parenchymal GATA3+ T cells in grey matter	0.013 (0.000-0.057)	0.080 (0.022-0.193)	116	**p=0.009***
Perivascular GATA3+ T cells in grey matter	0.004 (0.000-0.022)	0.032 (0.013-0.053)	97	**p=0.002***
GATA3+ T cells in white matter	0.020 (0.000-0.101)	0.085 (0.008-0.233)	161	p=0.134
Parenchymal GATA3+ T cells in white matter	0.018 (0.000-0.059)	0.057 (0.003-0.195)	162	p=0.138
Perivascular GATA3+ T cells in white matter	0.006 (0.000-0.036)	0.032 (0.000-0.053)	161	p=0.128

Data presented as median (IQR) based on non-parametric distribution.
*p<0.05

There was a significant increase in the total number of GATA3+ T cells/100mm^2 in the DLB group compared to the control group (DLB: median 0.112 [IQR 0.262], Control: median 0.038 [IQR 0.094], p=0.017). The number of GATA3+ T cells in grey matter/100mm^2 was significantly higher in DLB cases compared to control cases (DLB: median 0.133 [IQR 0.196], Control: median 0.016 [IQR 0.064], p=0.005). This significant difference was found in both the parenchymal compartment (DLB: median 0.080 [IQR 0.171], Control: median 0.013 [IQR 0.057], p=0.009) and perivascular compartment (DLB: median 0.032 [IQR 0.040], Control: median 0.004 [IQR 0.022], p=0.002) of grey matter.

Between DLB and control groups, there was no significant difference in the number of GATA3+ T cells/100mm^2 in white matter, number of parenchymal GATA3+ T cells/100mm^2 in white matter and the number of perivascular GATA3+ T cells/100mm^2 in white matter. These data are presented graphically in composite **Figure 4.17**.

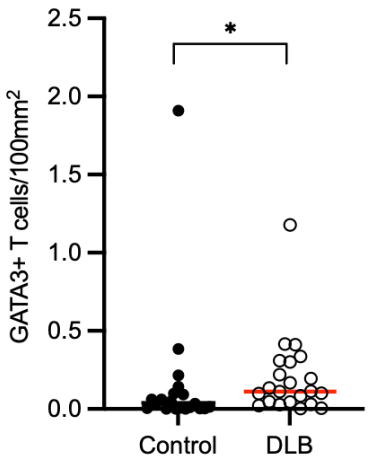

Scatter plot of total GATA3+ T cells in brain (grey and white) matter
The total number of GATA3+ T cells in brain matter was significantly higher in DLB compared to controls. *p=0.017.
Red line represents median.

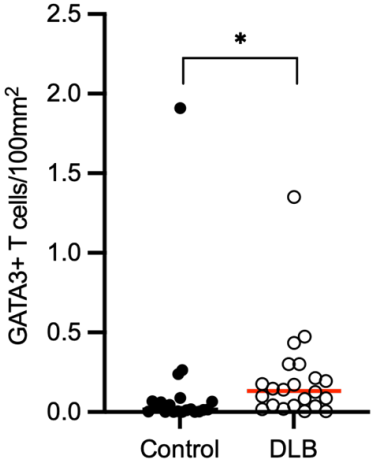

Scatter plot of total Tbet+ T cells in grey matter
The number of GATA3+ T cells in grey matter was significantly higher in DLB compared to controls. *p=0.005.
Red line represents median.

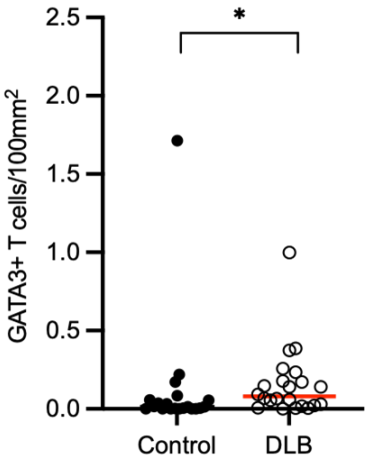

Scatter plot of parenchymal GATA3+ T cells in grey matter
The number of parenchymal GATA3+ T cells in grey matter was significantly higher in DLB compared to controls. *p=0.009.
Red line represents median.

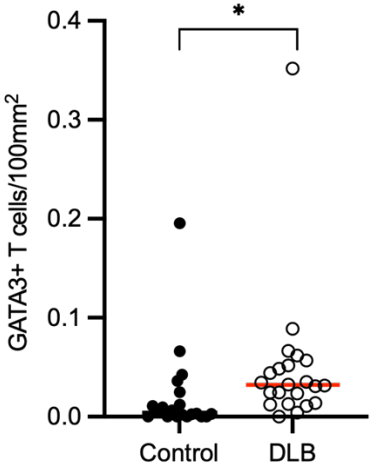

Scatter plot of perivascular GATA3+ T cells in grey matter
The number of perivascular GATA3+ T cells in grey matter was significantly higher in DLB compared to controls. *p=0.002.
Red line represents median.

Figure 4.17 Scatter plot graphs of total, parenchymal and perivascular GATA3+ T cells/100mm^2 in grey and white matter

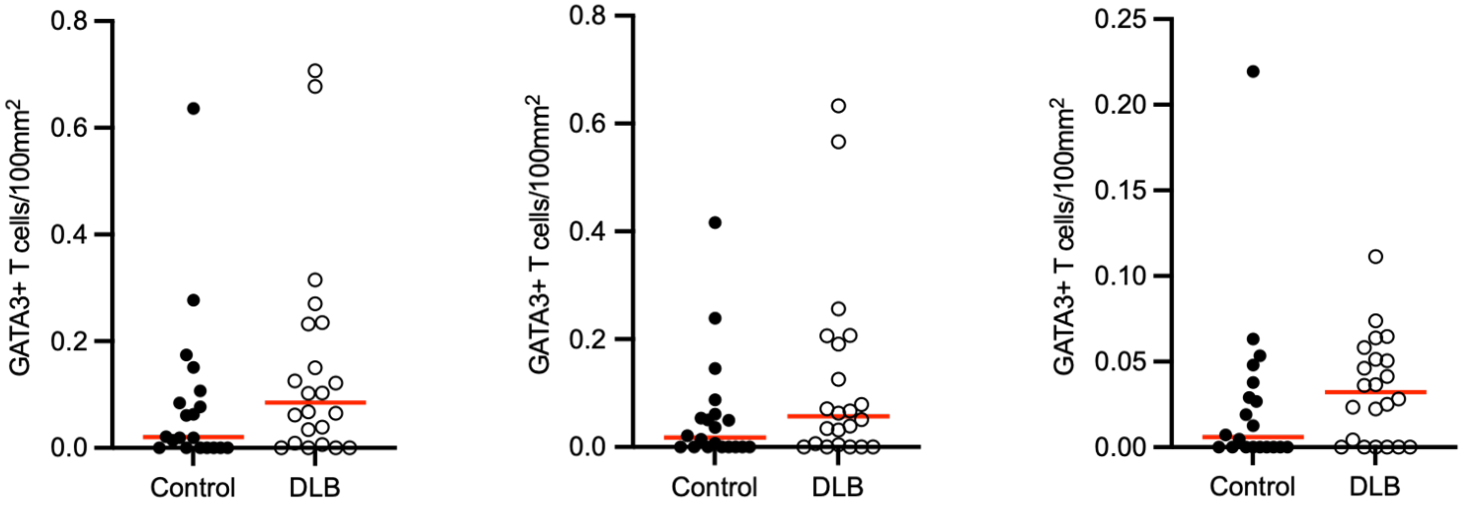

Scatter plot of total GATA3+ T cells in white matter
No significant difference in number of GATA3+ T cells in white matter between control and DLB groups. p=0.134. Red line represents median.

Scatter plot of parenchymal GATA3+ T cells in white matter
No significant difference in number of parenchymal GATA3+ T cells in white matter between control and DLB groups. p=0138. Red line represents median.

Scatter plot of perivascular GATA3+ T cells in white matter
No significant difference in number of perivascular GATA3+ T cells in white matter between control and DLB groups. p=0.128. Red line represents median.

Figure 4.17 (continued) **Scatter plot graphs of total, parenchymal and perivascular GATA3+ T cells/100mm^2 in grey and white matter**

4.12 Profile of T cell markers

The number of CD4+, CD8+, Foxp3+, Tbet+ and GATA3+ T cells/100mm^2 present in each defined location (total brain matter, grey matter, white matter, parenchymal and perivascular compartments of grey and white matter) for DLB and control groups are presented graphically in **Figure 4.18 – Figure 4.24**. This allows the relative comparison of examined T cell subsets present in control and DLB brain matter.

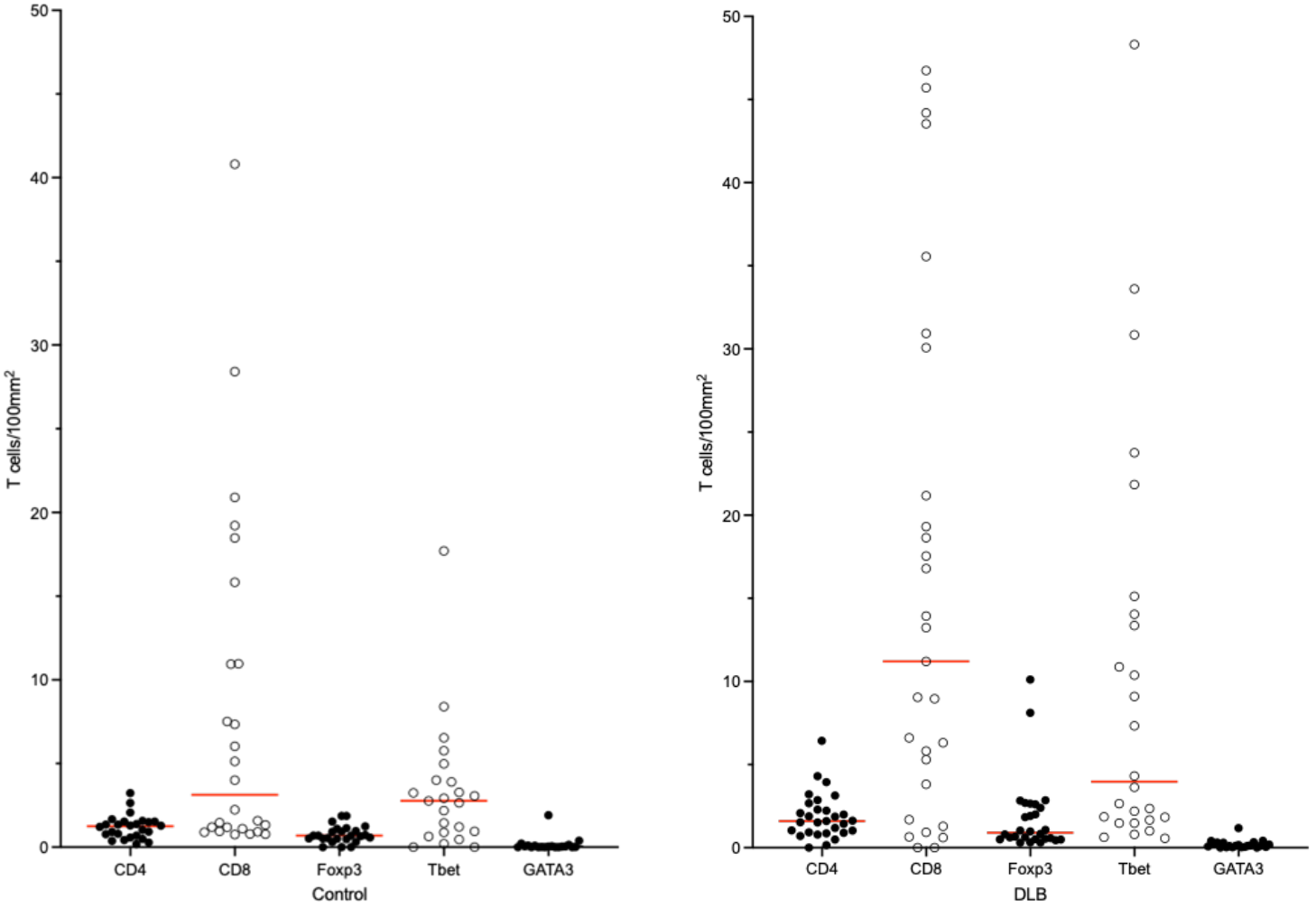

Figure 4.18 Scatter plot graphs of T cell subsets/100mm² in total brain matter (grey and white matter) in control and DLB groups

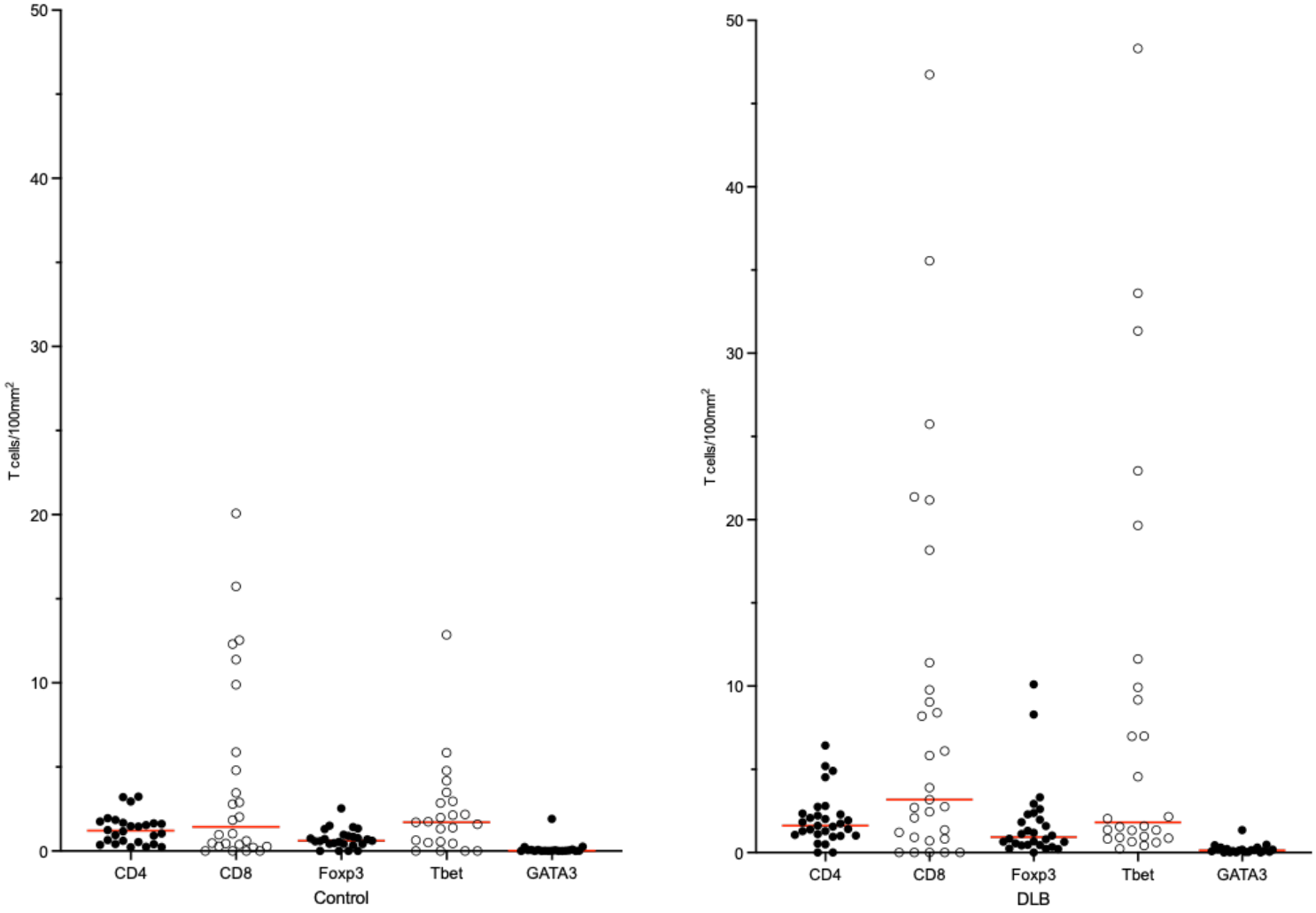

Figure 4.19 Scatter plot graphs of T cell subsets/100mm² in grey matter in control and DLB groups

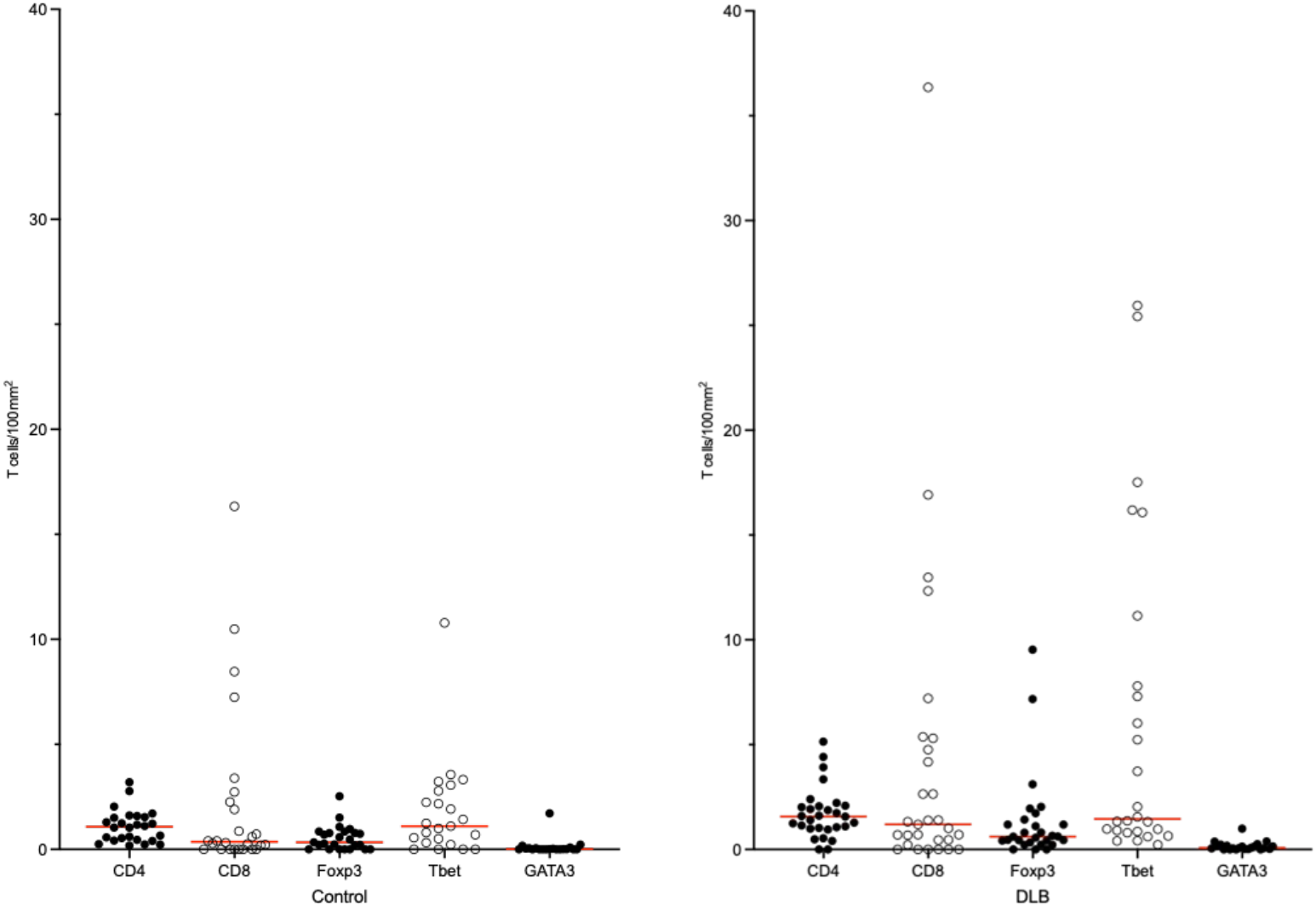

Figure 4.20 Scatter plot graphs of T cell subsets/100mm^2 in parenchymal compartment of grey matter in control and DLB groups

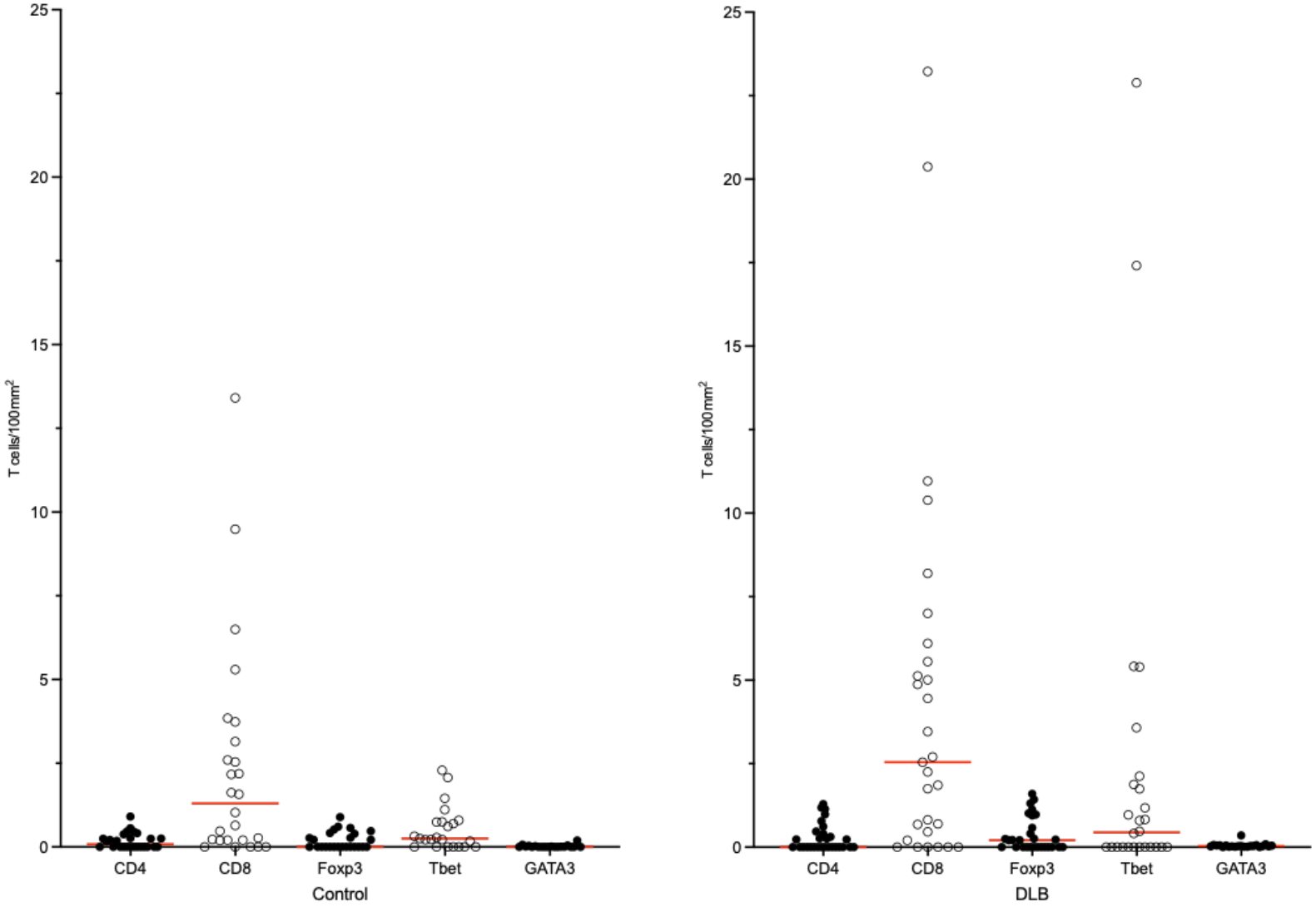

Figure 4.21 Scatter plot graphs of T cell subsets/100mm² in perivascular compartment of grey matter in control and DLB groups

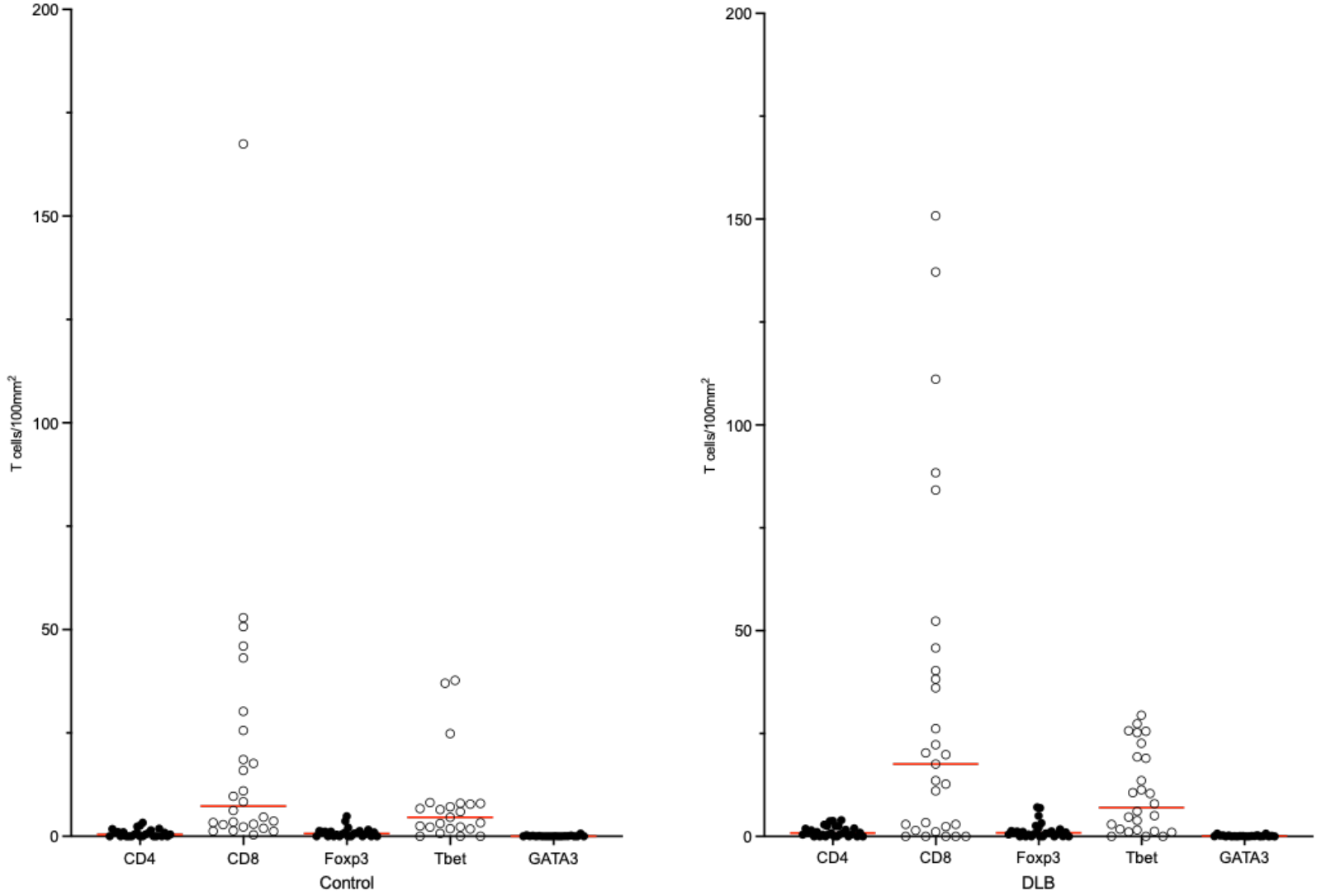

Figure 4.22 Scatter plot graphs of T cell subsets/100mm² in white matter in control and DLB groups

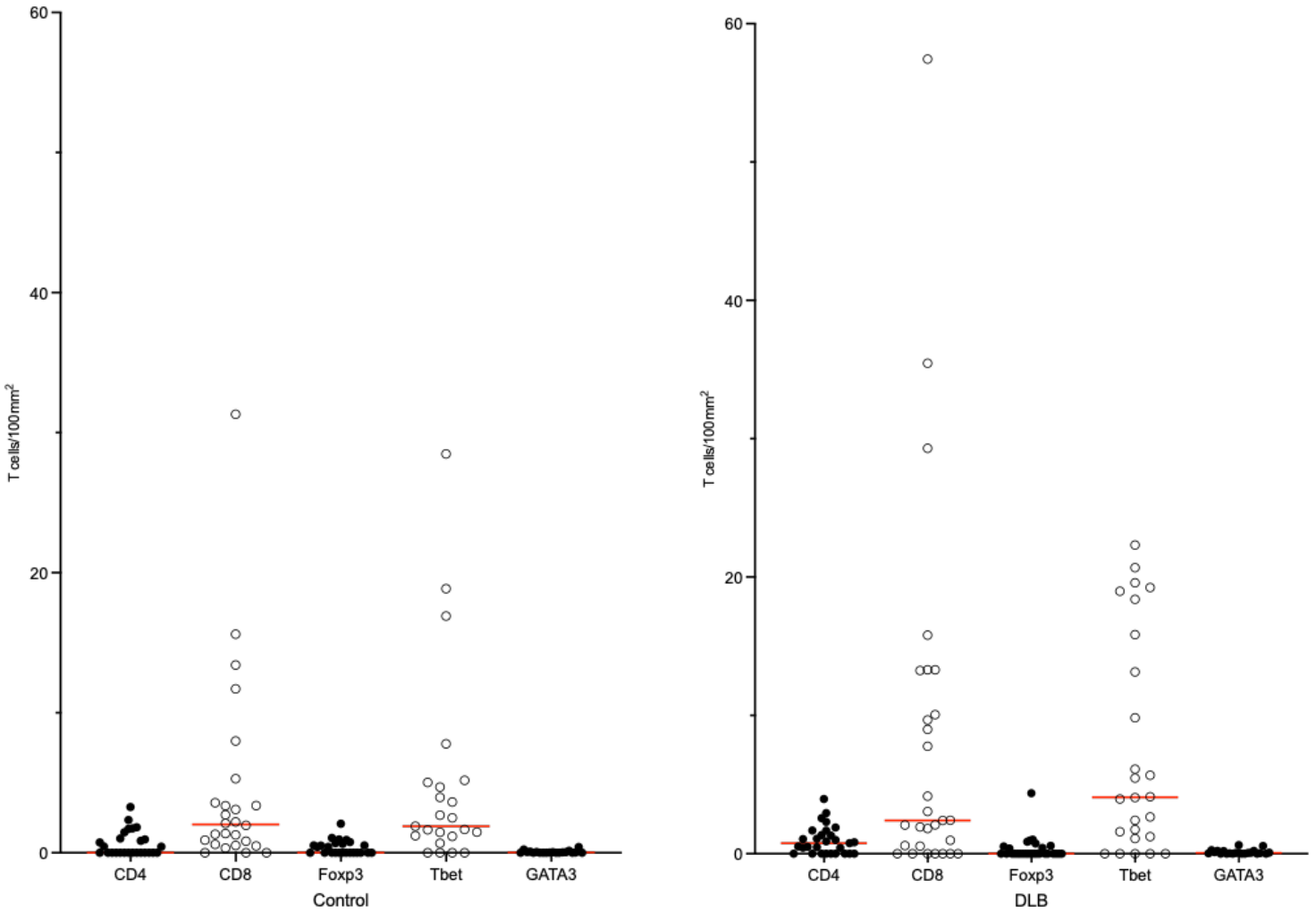

Figure 4.23 **Scatter plot graphs of T cell subsets/100mm^2 in parenchymal compartment of white matter in control and DLB groupsk**

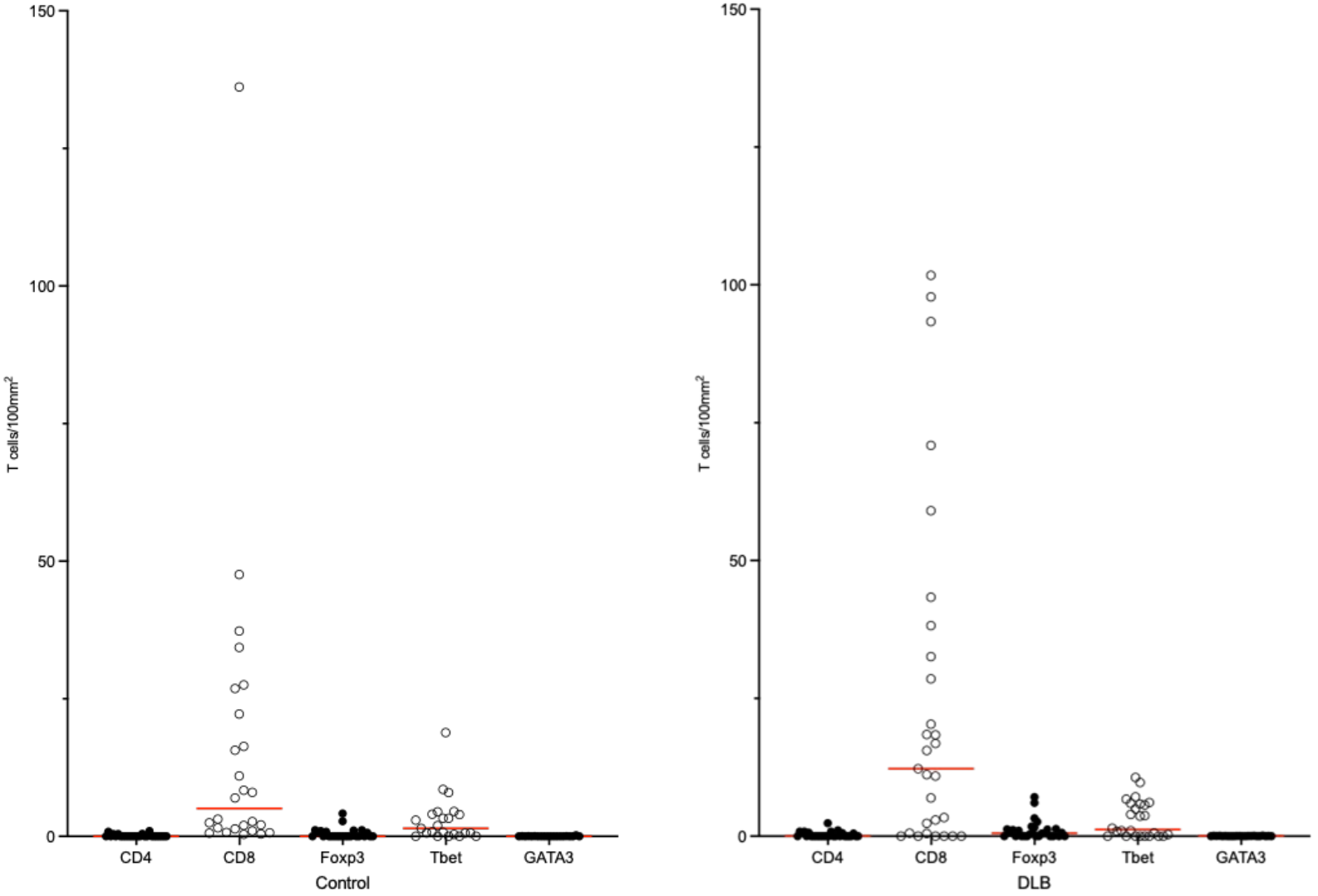

Figure 4.24 **Scatter plot graphs of T cell subsets/100mm² in perivascular compartment of white matter in control and DLB groups**

4.13 T cell ratios

T cell ratios for CD8:CD4 and Tbet:GATA3 in total brain matter and grey matter parenchyma were calculated for control and DLB cases. A Mann-Whitney U test was used to test for significant differences between the groups. The cases previously selected as outliers were excluded from analysis. A summary of the data is presented in in **Table 4.10**.

Table 4.10 CD8:CD4 and Tbet:GATA3 T cell ratios in total brain matter and grey matter parenchyma

	Control (26)	DLB (29)	Mann-Whitney U test statistic	p value
CD8:CD4 ratio in total brain matter	4.985 (0.748-12.820)	5.060 (2.220-17.180)	354	p=0.698
CD8:CD4 ratio in grey matter parenchyma	0.395 (0.000-3.503)	0.630 (0.100-2.155)	343	p=0.563
Tbet:GATA3 ratio in total brain matter	9.460 (0.000-79.180)	32.050 (11.723-109.608)	140	p=0.071
Tbet:GATA3 ratio in grey matter parenchyma	0.190 (0.000-41.110)	21.520 (5.893-143.535)	125	**p=0.028***

Data presented as median (IQR) based on non-parametric distribution.
*p<0.05

There was a significant increase in the ratio of Tbet:GATA3 cells in grey matter parenchyma in the DLB group compared to the control group (DLB: median 21.520 [IQR 137.642], Control: median 0.190 [IQR 41.110], p=0.028).

Between DLB and control groups, there was no significant difference in the ratio of CD8:CD4 T cells in total brain matter or grey matter parenchyma. There was no significant difference in the ratio of Tbet:GATA3 T cells in total brain matter between groups.

4.14 CXCL12 and CXCR4 markers

Post-mortem brain tissue sections from a sample of 8 DLB cases were immunostained for CXCL12 and CXCR4. Images were reviewed to observe the quality and localisation of positive staining. Staining for CXCL12 was localised to the meninges with minimal staining in the majority of cases. A positive control of breast tumour tissue was used in the run to confirm successful experiments. Example images of immunostaining for CXCL12 are shown in **Figure 4.25**.

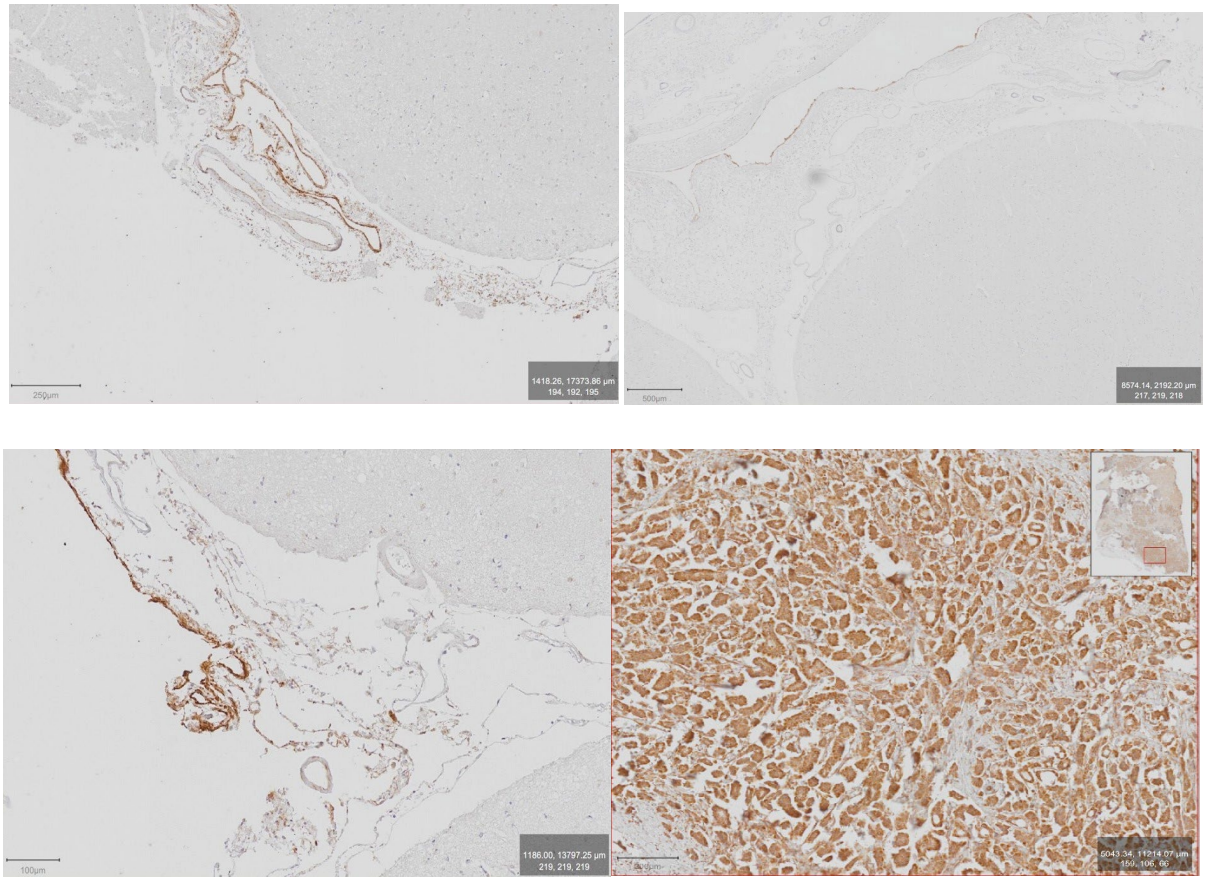

Figure 4.25 CXCL12 immunostaining

Example digital images showing CXCL12 immunostaining in the grey matter (x20 magnification, scale bar: top left =250µm, top right =500µm, bottom left =100µm). CXCL12 immunostaining in breast tumour tissue (bottom right) (x20 magnification, scale bar =20µm).

Immunostaining for CXCR4 revealed localisation of staining throughout the grey matter that appeared to be non-specific to any cell type. This presented difficulty in determining expression of this marker by T cells. Example images of brain tissue immunostained for CXCR4 and a positive control of tonsil are provided in **Figure 4.26**. Due to minimal positive staining for CXCL12 isolated to the meninges and non-specific staining for CXCR4, no further analysis was conducted using these markers.

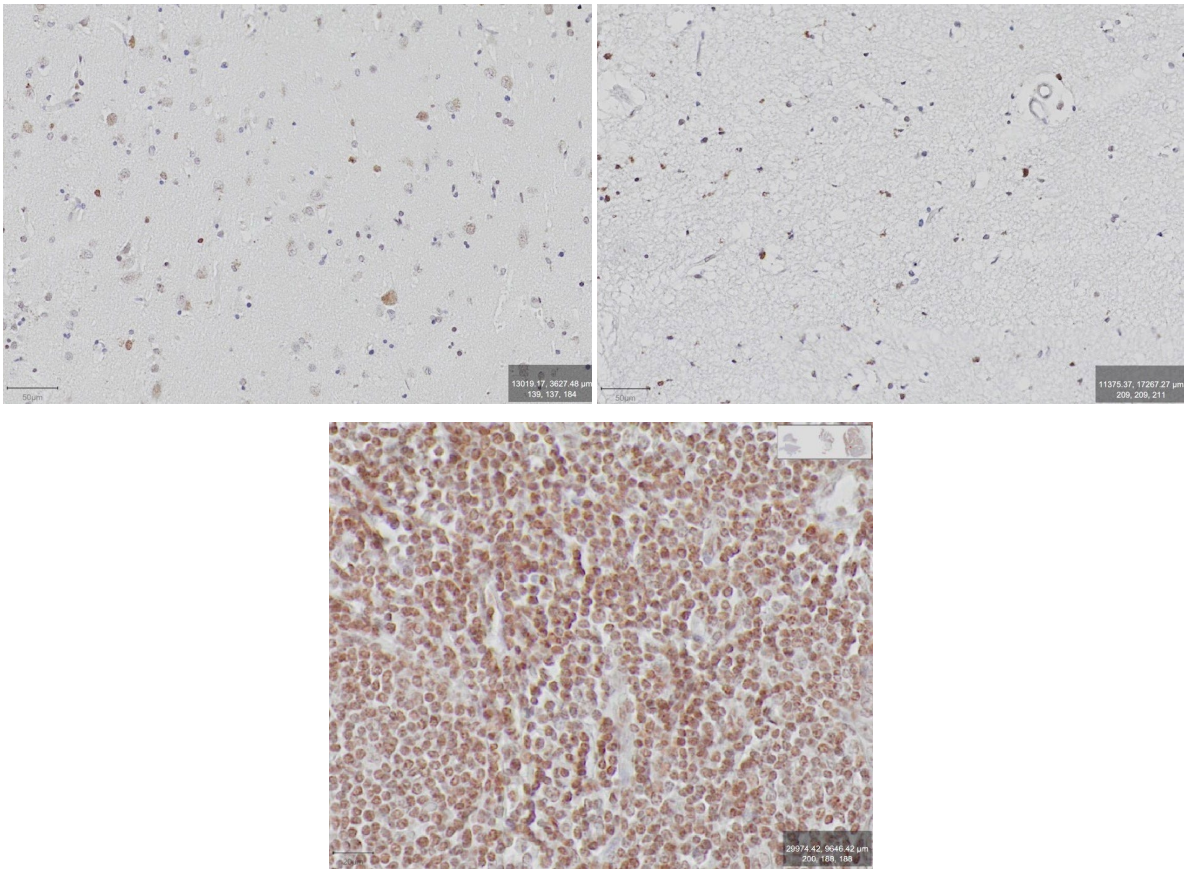

Figure 4.26 CXCR4 immunostaining
Example digital images showing CXCR4 immunostaining in the grey matter (top left and top right) (x20 magnification, scale bar =50μm) and in tonsil (bottom) (x20 magnification, scale bar =20μm).

4.15 Correlation between T cells and neuropathological markers

Neuropathological markers had already been quantified as part of a previous study using the same cohort of cases and included α-syn, ptau and Aβ (95). The number of T cells/100mm^2 in the parenchymal and perivascular compartments of grey and white matter, and markers of neuropathology, were assessed for correlation. Spearman's rank correlations were used for each T cell subset (CD4+, CD8+, Foxp3+, Tbet+ and GATA3+), with P values of less than 0.002 deemed significant to account for 21 multiple correlations. The P value was adjusted using the Bonferroni correction, resulting in a family wise error rate of 0.05 (5% chance of a Type 1 error). Control cases 803, 894, 943 and DLB case A304/06 were excluded from analysis due to being previously identified as outliers not meeting inclusion criteria.

4.15.1 Correlation between CD4+ T cells and markers of neuropathology

There were no significant correlations found between CD4+ T cells and neuropathological markers in the control or DLB group. Correlation tables for the control and DLB groups are presented in **Table 4.11** and **Table 4.12,** respectively.

Table 4.11 Correlations for CD4+ T cells and neuropathological markers in control group (n=26)

T cells/100mm²		Aβ	Ptau
Total CD4+ T cells	Correlation coefficient	-0.177	0.048
	Sig. (2-tailed)	0.386	0.816
CD4+ T cells in grey matter	Correlation coefficient	-0.142	-0.023
	Sig. (2-tailed)	0.489	0.910
Parenchymal CD4+ T cells in grey matter	Correlation coefficient	0.002	0.012
	Sig. (2-tailed)	0.993	0.952
Perivascular CD4+ T cells in grey matter	Correlation coefficient	-0.338	-0.093
	Sig. (2-tailed)	0.091	0.652
CD4+ T cells in white matter	Correlation coefficient	-0.092	0.049
	Sig. (2-tailed)	0.655	0.810
Parenchymal CD4+ T cells in white matter	Correlation coefficient	-0.107	0.052
	Sig. (2-tailed)	0.604	0.800
Perivascular CD4+ T cells in white matter	Correlation coefficient	-0.057	0.029
	Sig. (2-tailed)	0.782	0.889

Data presented as Spearman's rank correlation coefficient, *p<0.05, **p<0.002

Table 4.12 Correlations for CD4+ T cells and neuropathological markers in DLB group (n=29)

T cells/100mm²		α-syn	Aβ	Ptau
Total CD4+ T cells	Correlation coefficient	-0.022	-0.240	0.051
	Sig. (2-tailed)	0.911	0.210	0.795
CD4+ T cells in grey matter	Correlation coefficient	-0.055	-0.202	0.082
	Sig. (2-tailed)	0.778	0.293	0.677
Parenchymal CD4+ T cells in grey matter	Correlation coefficient	-0.122	-0.255	0.123
	Sig. (2-tailed)	0.530	0.182	0.534
Perivascular CD4+ T cells in grey matter	Correlation coefficient	0.057	-0.105	-0.199
	Sig. (2-tailed)	0.771	0.589	0.310
CD4+ T cells in white matter	Correlation coefficient	0.146	0.145	0.120
	Sig. (2-tailed)	0.450	0.453	0.544
Parenchymal CD4+ T cells in white matter	Correlation coefficient	0.037	0.089	0.077
	Sig. (2-tailed)	0.850	0.646	0.697
Perivascular CD4+ T cells in white matter	Correlation coefficient	0.341	0.047	0.271
	Sig. (2-tailed)	0.071	0.810	0.163

Data presented as Spearman's rank correlation coefficient, *p<0.05, **p<0.002

4.15.2 Correlation between CD8+ T cells and markers of neuropathology

No significant correlations were found between CD8+ T cells and markers of neuropathology in the control or DLB group. Correlation tables for the control group and DLB group are presented in **Table 4.13** and **Table 4.14**, respectively.

Table 4.13 Correlations for CD8+ T cells and neuropathological markers in control group (n=26)

T cells/100mm^2		Aβ	Ptau
Total CD8+ T cells	Correlation coefficient	-0.154	-0.178
	Sig. (2-tailed)	0.452	0.384
CD8+ T cells in grey matter	Correlation coefficient	-0.187	-0.052
	Sig. (2-tailed)	0.360	0.799
Parenchymal CD8+ T cells in grey matter	Correlation coefficient	-0.281	-0.051
	Sig. (2-tailed)	0.165	0.805
Perivascular CD8+ T cells in grey matter	Correlation coefficient	-0.155	-0.061
	Sig. (2-tailed)	0.450	0.768
CD8+ T cells in white matter	Correlation coefficient	-0.201	-0.240
	Sig. (2-tailed)	0.324	0.238
Parenchymal CD8+ T cells in white matter	Correlation coefficient	-0.392	-0.139
	Sig. (2-tailed)	0.048*	0.499
Perivascular CD8+ T cells in white matter	Correlation coefficient	-0.179	-0.193
	Sig. (2-tailed)	0.382	0.345

Data presented as Spearman's rank correlation coefficient, *p<0.05, **p<0.002

Table 4.14 Correlations for CD8+ T cells and neuropathological markers in DLB group (n=29)

T cells/100mm^2		α-syn	Aβ	Ptau
Total CD8+ T cells	Correlation coefficient	-0.116	-0.210	0.014
	Sig. (2-tailed)	0.551	0.275	0.944
CD8+ T cells in grey matter	Correlation coefficient	0.017	-0.261	-0.004
	Sig. (2-tailed)	0.929	0.172	0.983
Parenchymal CD8+ T cells in grey matter	Correlation coefficient	0.022	-0.332	-0.049
	Sig. (2-tailed)	0.908	0.078	0.806
Perivascular CD8+ T cells in grey matter	Correlation coefficient	-0.009	-0.245	-0.086
	Sig. (2-tailed)	0.961	0.201	0.663
CD8+ T cells in white matter	Correlation coefficient	-0.140	0.011	0.023
	Sig. (2-tailed)	0.468	0.955	0.909
Parenchymal CD8+ T cells in white matter	Correlation coefficient	-0.245	-0.210	-0.072
	Sig. (2-tailed)	0.200	0.273	0.716
Perivascular CD8+ T cells in white matter	Correlation coefficient	-0.102	0.037	0.054
	Sig. (2-tailed)	0.599	0.848	0.786

Data presented as Spearman's rank correlation coefficient, *p<0.05, **p<0.002

4.15.3 Correlation between Foxp3+ T cells and markers of neuropathology

No significant correlations were found between Foxp3+ T cells and markers of neuropathology in the control or DLB group. Correlation tables for the control group and DLB group are presented in **Table 4.15** and **Table 4.16**, respectively.

Table 4.15 Correlations for Foxp3+ T cells and neuropathological markers in control group (n=25)

T cells/100mm²		Aβ	Ptau
Total Foxp3+ T cells	Correlation coefficient	-0.140	-0.053
	Sig. (2-tailed)	0.504	0.801
Foxp3+ T cells in grey matter	Correlation coefficient	-0.156	-0.137
	Sig. (2-tailed)	0.456	0.513
Parenchymal Foxp3+ T cells in grey matter	Correlation coefficient	-0.133	-0.319
	Sig. (2-tailed)	0.526	0.120
Perivascular Foxp3+ T cells in grey matter	Correlation coefficient	0.040	0.107
	Sig. (2-tailed)	0.850	0.611
Foxp3+ T cells in white matter	Correlation coefficient	-0.028	-0.003
	Sig. (2-tailed)	0.893	0.990
Parenchymal Foxp3+ T cells in white matter	Correlation coefficient	0.222	-0.070
	Sig. (2-tailed)	0.286	0.739
Perivascular Foxp3+ T cells in white matter	Correlation coefficient	-0.330	-0.045
	Sig. (2-tailed)	0.107	0.830

Data presented as Spearman's rank correlation coefficient, *p<0.05, **p<0.002

Table 4.16 Correlations for Foxp3+ T cells and neuropathological markers in DLB group (n=28)

T cells/100mm²		α-syn	Aβ	Ptau
Total Foxp3+ T cells	Correlation coefficient	-0.192	0.025	0.241
	Sig. (2-tailed)	0.328	0.901	0.225
Foxp3+ T cells in grey matter	Correlation coefficient	-0.267	-0.013	0.267
	Sig. (2-tailed)	0.169	0.947	0.178
Parenchymal Foxp3+ T cells in grey matter	Correlation coefficient	-0.086	-0.173	0.422
	Sig. (2-tailed)	0.664	0.379	0.028*
Perivascular Foxp3+ T cells in grey matter	Correlation coefficient	-0.364	0.999	-0.015
	Sig. (2-tailed)	0.057	0.618	0.941
Foxp3+ T cells in white matter	Correlation coefficient	-0.076	-0.020	-0.162
	Sig. (2-tailed)	0.702	0.920	0.419
Parenchymal Foxp3+ T cells in white matter	Correlation coefficient	-0.285	-0.018	-0.071
	Sig. (2-tailed)	0.142	0.926	0.726
Perivascular Foxp3+ T cells in white matter	Correlation coefficient	0.058	-0.020	-0.159
	Sig. (2-tailed)	0.771	0.918	0.428

Data presented as Spearman's rank correlation coefficient, *p<0.05, **p<0.002

4.15.4 Correlation between Tbet+ T cells and markers of neuropathology

No significant correlations were found between Tbet+ T cells and markers of neuropathology in the control or DLB group. Correlation tables for the control group and DLB group are presented in **Table 4.17** and **Table 4.18**, respectively.

Table 4.17 Correlations for Tbet+ T cells and neuropathological markers in control group (n=23)

T cells/100mm^2		Aβ	Ptau
Total Tbet+ T cells	Correlation coefficient	0.007	-0.035
	Sig. (2-tailed)	0.975	0.875
Tbet+ T cells in grey matter	Correlation coefficient	0.197	0.108
	Sig. (2-tailed)	0.367	0.622
Parenchymal Tbet+ T cells in grey matter	Correlation coefficient	0.126	0.080
	Sig. (2-tailed)	0.567	0.716
Perivascular Tbet+ T cells in grey matter	Correlation coefficient	0.243	0.043
	Sig. (2-tailed)	0.265	0.845
Tbet+ T cells in white matter	Correlation coefficient	0.006	-0.141
	Sig. (2-tailed)	0.979	0.520
Parenchymal Tbet+ T cells in white matter	Correlation coefficient	0.087	0.018
	Sig. (2-tailed)	0.694	0.936
Perivascular Tbet+ T cells in white matter	Correlation coefficient	-0.257	-0.076
	Sig. (2-tailed)	0.236	0.729

Data presented as Spearman's rank correlation coefficient, *p<0.05, **p<0.002

Table 4.18 Correlations for Tbet+ T cells and neuropathological markers in DLB group (n=26)

T cells/100mm^2		α-syn	Aβ	Ptau
Total Tbet+ T cells	Correlation coefficient	-0.131	-0.422	0.057
	Sig. (2-tailed)	0.523	0.032*	0.788
Tbet+ T cells in grey matter	Correlation coefficient	-0.140	-0.378	-0.034
	Sig. (2-tailed)	0.495	0.057	0.871
Parenchymal Tbet+ T cells in grey matter	Correlation coefficient	-0.119	-0.446	0.044
	Sig. (2-tailed)	0.563	0.022*	0.836
Perivascular Tbet+ T cells in grey matter	Correlation coefficient	-0.118	-0.258	-0.083
	Sig. (2-tailed)	0.565	0.203	0.695
Tbet+ T cells in white matter	Correlation coefficient	-0.019	-0.002	0.154
	Sig. (2-tailed)	0.927	0.991	0.463
Parenchymal Tbet+ T cells in white matter	Correlation coefficient	0.044	0.109	0.093
	Sig. (2-tailed)	0.832	0.597	0.658
Perivascular Tbet+ T cells in white matter	Correlation coefficient	-0.049	-0.169	0.153
	Sig. (2-tailed)	0.812	0.409	0.464

Data presented as Spearman's rank correlation coefficient, *p<0.05, **p<0.002

4.15.5 Correlation between GATA3+ T cells and markers of neuropathology

No significant correlations were found between GATA3+ T cells and markers of neuropathology in the control group. In the DLB group, a significant positive correlation was found between Aβ and GATA3+ T cells in the white matter parenchyma. Correlation tables for the control group and DLB group are presented in **Table 4.19** and **Table 4.20**, respectively.

Table 4.19 Correlations for GATA3+ T cells and neuropathological markers in control group (n=20)

T cells/100mm²		Aβ	Ptau
Total GATA3+ T cells	Correlation coefficient	0.122	0.032
	Sig. (2-tailed)	0.608	0.892
GATA3+ T cells in grey matter	Correlation coefficient	0.141	-0.017
	Sig. (2-tailed)	0.553	0.945
Parenchymal GATA3+ T cells in grey matter	Correlation coefficient	0.098	-0.066
	Sig. (2-tailed)	0.680	0.784
Perivascular GATA3+ T cells in grey matter	Correlation coefficient	0.122	0.011
	Sig. (2-tailed)	0.609	0.964
GATA3+ T cells in white matter	Correlation coefficient	-0.077	0.131
	Sig. (2-tailed)	0.748	0.583
Parenchymal GATA3+ T cells in white matter	Correlation coefficient	-0.088	0.207
	Sig. (2-tailed)	0.713	0.381
Perivascular GATA3+ T cells in white matter	Correlation coefficient	-0.128	0.204
	Sig. (2-tailed)	0.592	0.388

Data presented as Spearman's rank correlation coefficient, *p<0.05, **p<0.002

Table 4.20 Correlations for GATA3+ T cells and neuropathological markers in DLB group (n=22)

T cells/100mm²		α-syn	Aβ	Ptau
Total GATA3+ T cells	Correlation coefficient	0.014	0.343	0.301
	Sig. (2-tailed)	0.952	0.118	0.185
GATA3+ T cells in grey matter	Correlation coefficient	-0.04	0.285	0.205
	Sig. (2-tailed)	0.986	0.198	0.372
Parenchymal GATA3+ T cells in grey matter	Correlation coefficient	-0.050	0.247	0.166
	Sig. (2-tailed)	0.825	0.268	0.471
Perivascular GATA3+ T cells in grey matter	Correlation coefficient	-0.076	0.243	0.114
	Sig. (2-tailed)	0.738	0.275	0.624
GATA3+ T cells in white matter	Correlation coefficient	0.110	0.604	0.480
	Sig. (2-tailed)	0.625	0.003*	0.027
Parenchymal GATA3+ T cells in white matter	Correlation coefficient	0.167	0.629	0.516
	Sig. (2-tailed)	0.457	**0.001****	0.017
Perivascular GATA3+ T cells in white matter	Correlation coefficient	0.184	0.475	0.391
	Sig. (2-tailed)	0.413	0.026*	0.080

Data presented as Spearman's rank correlation coefficient, *p<0.05, **p<0.002

4.16 Correlation between T cells and inflammatory markers

Protein loads for the inflammatory markers Iba1, HLA-DR, CD68, CD64, CD32a, CD32b, CD16, CHI3L1 and IL4R had already been quantified for each DLB and control case in a previous study, (95). These data were used to assess for correlations between the number of T cells/100mm^2 in the parenchymal and perivascular compartments of grey and white matter, and inflammatory markers. Spearman's rank correlations were performed for each T cell subset (CD4+, CD8+, Foxp3+, Tbet+ and GATA3+ T cells), with P values of less than 0.001 deemed to be significant. The P value was adjusted using the Bonferroni correction, resulting in a family wise error rate of 0.05 (5% chance of a Type 1 error). Control cases 803, 894, 943 and DLB case A304/06 were excluded from analysis due to being previously identified as outliers not meeting inclusion criteria.

4.16.1 Correlations between CD4+ T cells and inflammatory markers

In both groups, there were no significant correlations found between CD4+ T cells and markers of inflammation. Correlation tables for control and DLB groups are presented in **Table 4.21** and **Table 4.22**, respectively.

Table 4.21 Correlations for CD4+ T cells and inflammatory markers in control group (n=26)

T cells/100mm²		Iba	CD68	HLADR	CD64	CD32a	CD32b	CD16	CHI3L1	IL4R
Total CD4+ T cells	Correlation coefficient	-0.234	-0.214	-0.086	-0.156	0.184	0.252	0.146	-0.080	0.077
	Sig. (2-tailed)	0.221	0.266	0.657	0.427	0.369	0.215	0.449	0.681	0.692
CD4+ T cells in grey matter	Correlation coefficient	-0.133	-0.211	-0.126	-0.122	0.161	0.281	0.277	-0.067	0.117
	Sig. (2-tailed)	0.490	0.272	0.516	0.537	0.432	0.164	0.146	0.729	0.545
Parenchymal CD4+ T cells in grey matter	Correlation coefficient	-0.121	-0.263	-0.218	-0.145	0.137	0.249	0.203	-0.084	0.076
	Sig. (2-tailed)	0.531	0.169	0.257	0.462	0.504	0.219	0.292	0.666	0.696
Perivascular CD4+ T cells in grey matter	Correlation coefficient	-0.286	-0.005	0.200	0.053	0.068	0.339	0.336	-0.030	0.002
	Sig. (2-tailed)	0.133	0.980	0.297	0.789	0.740	0.090	0.075	0.878	0.992
CD4+ T cells in white matter	Correlation coefficient	-0.041	-0.085	-0.034	-0.143	-0.109	-0.227	-0.415	-0.206	-0.102
	Sig. (2-tailed)	0.834	0.660	0.862	0.467	0.596	0.266	0.025*	0.284	0.598
Parenchymal CD4+ T cells in white matter	Correlation coefficient	-0.033	-0.195	-0.113	-0.242	-0.132	-0.290	-0.461	-0.182	-0.008
	Sig. (2-tailed)	0.865	0.310	0.560	0.215	0.521	0.151	0.012*	0.346	0.966
Perivascular CD4+ T cells in white matter	Correlation coefficient	-0.136	0.250	0.236	0.202	-0.205	0.011	0.114	-0.031	-0.340
	Sig. (2-tailed)	0.482	0.192	0.217	0.302	0.315	0.958	0.555	0.874	0.071

Data presented as Spearman's rank correlation coefficient, *p<0.05, **p<0.001

Table 4.22 Correlations for CD4+ T cells and inflammatory markers in DLB group (n=29)

T cells/100mm²		Iba	CD68	HLADR	CD64	CD32a	CD32b	CD16	CHI3L1	IL4R
Total CD4+ T cells	Correlation coefficient	-0.106	0.113	-0.036	0.029	-0.025	-0.057	-0.122	-0.131	0.046
	Sig. (2-tailed)	0.593	0.559	0.853	0.883	0.900	0.777	0.528	0.498	0.833
CD4+ T cells in grey matter	Correlation coefficient	-0.111	0.166	-0.055	-0.019	-0.031	-0.102	-0.112	-0.154	-0.030
	Sig. (2-tailed)	0.574	0.389	0.777	0.924	0.879	0.614	0.564	0.424	0.893
Parenchymal CD4+ T cells in grey matter	Correlation coefficient	-0.081	0.140	-0.109	-0.088	0.015	-0.069	-0.109	-0.176	-0.094
	Sig. (2-tailed)	0.681	0.469	0.575	0.657	0.942	0.731	0.575	0.361	0.670
Perivascular CD4+ T cells in grey matter	Correlation coefficient	0.061	0.053	0.121	0.068	-0.020	-0.080	-0.169	-0.222	0.074
	Sig. (2-tailed)	0.757	0.784	0.531	0.732	0.921	0.691	0.380	0.246	0.739
CD4+ T cells in white matter	Correlation coefficient	-0.180	-0.085	-0.194	0.060	-0.268	-0.077	0.041	0.275	-0.059
	Sig. (2-tailed)	0.360	0.662	0.313	0.762	0.177	0.701	0.834	0.149	0.789
Parenchymal CD4+ T cells in white matter	Correlation coefficient	-0.075	-0.183	-0.260	-0.012	-0.242	-0.127	-0.018	0.183	-0.093
	Sig. (2-tailed)	0.704	0.342	0.174	0.953	0.224	0.528	0.928	0.343	0.672
Perivascular CD4+ T cells in white matter	Correlation coefficient	-0.139	0.208	0.155	0.115	-0.110	0.094	0.116	-0.139	0.474
	Sig. (2-tailed)	0.482	0.279	0.422	0.561	0.586	0.639	0.550	0.471	0.022*

Data presented as Spearman's rank correlation coefficient, *p<0.05, **p<0.001

4.16.2 Correlations between CD8+ T cells and inflammatory markers

There were no significant correlations found between CD8+ T cells and markers of inflammation in the control group.

Significant positive correlations between the following variables were found in the DLB group:

- CD32b and CD8+ T cells in grey matter (rs[27]=0.631, p=<0.001)
- CD32b and perivascular CD8+ T cells in grey matter (rs[27]=0.690, p=<0.001)

Correlation tables are shown in **Table 4.23** for the control group and in **Table 4.24** for the DLB group.

Table 4.23 Correlations for CD8+ T cells and inflammatory markers in control group (n=26)

T cells/100mm^2		Iba	CD68	HLADR	CD64	CD32a	CD32b	CD16	CHI3L1	IL4R
Total CD8+ T cells	Correlation coefficient	0.069	0.299	0.089	0.436	0.250	0.406	0.181	0.098	0.236
	Sig. (2-tailed)	0.736	0.138	0.667	0.029*	0.238	0.049*	0.376	0.633	0.245
CD8+ T cells in grey matter	Correlation coefficient	-0.104	0.314	0.170	0.482	0.186	0.263	0.305	0.111	0.281
	Sig. (2-tailed)	0.613	0.118	0.408	0.015*	0.383	0.215	0.129	0.588	0.165
Parenchymal CD8+ T cells in grey matter	Correlation coefficient	-0.089	0.251	0.178	0.546	0.216	0.157	0.218	0.027	0.394
	Sig. (2-tailed)	0.665	0.216	0.385	0.005*	0.310	0.465	0.285	0.894	0.046*
Perivascular CD8+ T cells in grey matter	Correlation coefficient	-0.099	0.284	0.142	0.418	0.143	0.332	0.261	0.129	0.230
	Sig. (2-tailed)	0.630	0.160	0.488	0.037*	0.504	0.113	0.197	0.531	0.259
CD8+ T cells in white matter	Correlation coefficient	0.125	0.219	0.125	0.321	0.357	0.476	0.175	0.120	0.216
	Sig. (2-tailed)	0.544	0.282	0.541	0.117	0.087	0.019*	0.393	0.558	0.290
Parenchymal CD8+ T cells in white matter	Correlation coefficient	0.355	0.330	0.335	0.317	0.513	0.358	0.187	0.169	0.401
	Sig. (2-tailed)	0.075	0.099	0.094	0.123	0.010*	0.086	0.361	0.409	0.042*
Perivascular CD8+ T cells in white matter	Correlation coefficient	0.089	0.187	0.062	0.286	0.288	0.477	0.134	0.102	0.183
	Sig. (2-tailed)	0.665	0.359	0.765	0.165	0.173	0.018*	0.513	0.619	0.371

Data presented as Spearman's rank correlation coefficient, *p<0.05, **p<0.001

Table 4.24 Correlations for CD8+ T cells and inflammatory markers in DLB group (n=29)

T cells/100mm²		Iba	CD68	HLADR	CD64	CD32a	CD32b	CD16	CHI3L1	IL4R
Total CD8+ T cells	Correlation coefficient	0.062	0.462	0.232	0.432	0.241	0.532	0.144	-0.240	0.391
	Sig. (2-tailed)	0.755	0.012*	0.226	0.022*	0.225	0.004*	0.457	0.209	0.065
CD8+ T cells in grey matter	Correlation coefficient	0.087	0.460	0.199	0.384	0.324	0.631	0.188	-0.363	0.337
	Sig. (2-tailed)	0.659	0.012*	0.301	0.044*	0.099	**<0.001****	0.328	0.053	0.116
Parenchymal CD8+ T cells in grey matter	Correlation coefficient	0.035	0.405	0.174	0.375	0.288	0.520	0.189	-0.278	0.323
	Sig. (2-tailed)	0.859	0.029*	0.368	0.049*	0.146	0.005*	0.326	0.145	0.133
Perivascular CD8+ T cells in grey matter	Correlation coefficient	0.181	0.405	0.163	0.348	0.339	0.690	0.122	-0.389	0.316
	Sig. (2-tailed)	0.355	0.029*	0.400	0.069	0.084	**<0.001****	0.527	0.037*	0.142
CD8+ T cells in white matter	Correlation coefficient	0.205	0.256	-0.117	0.224	-0.003	0.330	-0.074	0.043	0.136
	Sig. (2-tailed)	0.295	0.180	0.547	0.251	0.989	0.093	0.703	0.824	0.535
Parenchymal CD8+ T cells in white matter	Correlation coefficient	0.252	0.210	-0.072	0.147	-0.088	0.296	-0.096	-0.120	0.211
	Sig. (2-tailed)	0.195	0.275	0.711	0.455	0.661	0.174	0.619	0.535	0.335
Perivascular CD8+ T cells in white matter	Correlation coefficient	0.184	0.279	-0.097	0.216	0.002	0.341	-0.068	0.024	0.139
	Sig. (2-tailed)	0.349	0.143	0.617	0.270	0.994	0.082	0.726	0.902	0.527

Data presented as Spearman's rank correlation coefficient, *p<0.05, **p<0.001

4.16.3 Correlations between Foxp3+ T cells and inflammatory markers

In both groups, there were no significant correlations found between Foxp3+ T cells and markers of inflammation. Correlation tables for control and DLB groups are presented in **Table 4.25** and **Table 4.26**, respectively.

Table 4.25 Correlations for Foxp3+ T cells and inflammatory markers in control group (n=25)

T cells/100mm²		Iba	CD68	HLADR	CD64	CD32a	CD32b	CD16	CHI3L1	IL4R
Total Foxp3+ T cells	Correlation coefficient	0.069	0.086	0.326	0.042	0.274	0.243	0.026	-0.161	0.500
	Sig. (2-tailed)	0.745	0.682	0.112	0.845	0.206	0.265	0.901	0.443	0.011*
Foxp3+ T cells in grey matter	Correlation coefficient	0.104	0.021	0.355	-0.024	0.396	0.222	-0.202	-0.262	0.377
	Sig. (2-tailed)	0.619	0.921	0.082	0.910	0.061	0.308	0.332	0.205	0.063
Parenchymal Foxp3+ T cells in grey matter	Correlation coefficient	-0.058	-0.040	0.117	0.064	0.221	0.193	-0.135	-0.268	0.278
	Sig. (2-tailed)	0.782	0.851	0.579	0.768	0.310	0.377	0.519	0.195	0.178
Perivascular Foxp3+ T cells in grey matter	Correlation coefficient	0.348	0.187	0.264	-0.001	0.584	0.195	0.111	0.110	0.218
	Sig. (2-tailed)	0.088	0.371	0.202	0.995	0.003*	0.372	0.599	0.600	0.295
Foxp3+ T cells in white matter	Correlation coefficient	-0.023	0.263	0.205	0.058	0.058	0.112	0.381	0.007	0.243
	Sig. (2-tailed)	0.914	0.204	0.326	0.789	0.792	0.612	0.060	0.975	0.241
Parenchymal Foxp3+ T cells in white matter	Correlation coefficient	0.171	0.085	0.024	-0.066	0.188	0.032	0.065	-0.168	0.201
	Sig. (2-tailed)	0.414	0.685	0.911	0.760	0.389	0.886	0.758	0.423	0.336
Perivascular Foxp3+ T cells in white matter	Correlation coefficient	-0.260	0.381	0.360	0.260	-0.129	0.042	0.482	0.009	0.139
	Sig. (2-tailed)	0.210	0.060	0.077	0.219	0.557	0.850	0.015*	0.964	0.507

Data presented as Spearman's rank correlation coefficient, *p<0.05, **p<0.001

Table 4.26 Correlations for Foxp3+ T cells and inflammatory markers in DLB group (n=28)

T cells/100mm²		Iba	CD68	HLADR	CD64	CD32a	CD32b	CD16	CHI3L1	IL4R
Total Foxp3+ T cells	Correlation coefficient	-0.189	0.311	0.021	0.332	0.091	0.334	0.380	0.226	0.309
	Sig. (2-tailed)	0.346	0.107	0.916	0.091	0.660	0.095	0.046*	0.247	0.151
Foxp3+ T cells in grey matter	Correlation coefficient	-0.225	0.258	-0.051	0.212	0.047	0.317	0.378	0.158	0.120
	Sig. (2-tailed)	0.260	0.185	0.797	0.287	0.819	0.115	0.048*	0.423	0.587
Parenchymal Foxp3+ T cells in grey matter	Correlation coefficient	-0.365	0.345	0.033	0.126	-0.006	0.313	0.283	-0.049	0.167
	Sig. (2-tailed)	0.061	0.072	0.868	0.532	0.978	0.119	0.145	0.803	0.446
Perivascular Foxp3+ T cells in grey matter	Correlation coefficient	0.067	0.162	-0.192	0.190	0.084	0.284	0.226	0.247	0.079
	Sig. (2-tailed)	0.741	0.411	0.327	0.341	0.682	0.160	0.249	0.204	0.720
Foxp3+ T cells in white matter	Correlation coefficient	0.044	0.193	0.038	0.209	0.106	0.259	0.098	0.026	0.326
	Sig. (2-tailed)	0.827	0.326	0.848	0.296	0.607	0.201	0.621	0.897	0.129
Parenchymal Foxp3+ T cells in white matter	Correlation coefficient	0.065	-0.082	-0.372	-0.203	-0.229	0.075	-0.061	-0.046	-0.087
	Sig. (2-tailed)	0.748	0.676	0.052	0.309	0.260	0.716	0.759	0.817	0.693
Perivascular Foxp3+ T cells in white matter	Correlation coefficient	0.176	0.176	0.139	0.191	0.189	0.160	0.075	0.115	0.334
	Sig. (2-tailed)	0.380	0.369	0.481	0.339	0.355	0.434	0.704	0.559	0.119

Data presented as Spearman's rank correlation coefficient, *p<0.05, **p<0.001

4.16.4 Correlations between Tbet+ T cells and inflammatory markers

In the control group, there were no significant correlations found between Tbet+ T cells and markers of inflammation.

Significant positive correlations between the following variables were found in the DLB group:

- CD64 and total Tbet+ T cells (rs[23]=0.796, p=<0.001)
- CD64 and Tbet+ T cells in grey matter (rs[23]=0.713, p=<0.001)
- CD64 and parenchymal Tbet+ T cells in grey matter (rs[23]=0.704, p=<0.001)
- CD64 and perivascular Tbet+ T cells in grey matter (rs[23]=0.640, p=<0.001)
- CD64 and perivascular Tbet+ T cells in white matter (rs[23]=0.620, p=<0.001)
- CD32b and Tbet+ T cells in grey matter (rs[22]=0.686, p=<0.001)
- CD32b and parenchymal Tbet+ T cells in grey matter (rs[22]=0.737, p=<0.001)

Correlation tables for control and DLB groups are presented in **Table 4.27** and **Table 4.28**, respectively.

Table 4.27 Correlations for Tbet+ T cells and inflammatory markers in control group (n=23)

T cells/100mm²		Iba	CD68	HLADR	CD64	CD32a	CD32b	CD16	CHI3L1	IL4R
Total Tbet+ T cells	Correlation coefficient	-0.139	-0.210	-0.269	0.221	-0.158	0.254	-0.132	-0.240	-0.144
	Sig. (2-tailed)	0.526	0.336	0.214	0.323	0.494	0.255	0.550	0.271	0.511
Tbet+ T cells in grey matter	Correlation coefficient	-0.022	-0.227	-0.400	0.061	-0.079	0.306	-0.131	-0.062	-0.018
	Sig. (2-tailed)	0.920	0.298	0.086	0.787	0.734	0.167	0.550	0.777	0.934
Parenchymal Tbet+ T cells in grey matter	Correlation coefficient	-0.032	-0.204	-0.350	0.087	-0.061	0.287	-0.095	-0.056	0.037
	Sig. (2-tailed)	0.884	0.351	0.101	0.700	0.794	0.196	0.667	0.798	0.866
Perivascular Tbet+ T cells in grey matter	Correlation coefficient	-0.236	0.079	-0.247	0.258	-0.275	0.264	-0.106	-0.092	-0.166
	Sig. (2-tailed)	0.277	0.721	0.256	0.190	0.227	0.235	0.629	0.676	0.448
Tbet+ T cells in white matter	Correlation coefficient	-0.159	-0.103	-0.122	0.275	-0.272	0.089	-0.147	-0.346	-0.159
	Sig. (2-tailed)	0.468	0.639	0.580	0.215	0.233	0.692	0.505	0.106	0.468
Parenchymal Tbet+ T cells in white matter	Correlation coefficient	-0.151	0.107	-0.144	0.288	-0.208	0.266	-0.124	-0.233	-0.108
	Sig. (2-tailed)	0.493	0.628	0.513	0.194	0.365	0.232	0.572	0.284	0.624
Perivascular Tbet+ T cells in white matter	Correlation coefficient	-0.093	-0.271	-0.035	0.028	-0.280	0.009	-0.212	-0.269	-0.090
	Sig. (2-tailed)	0.672	0.211	0.873	0.902	0.219	0.970	0.332	0.214	0.682

Data presented as Spearman's rank correlation coefficient, *p<0.05, **p<0.001

Table 4.28 Correlations for Tbet+ T cells and inflammatory markers in DLB group (n=26)

T cells/100mm²		Iba	CD68	HLADR	CD64	CD32a	CD32b	CD16	CHI3L1	IL4R
Total Tbet+ T cells	Correlation coefficient	-0.015	0.505	0.301	0.796	0.419	0.608	0.571	-0.300	0.426
	Sig. (2-tailed)	0.942	0.008*	0.135	**<0.001****	0.037*	0.002*	0.002*	0.136	0.054
Tbet+ T cells in grey matter	Correlation coefficient	-0.044	0.492	0.301	0.713	0.506	0.686	0.538	-0.357	0.401
	Sig. (2-tailed)	0.835	0.011*	0.135	**<0.001****	0.010*	**<0.001****	0.005*	0.073	0.071
Parenchymal Tbet+ T cells in grey matter	Correlation coefficient	-0.025	0.543	0.264	0.704	0.485	0.737	0.513	-0.348	0.426
	Sig. (2-tailed)	0.904	0.004*	0.193	**<0.001****	0.014*	**<0.001****	0.007*	0.081	0.054
Perivascular Tbet+ T cells in grey matter	Correlation coefficient	-0.060	0.285	0.217	0.640	0.414	0.564	0.379	-0.257	0.386
	Sig. (2-tailed)	0.774	0.158	0.288	**<0.001****	0.040*	0.004*	0.056	0.205	0.084
Tbet+ T cells in white matter	Correlation coefficient	0.185	0.408	-0.063	0.603	0.139	0.477	0.329	0.081	0.244
	Sig. (2-tailed)	0.377	0.039*	0.759	0.001*	0.509	0.018*	0.101	0.692	0.286
Parenchymal Tbet+ T cells in white matter	Correlation coefficient	0.225	0.329	-0.086	0.442	0.022	0.470	0.243	0.052	0.238
	Sig. (2-tailed)	0.279	0.101	0.676	0.027*	0.917	0.021*	0.233	0.802	0.299
Perivascular Tbet+ T cells in white matter	Correlation coefficient	0.125	0.410	0.052	0.620	0.211	0.325	0.366	-0.083	0.195
	Sig. (2-tailed)	0.551	0.038*	0.801	**<0.001****	0.310	0.121	0.066	0.688	0.397

Data presented as Spearman's rank correlation coefficient, *p<0.05, **p<0.001

4.16.5 Correlations between GATA3+ T cells and inflammatory markers

In both groups, there were no significant correlations found between GATA3+ T cells and markers of inflammation. Correlation tables for control and DLB groups are presented in **Table 4.29** and **Table 4.30**, respectively.

Table 4.29 Correlations for GATA3+ T cells and inflammatory markers in Control group (n=20)

T cells/100mm^2		Iba	CD68	HLADR	CD64	CD32a	CD32b	CD16	CHI3L1	IL4R
Total GATA3+ T cells	Correlation coefficient	0.053	-0.164	-0.276	-0.150	-0.027	0.021	0.110	0.205	-0.259
	Sig. (2-tailed)	0.825	0.489	0.238	0.539	0.912	0.932	0.644	0.386	0.270
GATA3+ T cells in grey matter	Correlation coefficient	0.072	-0.064	-0.213	-0.149	-0.019	0.101	0.221	0.189	-0.321
	Sig. (2-tailed)	0.764	0.789	0.367	0.544	0.937	0.680	0.350	0.424	0.168
Parenchymal GATA3+ T cells in grey matter	Correlation coefficient	0.101	-0.042	-0.251	-0.059	-0.071	0.076	0.314	0.175	-0.367
	Sig. (2-tailed)	0.673	0.862	0.286	0.810	0.773	0.757	0.177	0.460	0.112
Perivascular GATA3+ T cells in grey matter	Correlation coefficient	-0.219	-0.247	-0.130	-0.346	-0.142	0.000	-0.076	-0.091	-0.139
	Sig. (2-tailed)	0.353	0.293	0.586	0.146	0.563	1.000	0.752	0.701	0.558
GATA3+ T cells in white matter	Correlation coefficient	0.413	-0.093	-0.188	-0.215	0.160	-0.177	-0.245	0.230	0.080
	Sig. (2-tailed)	0.070	0.697	0.427	0.377	0.512	0.470	0.299	0.328	0.738
Parenchymal GATA3+ T cells in white matter	Correlation coefficient	0.275	-0.203	-0.206	-0.340	0.029	-0.092	-0.352	0.110	0.105
	Sig. (2-tailed)	0.241	0.390	0.384	0.154	0.907	0.708	0.128	0.643	0.660
Perivascular GATA3+ T cells in white matter	Correlation coefficient	0.497	-0.065	-0.129	-0.190	0.259	-0.304	-0.155	0.355	0.211
	Sig. (2-tailed)	0.026*	0.787	0.587	0.437	0.285	0.205	0.515	0.125	0.371

Data presented as Spearman's rank correlation coefficient, *p<0.05, **p<0.001

Table 4.30 Correlations for GATA3+ T cells and inflammatory markers in DLB group (n=22)

T cells/100mm^2		Iba	CD68	HLADR	CD64	CD32a	CD32b	CD16	CHI3L1	IL4R
Total GATA3+ T cells	Correlation coefficient	-0.277	0.028	0.324	0.126	-0.160	-0.051	0.387	0.005	0.372
	Sig. (2-tailed)	0.225	0.903	0.142	0.586	0.487	0.827	0.075	0.984	0.117
GATA3+ T cells in grey matter	Correlation coefficient	-0.326	0.062	0.340	0.212	-0.103	-0.006	0.476	0.003	0.377
	Sig. (2-tailed)	0.149	0.786	0.121	0.357	0.656	0.978	0.025*	0.988	0.111
Parenchymal GATA3+ T cells in grey matter	Correlation coefficient	-0.326	0.018	0.360	0.169	-0.160	-0.066	0.458	0.008	0.405
	Sig. (2-tailed)	0.149	0.938	0.100	0.464	0.489	0.777	0.032*	0.972	0.085
Perivascular GATA3+ T cells in grey matter	Correlation coefficient	-0.462	0.174	0.399	0.243	-0.118	0.168	0.518	0.023	0.465
	Sig. (2-tailed)	0.035*	0.437	0.066	0.289	0.610	0.468	0.014*	0.919	0.045*
GATA3+ T cells in white matter	Correlation coefficient	-0.100	0.057	-0.095	-0.047	-0.234	-0.045	0.059	0.238	0.023
	Sig. (2-tailed)	0.666	0.800	0.674	0.840	0.307	0.847	0.793	0.287	0.926
Parenchymal GATA3+ T cells in white matter	Correlation coefficient	-0.126	0.047	-0.108	0.038	-0.328	-0.151	0.132	0.259	-0.044
	Sig. (2-tailed)	0.585	0.835	0.631	0.870	0.147	0.513	0.557	0.244	0.857
Perivascular GATA3+ T cells in white matter	Correlation coefficient	-0.183	0.073	-0.006	-0.181	-0.235	0.041	-0.018	0.186	0.074
	Sig. (2-tailed)	0.427	0.747	0.978	0.432	0.305	0.859	0.936	0.407	0.764

Data presented as Spearman's rank correlation coefficient, *p<0.05, **p<0.001

Chapter 5 Conclusions

This novel study aimed to define the profile of T cells in the brain in DLB using immunohistochemistry. To date, this is the first human *post-mortem* study to examine different T cell subsets in the parenchymal and perivascular compartments of grey and white brain matter in DLB. Quantification of T cell subsets identified alterations in the cerebral profile of T cells in DLB compared to controls. Associations between T cells and markers of inflammation revealed potential T cell interactions with microglia and neurons. These findings suggest that T cell infiltration into the brain may play a role in the pathogenesis of DLB.

5.1.1 CD4+ T cells in DLB

Analysis of CD4+ T cell data revealed increased numbers of CD4+ T cells in grey matter in DLB, which was reflected in the parenchymal compartment but not in the perivascular compartment. This is in keeping with previous literature, which has reported increased numbers of CD4+ T cells in human brain parenchyma in DLB (158) and in PDD (159). Preclinical studies examining cerebral T cell populations have consistently demonstrated increased infiltration of CD4+ cells in mouse models of LBD (158, 172). Although not defined into T cell subsets, there is a body of evidence showing the increased presence of CD3+ T cells in DLB brains (160, 161), specifically in grey matter parenchyma (95). The detection of CD4+IL-17A+ T cells in one study by Gate *et al*. supports an infiltrating CD4+ T cell population that includes Th17 cells (161).

Preclinical and human *post-mortem* studies in PD reveal similar findings, with increased CD4+ T cell infiltration observed in the SN (144, 145). The presence of peripheral α-syn-specific CD4+ T cells has been reported in PD, and if able to infiltrate the brain, these may contribute to an increased cerebral CD4+ T cell population (153, 156). Previous literature has shown reduced proportions of peripheral CD4+ T cells in DLB (178), possibly a consequence of increased recruitment into the brain.

Correlations between the number of CD4+ T cells and neuropathological markers of DLB did not show any significant associations in the DLB or control group. This suggests that the extent of T cell infiltration is independent of neuropathology. However, this does not exclude the possibility of potential interactions between T cells and α-syn, as proposed in previous studies (153, 160, 161). The burden of neuropathology does not necessarily reflect the extent of T cell reactivity in the DLB brain, and it is possible that other factors such as neuronal or synaptic degeneration play a prominent role in driving T cell recruitment. These potential interactions are supported by previous observations of CD3+ T cells adjacent to neuronal processes in LBD brains (148, 161).

There were no associations found between CD4+ T cells and markers of inflammation in the DLB or control groups. Notably, there were no correlations identified between CD4+ T cells and the microglial markers Iba1, HLA-DR and CD68, suggesting the antigen presenting properties of microglia are not a prominent mechanism of CD4+ T cell activation in DLB. Previous *post-mortem* brain studies have reported an absence of microglial activation in DLB which further supports that activation of microglia may not be driving neuroinflammatory processes (95-97). A lack of interaction between T cells and activated microglia is conflicting with some of the previous literature in this area. CD3+ T cells have been detected in close proximity to Iba1+ microglia in the SN in DLB and PDD human brains (161). Furthermore, in PDD brains, Kouli *et al.* detected a significant correlation between HLA-DR+ microglia and CD4+ T cells in the amygdala (159). It is important to note the variation in brain regions examined and that these findings may not be applicable to all brain areas.

5.1.2 CD8+ T cells in DLB

Although higher numbers of CD8+ T cells were detected within grey and white matter brain compartments in DLB cases compared to controls, these differences did not reach statistical significance. It is possible that the high variance in data may have reduced the power to detect such differences. Nevertheless, the findings are consistent with previous literature indicating a lack of significant difference in numbers of CD8+ T cells in human DLB/PDD versus control brains (158, 159). A similar non-significant trend of increased CD8+ T cells was previously observed in the hippocampus in DLB (158), and the SN and amygdala in PDD (159).

In both groups, the overall number of CD8+ T cells was higher than CD4+ T cells, with a predominance in perivascular areas of white matter. This is in keeping with the profile of T cells observed in non-pathological aged brains (127-129) and infers a role for CD8+ T cells in the ageing brain that may be independent of neuropathology. There were no associations between CD8+ T cells and neuropathological markers, further supporting this hypothesis.

Positive associations between CD8+ T cells in grey matter and the inflammatory marker, CD32b were identified in the DLB group. CD32b (FcγRIIb) is a cell surface receptor expressed on microglia that binds to immune complex and is the only FcγR with an inhibitory action (204). In a previous study using cell cultures, microglial phagocytosis was inhibited when aggregated α-syn bound to CD32b expressed by microglia (205). This inhibition may contribute to neurodegeneration by reducing the effective clearance of α-syn, however, the role of CD8+ T cells in these interactions is not yet clear.

It is notable that immunostaining for CD32b was observed to be localised to neuronal nuclei, with no localisation to microglia. Choi *et al.* demonstrated that neuronal CD32b functions as a

receptor for α-syn fibrils to mediate cell-to-cell transmission of α-syn (206). CD8+ T cells may play a role in these interactions, potentially contributing to synaptic dysfunction in DLB. The lack of association between CD8+ T cells and α-syn does not necessarily support this, although interactions earlier in the disease course cannot be excluded. A further consideration is that the quantification of LRP in this study related to the presence of LB and LN. It has been proposed that pre-synaptic α-syn aggregates may contribute to neurodegeneration to a greater extent, through synaptic dysfunction and impairment of neurotransmitter release (207).

Whilst there is limited literature relating to neuronal CD32b expression in DLB, this area has been further investigated in AD. In a human *post-mortem* brain study, neuronal CD32b was shown to be upregulated in the hippocampus and contributed to Aβ-induced synaptic loss in AD (208). It is plausible that neuronal CD32b expression could be a shared pathological response to immune complexes and aggregated protein deposition in DLB. However, potential interactions between CD8+ T cells and neuronal CD32b have not yet been established.

5.1.3 Foxp3+ T cells in DLB

The expression of Foxp3, a marker of Treg cells, has not been previously reported in the DLB brain. Existing literature is therefore limited in this area, however, increased Treg cell responses have been reported previously in PD. Cerebral Foxp3 expression was increased in a mouse model of PD, supported by an increase in IL-10, the cytokine expressed by Treg cells (144).

In contrast, this study revealed no significant differences in the number of Foxp3+ T cells in grey or white matter between DLB and control cases. Furthermore, no associations were found with markers of neuropathology or inflammation. These findings suggest that Treg cell recruitment is not altered in the DLB brain and does not occur in response to the presence of neuropathology or activated microglia.

5.1.4 Tbet+ T cells in DLB

Increased numbers of Tbet+ T cells were detected in total brain matter and parenchymal grey matter in DLB brains in this study, suggesting recruitment of Th1 and/or Tc1 cells. The increased CD4+ T cell population within the same brain compartments implicate Th1 cells as the infiltrating T cell subset, although this cannot be confirmed in the absence of double immunostaining. If proven, this is consistent with previous reports of increased cerebral Th1 cells in mouse models of LBD, supporting a proinflammatory response to the overexpression of α-syn (144, 158). CD4+ T cells expressing IFN-γ were the most prevalent cytokine producing cells, indicating a prominent Th1 response in LBD (144).

Correlations between Tbet+ T cells and markers of inflammation showed associations with the markers, CD64 and CD32b in grey matter. The FcγR CD64 is known to be activating and contributes to proinflammatory responses. Immunostaining for CD64 showed extensive staining of microglial cell bodies and processes. This raises the possibility of interactions between Th1 cells and microglia to promote proinflammatory responses, particularly within the grey matter compartment in DLB. One previous study in PD found increased expression of CD64 on phagocytic microglia, which were found to contain remnants from pigmented neurons (209). This is however, in contrast to a previous *post-mortem* human study that found no alteration in CD64 expression in DLB brain tissue compared to controls (95). The potential interactions between Tbet+ T cells and microglia expressing CD64 remain unclear, although prominent Th1 cell infiltration supports the involvement of proinflammatory responses.

In addition to the association found between the inhibitory receptor CD32b and CD8+ T cells, there was also a positive correlation detected between CD32b and Tbet+ T cells in total grey matter in DLB. The CD8+ T cells potentially interacting with neuronal CD32b in this compartment may therefore include Tc1 cells. However, in the absence of double staining, it is not possible to confirm if these Tbet+ T cells are CD4+ T cells or CD8+ T cells.

The lack of association with markers of neuropathology suggests a limited role for Tbet+ T cell reactivity in response to protein deposition in DLB. Increased Th1 cell recruitment into the DLB brain may occur independently of protein accumulation. This is surprising based on previous evidence of peripheral T cell responses involving an α-syn-specific subset of Th1 cells in PD (153). One possible explanation is that T cell responses to α-syn in the periphery in PD are not replicated in the DLB brain. Other factors such as disease course should also be considered, given that T cell responses were reported to be most pronounced during early stages of PD (153). Furthermore, the capacity for α-syn-specific T cell recruitment from the periphery into the brain is yet to be established.

5.1.5 GATA3+ T cells in DLB

Although GATA3+ T cells constituted the least abundant cerebral T cell subset in both groups, there were significantly increased numbers present in total brain matter and grey matter compartments in the DLB group compared to the control group. Increased CD4+ T cells within the total brain matter and grey matter parenchyma indicate that these represent Th2 cells. This is consistent with previous studies in PD that have evidenced an increased Th2 cell response to α-syn, however this was in relation to peripheral T cells, rather than cerebral T cells (153, 156).

No previous *post-mortem* brain studies have investigated the presence of Th2 cells or IL-4 expression in DLB. One previous study using a mouse model of PD reported no change in

expression of the Th2 associated cytokine, IL-4 in the midbrain. Furthermore, there was no increase in GATA3 expression (144), supporting an absence of altered Th2 cell responses in the PD brain. This contrasting observation in PD suggests that additional T cell responses may be present in the DLB brain. It is important to recognise that T cell responses in the brains of mice and humans may differ and vary according to the brain region examined.

The positive correlation found between Aβ and GATA3+ T cells in white matter parenchyma in DLB is particularly interesting, given that Aβ deposition was only quantified in grey matter. This suggests that Th2 or Tc2 cells may home to white matter areas in response to damage associated signals from grey matter. A study including 45 patients with DLB or mild cognitive impairment with LB, and 45 matched controls has investigated the influences of AD pathology on white matter neurite alterations, using diffusion tensor imaging and neurite orientation dispersion and density imaging. Cortical Aβ deposition in DLB was found to have significant effects on white matter microstructural injury through its influence on tau deposition (210). This evidence supports the possibility that Th2/Tc2 cells contribute to immune interactions in response to AD pathology, potentially resulting in white matter injury.

5.1.6 The profile of T cell subsets in DLB

When comparing the numbers of CD4+ and CD8+ T cells detected in control and DLB brains, CD8+ T cells were found to be the most abundant in all brain compartments except grey matter parenchyma. In both groups, there was a higher number of CD4+ T cells compared to CD8+ T cells in this area, although differences did not reach statistical significance. The predominant presence of CD8+ T cells in the perivascular compartment of white matter in control brains is in keeping with previous literature (128-130, 132). In a human *post-mortem* study, increased numbers of CD8+ T cells were detected in the white matter of healthy older aged brains (>65 years), compared to younger aged brains (<58 years) (129). The overall profile of CD4+ and CD8+ T cells in the DLB brain appears to reflect a similar profile to that observed in healthy ageing brains. This is further supported by similar CD8:CD4 T cell ratios in both control and DLB groups.

Further insights into the T cell profile in the DLB brain were gained through comparison of different T cell subsets between groups. Notable findings were increased numbers of CD4+ T cells, Tbet+ T cells and GATA3+ T cells in DLB brains, specifically within total brain matter and the parenchymal compartment of grey matter. The presence of increased CD4+ T cells within these compartments, implicates increased recruitment of Th1 and Th2 cells into the DLB brain. Tbet+ T cells were detected in higher numbers than GATA3+ T cells, with the latter representing the lowest population of T cell subset in both groups. This raises the possibility of a predominant

proinflammatory Th1 cell response and is further supported by the increased ratio of Tbet:GATA3 T cells within grey matter parenchyma in the DLB group. The regulation of immune responses would likely depend on the balance between cytokines expressed by Th1 and Th2 cells. It can be hypothesised that T cell responses in DLB balance in favour of Th1 cells contributing to a proinflammatory environment, however the lack of data regarding cytokine expression in this study limits evaluation of potential Th2 cell responses. Th2 cells are generally considered to be neuroprotective and can supress Th1 cell responses through expression of IL-4 (104). Despite being present in lower numbers, Th2 cell reactivity in DLB may still contribute to a downregulation of proinflammatory Th1 cell responses.

The lack of association between T cells and neuropathology implies that cerebral T cell infiltration may occur independently of protein deposition in DLB, however this does not exclude interactions between T cells and α-syn. The occurrence of α-syn in the periphery, as well as drainage of α-syn into the lymphatic system provides possible mechanisms for T cell activation and recruitment into the brain. Following activation in the periphery, Th1 and Th2 cells may infiltrate the brain where they recognise α-syn derived antigens presented on MHCII expressed by microglia. The associations found between Tbet+ T cells and FcγR CD64 in DLB grey matter support potential interactions between Th1 cells and microglia, possibly contributing to increased phagocytic activity. However, these mechanisms remain unclear, particularly as previous *post-mortem* brain studies have revealed a lack of microglial activation in DLB (95-97).

When considering the mechanism of T cell entry into the brain, Th2 cells have been shown to migrate in higher numbers than Th1 cells across human adult brain endothelial cell monolayers, suggesting the BBB preferentially protects the brain from proinflammatory Th1 cells (211). The authors proposing this examined brain tissue taken from the temporal lobes of young adults with intractable epilepsy (211). This cohort may therefore not reflect DLB subjects or aged controls. In DLB, the integrity of the BBB is altered as evidenced in a recent study using DCE-MRI. BBB permeability was higher within the cerebral cortex of DLB participants, compared to AD and control groups (212). A more permeable BBB in DLB may explain the mechanism of increased Th1 cell infiltration into the brain. It is worth noting that there were higher numbers of Th1 cells compared to Th2 cells in control brains which does not support a preferential restriction of Th1 cells into normal physiologically aged brains.

An alternative route of T cell infiltration into the brain parenchyma is migration from the CSF through the ependymal layer of the lateral ventricle. One study examining the recruitment of Aβ-specific CD4+ T cell subsets via the lateral ventricle in mice, demonstrated increased infiltration of Th1 cells in comparison to Th2 and Th17 cell subsets. The authors proposed that Th1 cells are more effective in migrating into the brain parenchyma to target their cognate antigen (125). In

relation to DLB, peripheral α-syn-specific Th1 cells may have the capability to infiltrate the lateral ventricle via the choroid plexus and preferentially migrate across the ependymal cell layer into the brain parenchyma. However, it is important to consider that mechanisms of T cell infiltration in mice may not be replicated in humans. Additionally, it remains unclear whether Th1 cells recruited the DLB brain are indeed specific to α-syn or co-morbid AD pathology.

Associations between CD32b with both CD8+ T cells and Tbet+ cells in total grey matter infer potential interactions between Tc1 cells and neurons expressing CD32b in DLB. These interactions do not appear to be dependent on increased CD8+ T cell infiltration. The role of Tc1 cells in DLB is yet to be established, although it has been proposed that interactions between CD8+ T cells and neurons can directly result in neuronal cell death, as well as damage to dendrites in grey matter (213). Although CD32b does not directly engage CD8+ T cells, Tc1 associated cytokines could promote neuronal MHCI expression and increase neuronal vulnerability to cytotoxic injury.

Overall, significant differences have been found in T cell subsets present in the brain between DLB and controls. **Figure 5.1** illustrates a proposed profile of T cells in the DLB brain based on the results of this study and previous literature.

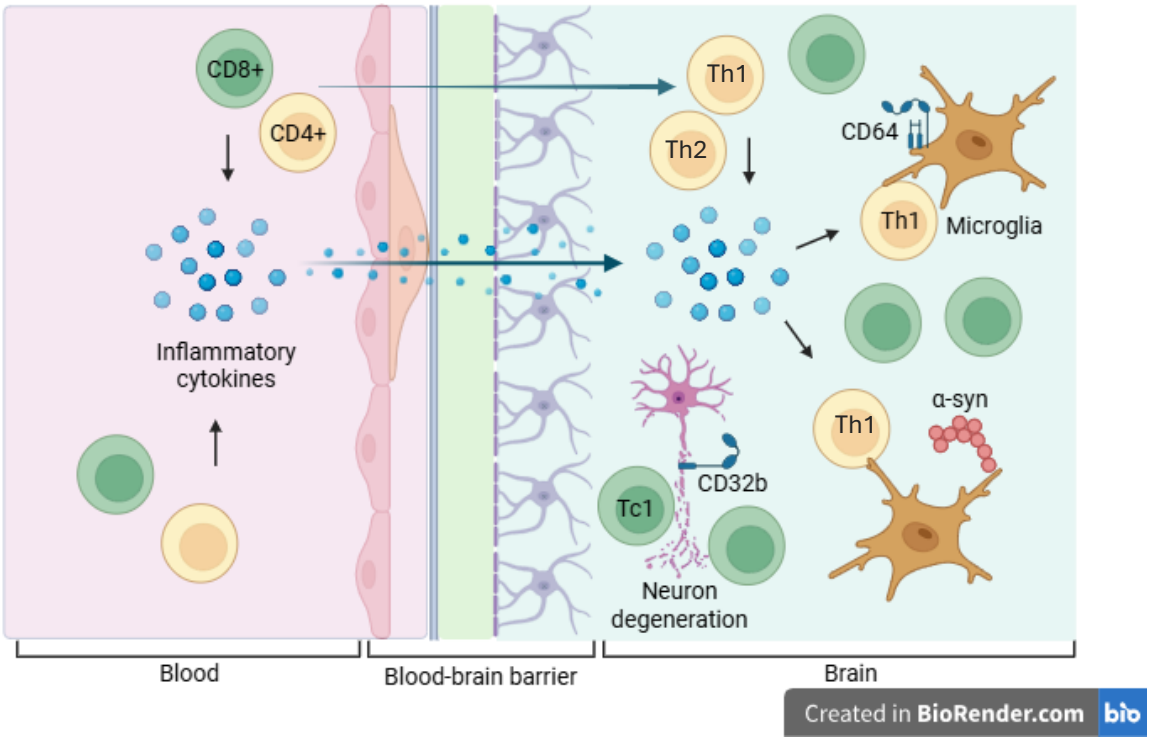

Figure 5.1 The potential profile of cerebral T cells in DLB
Increased numbers of Th1 and Th2 cells infiltrate the DLB brain through a more permeable BBB. Following recognition of α-syn derived antigens, Th1 cells promote proinflammatory responses via interactions with microglia. Additionally, Tc1 cells interact with neurons expressing CD32b, contributing to neuronal damage. Created by Biorender.com.

5.1.7 Strengths and limitations

This study includes the largest sample size to date for the examination of T cells in the human DLB brain, providing a higher level of power to detect significant differences. The DLB and control groups were well matched for age, sex and *post-mortem* delay to limit confounding factors. However, there was a lack of clinical information regarding infection or inflammation at the time of death, preventing comparison between groups. The use of *post-mortem* human brain tissue is an additional strength of the study. This provided a true representation of the human brain in DLB and did not rely on the use of animal models, which may not replicate disease processes accurately. DLB cases with co-existing AD pathology were minimised by the inclusion of cases with a Braak ptau score of 3 or below. Cases with a neuropathological diagnosis of cerebral amyloid angiopathy or argyrophilic grain disease were excluded from analysis to remove potential confounding effects associated with these comorbidities.

The existing cohort of cases did not include adequate numbers of tissue slides to enable inclusion of all eligible cases, resulting in reduced sample sizes for the T cell markers Foxp3, Tbet and GATA3. This may have influenced the power of the study to detect significant differences for those markers. Ideally, additional cases would have been sourced to maintain the sample size, however, resource constraints did not allow for this.

The same region of the brain was examined in each case which provided consistency of sampling. This could be considered a limitation as the single neocortical area examined may not represent the T cell profile and distribution of neuropathology in other brain regions. For example, T cell alterations in cases where LRP is prominent in limbic, brainstem and amygdala areas may not have been accurately represented. Evidence of an altered T cell profile in different brain regions including the brainstem and amygdala was provided in a *post-mortem* study in PDD (158). An alternative methodology would have been to examine several cortical and subcortical brain regions, however, a restriction to one area was maintained due to limited resources.

A further limitation is the use of *post-mortem* brain tissue which largely examines late-stage disease. It is possible that that T cell responses show variation according to disease course. An *in vivo* brain imaging study using TSPO PET reported increased TSPO ligand binding in DLB cases of mild severity and reduced binding in DLB cases of moderate to severe severity (89). This raises the possibility of microglial activation and subsequent interactions with T cells, being specific to early stages of disease. *Post-mortem* brain tissue from subjects in early stages of DLB would enable exploration of earlier disease mechanisms, however these cases would not be as readily available and would be unlikely to allow for a large sample size.

The quantification of T cell subsets in the DLB brain is a novel area of research that had not been previously explored. The detection of Foxp3+, Tbet+ and GATA3+ T cells in this study has revealed important information on the profile T cell subsets in the brain. However, the absence of double staining means it was not possible to confirm if these subsets belong to CD4+ or CD8+ T cell populations. Double immunohistochemistry would allow investigation of T cell marker co-localisation to further define specific T cell subsets.

CXCL12 and CXCR4 markers were not analysed due to inadequate optimisation of staining. Immunostaining for CXCL12 provided minimal areas of positive staining and positive staining for CXCR4 was not specific to T cells. CXCL12 and CXCR4 markers were successfully examined in a previous *post-mortem* study (161) and the same primary antibodies were sourced for this study. It is important to consider the different methodology used in the previous study which included fluorescence confocal microscopy. This allows for higher definition, the elimination of out-of-focus flare and may have enabled more accurate visualisation of the positive staining. Continued trials of primary antibody optimisation or the use of fluorescence confocal microscopy could allow for successful experiments in the future.

QuPath has been previously validated as a method for T cell detection in a study using *post-mortem* human brain tissue (193). All analysis was performed whilst blinded to groups using the same version of QuPath software. This prevented bias and ensured consistency during T cell detection. During T cell quantification, all positive detections were visualised and defined to be either parenchymal or perivascular. Due to the slide images representing two-dimensional sections of brain tissue, T cells within perpendicular capillaries may have been missed resulting in the number of perivascular T cells being underrepresented. Combined immunostaining with CD31, a marker for endothelial cells, would be an appropriate method to further investigate the distribution of blood vessels in relation to T cells.

5.1.8 Implications for future work

The identification of an altered profile of cerebral T cells in DLB warrants further investigation to improve our understanding of the adaptive immune response and how this may be contributing to disease pathogenesis in DLB.

The profile of T cell subsets could be further defined using multiplex immunohistochemistry, allowing for the identification of specific Th and Tc subsets. For example, the T cell markers CD3, CD4 and CD8 could be immunolabeled with Foxp3, Tbet and GATA3 T cell markers. Markers of inflammation and neuropathology could be included to examine the localisation of T cells to microglia and protein deposits.

Previous studies in LBD have investigated the expression of cytokines in *post-mortem* brain tissue to indicate T cell immunoreactivity, supporting the presence of different T cell subsets (144, 158, 161). Double immunolabelling using antibody combinations such as IFN-γ/CD4 and IFN-γ/CD8 could be used to further examine Th1 and Tc1 cell responses. Similarly, cytokines IL-4 and IL-10 could determine T cell reactivity associated with Th2/Tc2 and Treg/Ts cells, respectively. The T cell subset, Th17 was not explored in this study but has previously been identified in LBD brains (161). I propose that future work investigates the presence of Th17 and Tc17 cells in the DLB brain. Immunohistochemistry using the transcription factor RORγt and/or associated cytokine IL-17A could be used to achieve this.

There are several additional markers that could be assessed when examining T cell responses in the brain. As previously discussed, immunohistochemistry using CD31 could be conducted to investigate the relationship between vascular density and T cell infiltration. Immunohistochemistry using markers of BBB permeability such as albumin, fibrinogen and IgG may be helpful to demonstrate a potential route of T cell transmigration into the brain, particularly in areas where there are positive correlations between T cell markers and CD31. CD69 is an early marker of T cell activation and a key marker of TRM cells. This marker could be used to confirm T cell activation and retention of T cells in the brain. The possibility of antigen-specific T cells could be further examined by investigating the expression of antigen Kiel 67 (Ki-67), a marker of T cell proliferation after antigen stimulation. This would provide insight into whether T cells are entering the brain due to an antigen-specific response or through an alternative mechanism, such as bystander activation.

An alternative method for examining T cells in *post-mortem* brain tissue is to use reverse transcription quantitative polymerase chain reaction (RT-qPCR). This involves the extraction of total ribonucleic acid (RNA) from isolated T cells, before being reversely transcribed to complementary deoxyribonucleic acid (cDNA). Specific primers are then used to determine the expression of T cell marker genes such as transcription factors and T cell associated cytokines. The disadvantage of using this technique is that it does not provide absolute numbers of T cells or distinguish whether gene expression is from within the parenchyma or perivascular compartments. Using this method alongside immunohistochemistry could therefore be beneficial. Another method of T cell detection in the brain is spatial transcriptomics which allows mapping of gene expression. In contrast to RT-qPCR, this technique enables simultaneous detection of multiple T cell markers and spatial information, including the location of T cells relative to blood vessels and glial cells. I propose that an optimal method would involve spatial transcriptomics combined with immunohistochemistry. This would allow for validation of T cell subsets and information on T cell location relative to protein deposits such as α-syn.

Future *post-mortem* studies would ideally include multiple brain regions rather than a single area, to investigate whether the profile of T cells differ by brain location. This may allow for the additional detection of correlations between T cells and neuropathology. Further correlations between T cells and duration of disease could be performed to examine alterations in the profile of T cells throughout the disease course. This would require brain banks to have detailed medical histories and ideally objective measures of disease severity. In recent years, in-vivo labelling of T cells has developed using radioactive tracers and PET imaging. The clinical application of this method is currently limited due to the potential risks of impaired T cell function and neurotoxicity (214). With ongoing advancements in this field, a direction for future research would be the investigation of temporal associations between T cell infiltration and clinical features using in-vivo neuroimaging modalities.

The ideal future study would aim to define the profile of T cells in the blood, CSF and brain in the same cohort of DLB cases. A longitudinal, prospective study including a large cohort of DLB cases would allow for regular clinical assessments, blood and CSF collection prior to *post-mortem* brain analysis. The required resources for such a study could be achieved through collaboration of international research groups and brain banks.

5.1.9 Concluding remarks

DLB is the second most common neurodegenerative cause of dementia, yet it remains an under-researched area. There is growing evidence to support a role for inflammation in the pathogenesis of neurodegenerative diseases, but to date the adaptive immune profile in DLB has not been extensively investigated.

This study has revealed novel findings in the profile of T cells in the DLB brain. Increased infiltration of CD4+, Tbet+ and GATA3+ T cells have implicated the involvement of Th1 and Th2 cells in the disease process, with T cell ratios supporting a predominant proinflammatory T cell response. Associations with inflammatory markers indicate interactions between recruited T cells with both microglia and neurons, potentially contributing to synaptic dysfunction and neurodegeneration.

The altered T cell profile observed in the DLB brain has clinical implications, such as the potential for T cell modulation. For example, enhancing Treg cell populations may have therapeutic benefit by shifting immune responses towards a neuroprotective profile. Further analysis of T cell subsets in the blood, CSF and brain in DLB is warranted to improve our knowledge of disease mechanisms and guide the development of immunotherapies.

Appendix A

Immunohistochemistry Protocol (Boche Laboratory)

1. Rehydration
Clearene 1: 10 mins
Clearene 2: 10 mins
100% Ethanol 1: 5 mins
100% Ethanol 2: 5 mins
70% Ethanol 2: 5 mins
(transfer slides into a container)
Tap water
Distilled water

2. Blocking endogenous peroxidase: 3% H_2O_2 (from 30% stock; 1/10) in Methanol, 10 mins RT (e.g. if you have 5.9 ml Methanol take 590 µl out and add 590 µl of 30% H_2O_2; use *universals tube* to make solution and green tray(s) to lay slides down)
OR ImmPRESS Kit: blocking agent; 10 mins RT.

3. TBS wash: 3x 10 secs RT

4. Antigen retrieval (method depends on the antibody)

- *Heat-mediated* (microwave or pressure cooker)

Microwave method: Slides, in plastic racks (with a handle for small slides and without one for the large ones), are placed into the *plastic white square containers* and microwaved (50% power; Sharp microwave, R-27STM-A 800W) in selected solution (~ 330 ml) for 25 mins (small slides) and 35 mins (large slides); after this, the containers are taken out (wear insulated large gloves when removing them from the microwave – caution: extremely hot) and filled with running cold tap water until cool down; 1-2 mins

Pressure cooker method: see the HRU protocol
Solutions:
- 1 mM **EDTA buffer** pH 8 (0.37 g EDTA in 1L dH_2O, pH to 8 with ~ 8 ml of 0.1 M NaOH); microwave with slides
- 10 mM **Citrate buffer** pH 6 (2.1 g citric acid-monoxydrate in 1L dH_2O, pH to 6 with ~ 25 ml of 1 M NaOH; add 0.05% Tween 20 (0.5 ml) - optional); microwave with slides

- *Enzymatic*

- 0.5% Pronase, 20 mins, RT (from 5% stock; 1/10; e.g. 40 µl of 5% pronase in 360 µl of TBS; use either *1.5 ml eppendorf* tubes or *5 ml bijoux*)

5. TBS wash: 3x 10 secs RT

6. Saturation step with blocking solution [depends on the host species used for production of secondary antibodies; e.g. for *anti-rabbit* antibody made in swine use blocking medium (contains DMEM, foetal calf serum and bovine serum albumin) made and aliquoted by HRU (kept at -20°C); for *anti-mouse* antibody made in goat use 5% normal goat serum – NGS (kept at 4oC; HRU fridge) and for *anti-goat* antibody made in rabbit use 5% normal rabbit serum – NRS (kept at 4oC; HRU fridge), both diluted in TBS (e.g. 50 µl of NGS or NRS in 950 µl of TBS); use either *1.5 ml eppendorf* tubes or *5 ml bijoux*] 20 mins RT

7. Primary antibody (usually kept in LD78, in the fridge or at -20°C), 90 mins RT or O/N fridge or O/N RT (e.g. if dilution is 1/400 use 1 µl of the antibody in 400 µl TBS or Dako diluent; use either *1.5 ml eppendorf* tubes or *5 ml bijoux*)

8. TBS wash: 3x 10 secs RT

9. Secondary antibody: (fridge, HRU: Delphine's box in fridge in small room or tray in fridge in main room), 30 mins RT [e.g. biotinylated goat anti-mouse or biotinylated swine anti-rabbit or biotinylated rabbit anti-goat (if dilution is 1/400 use 1 µl of the antibody in 400 µl TBS or Dako diluent; use either *1.5 ml eppendorf* tubes or *5 ml bijoux*)
OR: **ImPRESS Polymer Kit:** ImmPRESS polymer reagent; 30 mins RT

10. TBS wash: 3x 10 secs RT

11. ABC-HRP complex (A: 1/75 and B: 1/75) Delphine's box, fridge, HRU; make it at the same time as secondary antibody; mix it well, 30 mins RT (e.g. 5.3 µl of A and 5.3 µl B in 400 µl of TBS; use either *1.5 ml eppendorf* tubes or *5 ml bijoux*)
OR: **ImPRESS Polymer Kit**

12. TBS wash: 3x 10 secs RT

13. Chromogenic reaction with DAB (Delphine's box, fridge, HRU; according to manufactory's instructions: 2 drops of buffer, 4 drops of DAB, 2 drops of H_2O_2 in 5 ml distilled water; use either *1.5 ml eppendorf* tubes or *5 ml bijoux*; duration of the reaction depends on the antibody and tissue)

14. Stop the DAB reaction with TBS and then with distilled water (transfer slides back to rack(s))

15. Counterstaining with Haematoxylin (by the waste sink) 20 secs RT

16. Stop the reaction with distilled water (poured into a glass dish) then tap water (poured into a slightly stained plastic container)

17. Dehydration (under the hood on the left; tip the solution out between the steps)

70% Ethanol: 1 min
100% Ethanol 1: 1 min
100% Ethanol 2: 1 min
Clearene 1: 3 mins
Clearene 2: 3 mins
Clearene 3: 3 mins

18. Mounting with Pertex manually (do not put too much of the mount) or using a machine

19. Check the reaction under the microscope.

Appendix B

Immunohistochemistry protocol (ImmPRESS Kit)

Staining procedure using HRP Horse Anti-Rabbit IgG Polymer Detection Kit

1. For paraffin sections, deparaffinize and hydrate tissue sections through xylenes or other clearing agents and graded alcohol series. For frozen sections or cell preparations fix with acetone or an appropriate fixative for the antigen under study, if necessary. Wash for 5 minutes in tap water.

2. If antigen unmasking is required, perform this procedure using a Vector® Antigen Unmasking Solution, Citrate-based, pH 6.0 (H-3300) or Tris-based, pH 9.0 (H-3301). 3. If quenching of endogenous peroxidase activity is required, incubate the sections in BLOXALL® Blocking Solution (SP-6000) for 10 minutes.

4. Wash in buffer for 5 minutes.

5. Incubate sections for 20 minutes with Normal Horse Serum, 2.5%.

6. Tip off excess serum from sections.

7. Incubate with rabbit primary antibody diluted in appropriate antibody diluent solution, such as diluted normal horse serum or BSA.

8. Wash in buffer for 5 minutes.

9. Incubate for 30 minutes with ImmPRESS Polymer Reagent.

10. Wash for 2 x 5 minutes in buffer.

11. Incubate in peroxidase substrate solution (not included) until desired stain intensity develops.

12. Rinse sections in tap water.

13. Counterstain (optional), clear and mount.

References

1. Collaborators GBDDF. Estimation of the global prevalence of dementia in 2019 and forecasted prevalence in 2050: an analysis for the Global Burden of Disease Study 2019. Lancet Public Health. 2022;7(2):e105-e25.

2. Velandia PP, Miller-Petrie MK, Chen C, Chakrabarti S, Chapin A, Hay S, et al. Global and regional spending on dementia care from 2000-2019 and expected future health spending scenarios from 2020-2050: An economic modelling exercise. EClinicalMedicine. 2022;45:101337.

3. Arvanitakis Z, Shah RC, Bennett DA. Diagnosis and Management of Dementia: Review. Jama. 2019;322(16):1589-99.

4. Hugo J, Ganguli M. Dementia and cognitive impairment: epidemiology, diagnosis, and treatment. Clin Geriatr Med. 2014;30(3):421-42.

5. World Health Organisation (WHO). The ICD-10 classification of mental and behavioural disorders. Geneva: World Health Organisation; 1993. p. 45-6.

6. Garre-Olmo J. [Epidemiology of Alzheimer's disease and other dementias]. Rev Neurol. 2018;66(11):377-86.

7. Chin KS, Teodorczuk A, Watson R. Dementia with Lewy bodies: Challenges in the diagnosis and management. Aust N Z J Psychiatry. 2019;53(4):291-303.

8. Outeiro TF, Koss DJ, Erskine D, Walker L, Kurzawa-Akanbi M, Burn D, et al. Dementia with Lewy bodies: an update and outlook. Mol Neurodegener. 2019;14(1):5.

9. Tolosa E, Garrido A, Scholz SW, Poewe W. Challenges in the diagnosis of Parkinson's disease. Lancet Neurol. 2021;20(5):385-97.

10. Aarsland D, Creese B, Politis M, Chaudhuri KR, Ffytche DH, Weintraub D, et al. Cognitive decline in Parkinson disease. Nat Rev Neurol. 2017;13(4):217-31.

11. Hely MA, Reid WG, Adena MA, Halliday GM, Morris JG. The Sydney multicenter study of Parkinson's disease: the inevitability of dementia at 20 years. Mov Disord. 2008;23(6):837-44.

12. McKeith IG, Boeve BF, Dickson DW, Halliday G, Taylor JP, Weintraub D, et al. Diagnosis and management of dementia with Lewy bodies: Fourth consensus report of the DLB Consortium. Neurology. 2017;89(1):88-100.

13. Walker Z, Possin KL, Boeve BF, Aarsland D. Lewy body dementias. Lancet. 2015;386(10004):1683-97.

14. Taylor JP, McKeith IG, Burn DJ, Boeve BF, Weintraub D, Bamford C, et al. New evidence on the management of Lewy body dementia. Lancet Neurol. 2020;19(2):157-69.

15. Vann Jones SA, O'Brien JT. The prevalence and incidence of dementia with Lewy bodies: a systematic review of population and clinical studies. Psychol Med. 2014;44(4):673-83.

16. Savica R, Grossardt BR, Bower JH, Ahlskog JE, Boeve BF, Graff-Radford J, et al. Survival and Causes of Death Among People With Clinically Diagnosed Synucleinopathies With Parkinsonism: A Population-Based Study. JAMA Neurol. 2017;74(7):839-46.

17. Sanford AM. Lewy Body Dementia. Clin Geriatr Med. 2018;34(4):603-15.

18. Merdes AR, Hansen LA, Jeste DV, Galasko D, Hofstetter CR, Ho GJ, et al. Influence of Alzheimer pathology on clinical diagnostic accuracy in dementia with Lewy bodies. Neurology. 2003;60(10):1586-90.

19. Prasad S, Katta MR, Abhishek S, Sridhar R, Valisekka SS, Hameed M, et al. Recent advances in Lewy body dementia: A comprehensive review. Dis Mon. 2023;69(5):101441.

20. Galvin JE, Duda JE, Kaufer DI, Lippa CF, Taylor A, Zarit SH. Lewy body dementia: the caregiver experience of clinical care. Parkinsonism Relat Disord. 2010;16(6):388-92.

21. Ojobo E, Walker Z. Dementia with Lewy Bodies. In: Katona C, Butler R, editors. Seminars in Old Age Psychiatry. College Seminars Series. 2 ed. Cambridge: Cambridge University Press; 2019. p. 88-100.

22. Fasano A, Canning CG, Hausdorff JM, Lord S, Rochester L. Falls in Parkinson's disease: A complex and evolving picture. Mov Disord. 2017;32(11):1524-36.

23. Ballard C, Grace J, McKeith I, Holmes C. Neuroleptic sensitivity in dementia with Lewy bodies and Alzheimer's disease. Lancet. 1998;351(9108):1032-3.

24. Williams MM, Xiong C, Morris JC, Galvin JE. Survival and mortality differences between dementia with Lewy bodies vs Alzheimer disease. Neurology. 2006;67(11):1935-41.

25. Mueller C, Ballard C, Corbett A, Aarsland D. The prognosis of dementia with Lewy bodies. Lancet Neurol. 2017;16(5):390-8.

26. Cummings JL. Dementia with lewy bodies: molecular pathogenesis and implications for classification. J Geriatr Psychiatry Neurol. 2004;17(3):112-9.

27. Stefanis L. α-Synuclein in Parkinson's disease. Cold Spring Harb Perspect Med. 2012;2(2):a009399.

28. Mehra S, Sahay S, Maji SK. α-Synuclein misfolding and aggregation: Implications in Parkinson's disease pathogenesis. Biochim Biophys Acta Proteins Proteom. 2019;1867(10):890-908.

29. Meade RM, Fairlie DP, Mason JM. Alpha-synuclein structure and Parkinson's disease - lessons and emerging principles. Mol Neurodegener. 2019;14(1):29.

30. Amin J, Erskine D, Donaghy PC, Surendranathan A, Swann P, Kunicki AP, et al. Inflammation in dementia with Lewy bodies. Neurobiol Dis. 2022;168:105698.

31. Ingelsson M. Alpha-Synuclein Oligomers-Neurotoxic Molecules in Parkinson's Disease and Other Lewy Body Disorders. Front Neurosci. 2016;10:408.

32. Calabresi P, Mechelli A, Natale G, Volpicelli-Daley L, Di Lazzaro G, Ghiglieri V. Alpha-synuclein in Parkinson’s disease and other synucleinopathies: from overt neurodegeneration back to early synaptic dysfunction. Cell Death & Disease. 2023;14(3):176.

33. Andersen KB, Hansen AK, Damholdt MF, Horsager J, Skjaerbaek C, Gottrup H, et al. Reduced Synaptic Density in Patients with Lewy Body Dementia: An [(11) C]UCB-J PET Imaging Study. Mov Disord. 2021;36(9):2057-65.

34. Kon T, Tomiyama M, Wakabayashi K. Neuropathology of Lewy body disease: Clinicopathological crosstalk between typical and atypical cases. Neuropathology. 2020;40(1):30-9.

35. Beach TG, Adler CH, Sue LI, Vedders L, Lue L, White Iii CL, et al. Multi-organ distribution of phosphorylated alpha-synuclein histopathology in subjects with Lewy body disorders. Acta Neuropathol. 2010;119(6):689-702.

36. Mougenot AL, Nicot S, Bencsik A, Morignat E, Verchère J, Lakhdar L, et al. Prion-like acceleration of a synucleinopathy in a transgenic mouse model. Neurobiol Aging. 2012;33(9):2225-8.

37. Ulusoy A, Phillips RJ, Helwig M, Klinkenberg M, Powley TL, Di Monte DA. Brain-to-stomach transfer of α-synuclein via vagal preganglionic projections. Acta Neuropathol. 2017;133(3):381-93.

38. Bohnen NI, Müller M, Frey KA. Molecular Imaging and Updated Diagnostic Criteria in Lewy Body Dementias. Curr Neurol Neurosci Rep. 2017;17(10):73.

39. Jellinger KA. Dementia with Lewy bodies and Parkinson's disease-dementia: current concepts and controversies. J Neural Transm (Vienna). 2018;125(4):615-50.

40. Howlett DR, Whitfield D, Johnson M, Attems J, O'Brien JT, Aarsland D, et al. Regional Multiple Pathology Scores Are Associated with Cognitive Decline in Lewy Body Dementias. Brain Pathol. 2015;25(4):401-8.

41. Barber R, Ballard C, McKeith IG, Gholkar A, O'Brien JT. MRI volumetric study of dementia with Lewy bodies: a comparison with AD and vascular dementia. Neurology. 2000;54(6):1304-9.

42. Jahn H. Memory loss in Alzheimer's disease. Dialogues Clin Neurosci. 2013;15(4):445-54.

43. Zhu H, Lu H, Wang F, Liu S, Shi Z, Gan J, et al. Characteristics of Cortical Atrophy and White Matter Lesions Between Dementia With Lewy Bodies and Alzheimer's Disease: A Case-Control Study. Front Neurol. 2021;12:779344.

44. Nedelska Z, Ferman TJ, Boeve BF, Przybelski SA, Lesnick TG, Murray ME, et al. Pattern of brain atrophy rates in autopsy-confirmed dementia with Lewy bodies. Neurobiol Aging. 2015;36(1):452-61.

45. Chatterjee A, Hirsch-Reinshagen V, Moussavi SA, Ducharme B, Mackenzie IR, Hsiung GR. Clinico-pathological comparison of patients with autopsy-confirmed Alzheimer's disease, dementia with Lewy bodies, and mixed pathology. Alzheimers Dement (Amst). 2021;13(1):e12189.

46. McKeith IG, Dickson DW, Lowe J, Emre M, O'Brien JT, Feldman H, et al. Diagnosis and management of dementia with Lewy bodies: third report of the DLB Consortium. Neurology. 2005;65(12):1863-72.

47. Braak H, Alafuzoff I, Arzberger T, Kretzschmar H, Del Tredici K. Staging of Alzheimer disease-associated neurofibrillary pathology using paraffin sections and immunocytochemistry. Acta Neuropathol. 2006;112(4):389-404.

48. Marshall JS, Warrington R, Watson W, Kim HL. An introduction to immunology and immunopathology. Allergy Asthma Clin Immunol. 2018;14(Suppl 2):49.

49. Chaplin DD. Overview of the immune response. J Allergy Clin Immunol. 2010;125(2 Suppl 2):S3-23.

50. Huber-Lang M, Lambris JD, Ward PA. Innate immune responses to trauma. Nat Immunol. 2018;19(4):327-41.

51. Franceschi C, Garagnani P, Parini P, Giuliani C, Santoro A. Inflammaging: a new immune-metabolic viewpoint for age-related diseases. Nat Rev Endocrinol. 2018;14(10):576-90.

52. Kasler H, Verdin E. How inflammaging diminishes adaptive immunity. Nat Aging. 2021;1(1):24-5.

53. Baylis D, Bartlett DB, Patel HP, Roberts HC. Understanding how we age: insights into inflammaging. Longev Healthspan. 2013;2(1):8.

54. Cunha LL, Perazzio SF, Azzi J, Cravedi P, Riella LV. Remodeling of the Immune Response With Aging: Immunosenescence and Its Potential Impact on COVID-19 Immune Response. Front Immunol. 2020;11:1748.

55. Soraci L, Corsonello A, Paparazzo E, Montesanto A, Piacenza F, Olivieri F, et al. Neuroinflammaging: A Tight Line Between Normal Aging and Age-Related Neurodegenerative Disorders. Aging Dis. 2024;15(4):1726-47.

56. Kinney JW, Bemiller SM, Murtishaw AS, Leisgang AM, Salazar AM, Lamb BT. Inflammation as a central mechanism in Alzheimer's disease. Alzheimers Dement (N Y). 2018;4:575-90.

57. Pasqualetti G, Brooks DJ, Edison P. The role of neuroinflammation in dementias. Curr Neurol Neurosci Rep. 2015;15(4):17.

58. Guan YH, Zhang LJ, Wang SY, Deng YD, Zhou HS, Chen DQ, et al. The role of microglia in Alzheimer's disease and progress of treatment. Ibrain. 2022;8(1):37-47.

59. Pan XD, Zhu YG, Lin N, Zhang J, Ye QY, Huang HP, et al. Microglial phagocytosis induced by fibrillar β-amyloid is attenuated by oligomeric β-amyloid: implications for Alzheimer's disease. Mol Neurodegener. 2011;6:45.

60. Ries M, Sastre M. Mechanisms of Aβ Clearance and Degradation by Glial Cells. Front Aging Neurosci. 2016;8:160.

61. Domingues C, da Cruz ESOAB, Henriques AG. Impact of Cytokines and Chemokines on Alzheimer's Disease Neuropathological Hallmarks. Curr Alzheimer Res. 2017;14(8):870-82.

62. Meda L, Cassatella MA, Szendrei GI, Otvos L, Jr., Baron P, Villalba M, et al. Activation of microglial cells by beta-amyloid protein and interferon-gamma. Nature. 1995;374(6523):647-50.

63. Hickman SE, Allison EK, El Khoury J. Microglial dysfunction and defective beta-amyloid clearance pathways in aging Alzheimer's disease mice. J Neurosci. 2008;28(33):8354-60.

64. Boche D, Perry VH, Nicoll JA. Review: activation patterns of microglia and their identification in the human brain. Neuropathol Appl Neurobiol. 2013;39(1):3-18.

65. Minett T, Classey J, Matthews FE, Fahrenhold M, Taga M, Brayne C, et al. Microglial immunophenotype in dementia with Alzheimer's pathology. J Neuroinflammation. 2016;13(1):135.

66. Karch CM, Goate AM. Alzheimer's disease risk genes and mechanisms of disease pathogenesis. Biol Psychiatry. 2015;77(1):43-51.

67. Heneka MT, Carson MJ, El Khoury J, Landreth GE, Brosseron F, Feinstein DL, et al. Neuroinflammation in Alzheimer's disease. Lancet Neurol. 2015;14(4):388-405.

68. Huang LT, Zhang CP, Wang YB, Wang JH. Association of Peripheral Blood Cell Profile With Alzheimer's Disease: A Meta-Analysis. Front Aging Neurosci. 2022;14:888946.

69. Zheng C, Zhou XW, Wang JZ. The dual roles of cytokines in Alzheimer's disease: update on interleukins, TNF-α, TGF-β and IFN-γ. Transl Neurodegener. 2016;5:7.

70. Togo T, Akiyama H, Iseki E, Kondo H, Ikeda K, Kato M, et al. Occurrence of T cells in the brain of Alzheimer's disease and other neurological diseases. J Neuroimmunol. 2002;124(1-2):83-92.

71. Merlini M, Kirabali T, Kulic L, Nitsch RM, Ferretti MT. Extravascular CD3+ T Cells in Brains of Alzheimer Disease Patients Correlate with Tau but Not with Amyloid Pathology: An Immunohistochemical Study. Neurodegener Dis. 2018;18(1):49-56.

72. Unger MS, Li E, Scharnagl L, Poupardin R, Altendorfer B, Mrowetz H, et al. CD8(+) T-cells infiltrate Alzheimer's disease brains and regulate neuronal- and synapse-related gene expression in APP-PS1 transgenic mice. Brain Behav Immun. 2020;89:67-86.

73. Chen X, Firulyova M, Manis M, Herz J, Smirnov I, Aladyeva E, et al. Microglia-mediated T cell infiltration drives neurodegeneration in tauopathy. Nature. 2023;615(7953):668-77.

74. Li JQ, Tan L, Yu JT. The role of the LRRK2 gene in Parkinsonism. Mol Neurodegener. 2014;9:47.

75. Wallings RL, Herrick MK, Tansey MG. LRRK2 at the Interface Between Peripheral and Central Immune Function in Parkinson's. Front Neurosci. 2020;14:443.

76. Witoelar A, Jansen IE, Wang Y, Desikan RS, Gibbs JR, Blauwendraat C, et al. Genome-wide Pleiotropy Between Parkinson Disease and Autoimmune Diseases. JAMA Neurol. 2017;74(7):780-92.

77. Mogi M, Harada M, Riederer P, Narabayashi H, Fujita K, Nagatsu T. Tumor necrosis factor-alpha (TNF-alpha) increases both in the brain and in the cerebrospinal fluid from parkinsonian patients. Neurosci Lett. 1994;165(1-2):208-10.

78. Hunot S, Dugas N, Faucheux B, Hartmann A, Tardieu M, Debré P, et al. FcepsilonRII/CD23 is expressed in Parkinson's disease and induces, in vitro, production of nitric oxide and tumor necrosis factor-alpha in glial cells. J Neurosci. 1999;19(9):3440-7.

79. Harms AS, Thome AD, Yan Z, Schonhoff AM, Williams GP, Li X, et al. Peripheral monocyte entry is required for alpha-Synuclein induced inflammation and Neurodegeneration in a model of Parkinson disease. Exp Neurol. 2018;300:179-87.

80. Thakur P, Breger LS, Lundblad M, Wan OW, Mattsson B, Luk KC, et al. Modeling Parkinson's disease pathology by combination of fibril seeds and α-synuclein overexpression in the rat brain. Proc Natl Acad Sci U S A. 2017;114(39):E8284-e93.

81. Guerreiro R, Ross OA, Kun-Rodrigues C, Hernandez DG, Orme T, Eicher JD, et al. Investigating the genetic architecture of dementia with Lewy bodies: a two-stage genome-wide association study. Lancet Neurol. 2018;17(1):64-74.

82. Chia R, Sabir MS, Bandres-Ciga S, Saez-Atienzar S, Reynolds RH, Gustavsson E, et al. Genome sequencing analysis identifies new loci associated with Lewy body dementia and provides insights into its genetic architecture. Nat Genet. 2021;53(3):294-303.

83. Zhu P, Jin Z, Wu S, Gao S, He Y, Hu S, et al. Genome-wide association study provides insights into the genetic basis of Lewy body dementia. Mol Psychiatry. 2025;30(12):5813-27.

84. King E, O'Brien JT, Donaghy P, Morris C, Barnett N, Olsen K, et al. Peripheral inflammation in prodromal Alzheimer's and Lewy body dementias. J Neurol Neurosurg Psychiatry. 2018;89(4):339-45.

85. de Rooij SE, van Munster BC, Korevaar JC, Levi M. Cytokines and acute phase response in delirium. J Psychosom Res. 2007;62(5):521-5.

86. van Munster BC, Korevaar JC, Zwinderman AH, Levi M, Wiersinga WJ, De Rooij SE. Time-course of cytokines during delirium in elderly patients with hip fractures. J Am Geriatr Soc. 2008;56(9):1704-9.

87. Gore RL, Vardy ER, O'Brien JT. Delirium and dementia with Lewy bodies: distinct diagnoses or part of the same spectrum? J Neurol Neurosurg Psychiatry. 2015;86(1):50-9.

88. Iannaccone S, Cerami C, Alessio M, Garibotto V, Panzacchi A, Olivieri S, et al. In vivo microglia activation in very early dementia with Lewy bodies, comparison with Parkinson's disease. Parkinsonism Relat Disord. 2013;19(1):47-52.

89. Surendranathan A, Su L, Mak E, Passamonti L, Hong YT, Arnold R, et al. Early microglial activation and peripheral inflammation in dementia with Lewy bodies. Brain. 2018;141(12):3415-27.

90. Mackenzie IR. Activated microglia in dementia with Lewy bodies. Neurology. 2000;55(1):132-4.

91. Imamura K, Hishikawa N, Ono K, Suzuki H, Sawada M, Nagatsu T, et al. Cytokine production of activated microglia and decrease in neurotrophic factors of neurons in the hippocampus of Lewy body disease brains. Acta Neuropathol. 2005;109(2):141-50.

92. Shepherd CE, Thiel E, McCann H, Harding AJ, Halliday GM. Cortical inflammation in Alzheimer disease but not dementia with Lewy bodies. Arch Neurol. 2000;57(6):817-22.

93. Streit WJ, Xue QS. Microglia in dementia with Lewy bodies. Brain Behav Immun. 2016;55:191-201.

94. Bachstetter AD, Van Eldik LJ, Schmitt FA, Neltner JH, Ighodaro ET, Webster SJ, et al. Disease-related microglia heterogeneity in the hippocampus of Alzheimer's disease, dementia with Lewy bodies, and hippocampal sclerosis of aging. Acta Neuropathol Commun. 2015;3:32.

95. Amin J, Holmes C, Dorey RB, Tommasino E, Casal YR, Williams DM, et al. Neuroinflammation in dementia with Lewy bodies: a human post-mortem study. Transl Psychiatry. 2020;10(1):267.

96. Rajkumar AP, Bidkhori G, Shoaie S, Clarke E, Morrin H, Hye A, et al. Postmortem Cortical Transcriptomics of Lewy Body Dementia Reveal Mitochondrial Dysfunction and Lack of Neuroinflammation. Am J Geriatr Psychiatry. 2020;28(1):75-86.

97. Erskine D, Ding J, Thomas AJ, Kaganovich A, Khundakar AA, Hanson PS, et al. Molecular changes in the absence of severe pathology in the pulvinar in dementia with Lewy bodies. Mov Disord. 2018;33(6):982-91.

98. Bernaus A, Blanco S, Sevilla A. Glia Crosstalk in Neuroinflammatory Diseases. Front Cell Neurosci. 2020;14:209.

99. Caplan IF, Maguire-Zeiss KA. Toll-Like Receptor 2 Signaling and Current Approaches for Therapeutic Modulation in Synucleinopathies. Front Pharmacol. 2018;9:417.

100. Tian L, Ma L, Kaarela T, Li Z. Neuroimmune crosstalk in the central nervous system and its significance for neurological diseases. J Neuroinflammation. 2012;9:155.

101. Schetters STT, Gomez-Nicola D, Garcia-Vallejo JJ, Van Kooyk Y. Neuroinflammation: Microglia and T Cells Get Ready to Tango. Front Immunol. 2017;8:1905.

102. Raphael I, Joern RR, Forsthuber TG. Memory CD4(+) T Cells in Immunity and Autoimmune Diseases. Cells. 2020;9(3).

103. Caza T, Landas S. Functional and Phenotypic Plasticity of CD4(+) T Cell Subsets. Biomed Res Int. 2015;2015:521957.

104. Coder B, Wang W, Wang L, Wu Z, Zhuge Q, Su DM. Friend or foe: the dichotomous impact of T cells on neuro-de/re-generation during aging. Oncotarget. 2017;8(4):7116-37.

105. Mittrücker HW, Visekruna A, Huber M. Heterogeneity in the differentiation and function of $CD8^+$ T cells. Arch Immunol Ther Exp (Warsz). 2014;62(6):449-58.

106. Konya C, Goronzy JJ, Weyand CM. Treating autoimmune disease by targeting CD8(+) T suppressor cells. Expert Opin Biol Ther. 2009;9(8):951-65.

107. Koh CH, Lee S, Kwak M, Kim BS, Chung Y. CD8 T-cell subsets: heterogeneity, functions, and therapeutic potential. Exp Mol Med. 2023;55(11):2287-99.

108. Gray JI, Westerhof LM, MacLeod MKL. The roles of resident, central and effector memory CD4 T-cells in protective immunity following infection or vaccination. Immunology. 2018;154(4):574-81.

109. Xu W, Larbi A. Markers of T Cell Senescence in Humans. Int J Mol Sci. 2017;18(8).

110. Laphanuwat P, Gomes DCO, Akbar AN. Senescent T cells: Beneficial and detrimental roles. Immunol Rev. 2023.

111. Gemechu JM, Bentivoglio M. T Cell Recruitment in the Brain during Normal Aging. Front Cell Neurosci. 2012;6:38.

112. Evans FL, Dittmer M, de la Fuente AG, Fitzgerald DC. Protective and Regenerative Roles of T Cells in Central Nervous System Disorders. Front Immunol. 2019;10:2171.

113. Marchetti L, Engelhardt B. Immune cell trafficking across the blood-brain barrier in the absence and presence of neuroinflammation. Vasc Biol. 2020;2(1):H1-H18.

114. Greenwood J, Heasman SJ, Alvarez JI, Prat A, Lyck R, Engelhardt B. Review: leucocyte-endothelial cell crosstalk at the blood-brain barrier: a prerequisite for successful immune cell entry to the brain. Neuropathol Appl Neurobiol. 2011;37(1):24-39.

115. Weng NP. Aging of the immune system: how much can the adaptive immune system adapt? Immunity. 2006;24(5):495-9.

116. Yosri M, Dokhan M, Aboagye E, Al Moussawy M, Abdelsamed HA. Mechanisms governing bystander activation of T cells. Front Immunol. 2024;15:1465889.

117. Galea I, Bernardes-Silva M, Forse PA, van Rooijen N, Liblau RS, Perry VH. An antigen-specific pathway for CD8 T cells across the blood-brain barrier. J Exp Med. 2007;204(9):2023-30.

118. Hickey WF, Hsu BL, Kimura H. T-lymphocyte entry into the central nervous system. J Neurosci Res. 1991;28(2):254-60.

119. Carrithers MD, Visintin I, Kang SJ, Janeway CA, Jr. Differential adhesion molecule requirements for immune surveillance and inflammatory recruitment. Brain. 2000;123 (Pt 6):1092-101.

120. Krakowski ML, Owens T. Naive T lymphocytes traffic to inflamed central nervous system, but require antigen recognition for activation. Eur J Immunol. 2000;30(4):1002-9.

121. Engelhardt B, Ransohoff RM. Capture, crawl, cross: the T cell code to breach the blood-brain barriers. Trends Immunol. 2012;33(12):579-89.

122. Ransohoff RM, Kivisäkk P, Kidd G. Three or more routes for leukocyte migration into the central nervous system. Nat Rev Immunol. 2003;3(7):569-81.

123. McManus RM, Mills KH, Lynch MA. T Cells-Protective or Pathogenic in Alzheimer's Disease? J Neuroimmune Pharmacol. 2015;10(4):547-60.

124. Reboldi A, Coisne C, Baumjohann D, Benvenuto F, Bottinelli D, Lira S, et al. C-C chemokine receptor 6-regulated entry of TH-17 cells into the CNS through the choroid plexus is required for the initiation of EAE. Nat Immunol. 2009;10(5):514-23.

125. Fisher Y, Strominger I, Biton S, Nemirovsky A, Baron R, Monsonego A. Th1 polarization of T cells injected into the cerebrospinal fluid induces brain immunosurveillance. J Immunol. 2014;192(1):92-102.

126. Rustenhoven J, Kipnis J. Bypassing the blood-brain barrier. Science. 2019;366(6472):1448-9.

127. Smolders J, Remmerswaal EB, Schuurman KG, Melief J, van Eden CG, van Lier RA, et al. Characteristics of differentiated CD8(+) and CD4 (+) T cells present in the human brain. Acta Neuropathol. 2013;126(4):525-35.

128. Smolders J, Heutinck KM, Fransen NL, Remmerswaal EBM, Hombrink P, Ten Berge IJM, et al. Tissue-resident memory T cells populate the human brain. Nat Commun. 2018;9(1):4593.

129. Moreno-Valladares M, Silva TM, Garcés JP, Saenz-Antoñanzas A, Moreno-Cugnon L, Álvarez-Satta M, et al. CD8(+) T cells are present at low levels in the white matter with physiological and pathological aging. Aging (Albany NY). 2020;12(19):18928-41.

130. Stichel CC, Luebbert H. Inflammatory processes in the aging mouse brain: participation of dendritic cells and T-cells. Neurobiol Aging. 2007;28(10):1507-21.

131. Clevers H, Alarcon B, Wileman T, Terhorst C. The T cell receptor/CD3 complex: a dynamic protein ensemble. Annu Rev Immunol. 1988;6:629-62.

132. Hara Y, Rapp PR, Morrison JH. Neuronal and morphological bases of cognitive decline in aged rhesus monkeys. Age (Dordr). 2012;34(5):1051-73.

133. Batterman KV, Cabrera PE, Moore TL, Rosene DL. T Cells Actively Infiltrate the White Matter of the Aging Monkey Brain in Relation to Increased Microglial Reactivity and Cognitive Decline. Front Immunol. 2021;12:607691.

134. Ellwardt E, Walsh JT, Kipnis J, Zipp F. Understanding the Role of T Cells in CNS Homeostasis. Trends Immunol. 2016;37(2):154-65.

135. Hrastelj J, Andrews R, Loveless S, Morgan J, Bishop SM, Bray NJ, et al. CSF-resident CD4(+) T-cells display a distinct gene expression profile with relevance to immune surveillance and multiple sclerosis. Brain Commun. 2021;3(3):fcab155.

136. de Graaf MT, Smitt PA, Luitwieler RL, van Velzen C, van den Broek PD, Kraan J, et al. Central memory CD4+ T cells dominate the normal cerebrospinal fluid. Cytometry B Clin Cytom. 2011;80(1):43-50.

137. Smolders J, van Luijn MM, Hsiao CC, Hamann J. T-cell surveillance of the human brain in health and multiple sclerosis. Semin Immunopathol. 2022.

138. Rodriguez IJ, Lalinde Ruiz N, Llano León M, Martínez Enríquez L, Montilla Velásquez MDP, Ortiz Aguirre JP, et al. Immunosenescence Study of T Cells: A Systematic Review. Front Immunol. 2020;11:604591.

139. Pfister G, Weiskopf D, Lazuardi L, Kovaiou RD, Cioca DP, Keller M, et al. Naive T cells in the elderly: are they still there? Ann N Y Acad Sci. 2006;1067:152-7.

140. Goronzy JJ, Fulbright JW, Crowson CS, Poland GA, O'Fallon WM, Weyand CM. Value of immunological markers in predicting responsiveness to influenza vaccination in elderly individuals. J Virol. 2001;75(24):12182-7.

141. Zhang J, Ma D, Zhu X, Qu X, Ji C, Hou M. Elevated profile of Th17, Th1 and Tc1 cells in patients with immune thrombocytopenic purpura. Haematologica. 2009;94(9):1326-9.

142. Lonati A, Licenziati S, Canaris AD, Fiorentini S, Pasolini G, Marcelli M, et al. Reduced production of both Th1 and Tc1 lymphocyte subsets in atopic dermatitis (AD). Clin Exp Immunol. 1999;115(1):1-5.

143. Sun HL, Ma CJ, Du XF, Yang SY, Lv X, Zhao H, et al. Soluble IL-2Rα correlates with imbalances of Th1/Th2 and Tc1/Tc2 cells in patients with acute brucellosis. Infect Dis Poverty. 2020;9(1):92.

144. Williams GP, Schonhoff AM, Jurkuvenaite A, Gallups NJ, Standaert DG, Harms AS. CD4 T cells mediate brain inflammation and neurodegeneration in a mouse model of Parkinson's disease. Brain. 2021;144(7):2047-59.

145. Brochard V, Combadière B, Prigent A, Laouar Y, Perrin A, Beray-Berthat V, et al. Infiltration of CD4+ lymphocytes into the brain contributes to neurodegeneration in a mouse model of Parkinson disease. J Clin Invest. 2009;119(1):182-92.

146. Zucca FA, Capucciati A, Bellei C, Sarna M, Sarna T, Monzani E, et al. Neuromelanins in brain aging and Parkinson's disease: synthesis, structure, neuroinflammatory, and neurodegenerative role. IUBMB Life. 2023;75(1):55-65.

147. Galiano-Landeira J, Torra A, Vila M, Bové J. CD8 T cell nigral infiltration precedes synucleinopathy in early stages of Parkinson's disease. Brain. 2020;143(12):3717-33.

148. Sommer A, Marxreiter F, Krach F, Fadler T, Grosch J, Maroni M, et al. Th17 Lymphocytes Induce Neuronal Cell Death in a Human iPSC-Based Model of Parkinson's Disease. Cell Stem Cell. 2018;23(1):123-31 e6.

149. Schroder JB, Pawlowski M, Meyer Zu Horste G, Gross CC, Wiendl H, Meuth SG, et al. Immune Cell Activation in the Cerebrospinal Fluid of Patients With Parkinson's Disease. Front Neurol. 2018;9:1081.

150. Baba Y, Kuroiwa A, Uitti RJ, Wszolek ZK, Yamada T. Alterations of T-lymphocyte populations in Parkinson disease. Parkinsonism Relat Disord. 2005;11(8):493-8.

151. Stevens CH, Rowe D, Morel-Kopp MC, Orr C, Russell T, Ranola M, et al. Reduced T helper and B lymphocytes in Parkinson's disease. J Neuroimmunol. 2012;252(1-2):95-9.

152. Kustrimovic N, Comi C, Magistrelli L, Rasini E, Legnaro M, Bombelli R, et al. Parkinson's disease patients have a complex phenotypic and functional Th1 bias: cross-sectional studies of CD4+ Th1/Th2/T17 and Treg in drug-naïve and drug-treated patients. J Neuroinflammation. 2018;15(1):205.

153. Lindestam Arlehamn CS, Dhanwani R, Pham J, Kuan R, Frazier A, Rezende Dutra J, et al. α-Synuclein-specific T cell reactivity is associated with preclinical and early Parkinson's disease. Nat Commun. 2020;11(1):1875.

154. Singhania A, Pham J, Dhanwani R, Frazier A, Rezende Dutra J, Marder KS, et al. The TCR repertoire of α-synuclein-specific T cells in Parkinson's disease is surprisingly diverse. Sci Rep. 2021;11(1):302.

155. Li H, Ye C, Ji G, Han J. Determinants of public T cell responses. Cell Res. 2012;22(1):33-42.

156. Sulzer D, Alcalay RN, Garretti F, Cote L, Kanter E, Agin-Liebes J, et al. T cells from patients with Parkinson's disease recognize alpha-synuclein peptides. Nature. 2017;546(7660):656-61.

157. Dai L, Shen Y. Insights into T-cell dysfunction in Alzheimer's disease. Aging Cell. 2021;20(12):e13511.

158. Iba M, Kim C, Sallin M, Kwon S, Verma A, Overk C, et al. Neuroinflammation is associated with infiltration of T cells in Lewy body disease and α-synuclein transgenic models. J Neuroinflammation. 2020;17(1):214.

159. Kouli A, Camacho M, Allinson K, Williams-Gray CH. Neuroinflammation and protein pathology in Parkinson's disease dementia. Acta Neuropathol Commun. 2020;8(1):211.

160. Castellani RJ, Nugent SL, Morrison AL, Zhu X, Lee HG, Harris PL, et al. CD3 in Lewy pathology: does the abnormal recall of neurodevelopmental processes underlie Parkinson's disease. J Neural Transm (Vienna). 2011;118(1):23-6.

161. Gate D, Tapp E, Leventhal O, Shahid M, Nonninger TJ, Yang AC, et al. CD4(+) T cells contribute to neurodegeneration in Lewy body dementia. Science. 2021;374(6569):868-74.

162. Taguchi K, Watanabe Y, Tsujimura A, Tatebe H, Miyata S, Tokuda T, et al. Differential expression of alpha-synuclein in hippocampal neurons. PLoS One. 2014;9(2):e89327.

163. Taguchi K, Watanabe Y, Tsujimura A, Tanaka M. Brain region-dependent differential expression of alpha-synuclein. J Comp Neurol. 2016;524(6):1236-58.

164. Chen L, Nagaraja C, Daniels S, Fisk ZA, Dvorak R, Meyerdirk L, et al. Synaptic location is a determinant of the detrimental effects of α-synuclein pathology to glutamatergic transmission in the basolateral amygdala. Elife. 2022;11.

165. Ineichen BV, Okar SV, Proulx ST, Engelhardt B, Lassmann H, Reich DS. Perivascular spaces and their role in neuroinflammation. Neuron. 2022;110(21):3566-81.

166. McCandless EE, Wang Q, Woerner BM, Harper JM, Klein RS. CXCL12 limits inflammation by localizing mononuclear infiltrates to the perivascular space during experimental autoimmune encephalomyelitis. J Immunol. 2006;177(11):8053-64.

167. Cruz-Orengo L, Holman DW, Dorsey D, Zhou L, Zhang P, Wright M, et al. CXCR7 influences leukocyte entry into the CNS parenchyma by controlling abluminal CXCL12 abundance during autoimmunity. J Exp Med. 2011;208(2):327-39.

168. Rockenstein E, Mallory M, Hashimoto M, Song D, Shults CW, Lang I, et al. Differential neuropathological alterations in transgenic mice expressing alpha-synuclein from the platelet-derived growth factor and Thy-1 promoters. J Neurosci Res. 2002;68(5):568-78.

169. Chesselet MF, Richter F, Zhu C, Magen I, Watson MB, Subramaniam SR. A progressive mouse model of Parkinson's disease: the Thy1-aSyn ("Line 61") mice. Neurotherapeutics. 2012;9(2):297-314.

170. Jang DI, Lee AH, Shin HY, Song HR, Park JH, Kang TB, et al. The Role of Tumor Necrosis Factor Alpha (TNF-alpha) in Autoimmune Disease and Current TNF-alpha Inhibitors in Therapeutics. Int J Mol Sci. 2021;22(5).

171. Harms AS, Cao S, Rowse AL, Thome AD, Li X, Mangieri LR, et al. MHCII is required for α-synuclein-induced activation of microglia, CD4 T cell proliferation, and dopaminergic neurodegeneration. J Neurosci. 2013;33(23):9592-600.

172. Earls RH, Menees KB, Chung J, Barber J, Gutekunst CA, Hazim MG, et al. Intrastriatal injection of preformed alpha-synuclein fibrils alters central and peripheral immune cell profiles in non-transgenic mice. J Neuroinflammation. 2019;16(1):250.

173. Luk KC, Kehm V, Carroll J, Zhang B, O'Brien P, Trojanowski JQ, et al. Pathological α-synuclein transmission initiates Parkinson-like neurodegeneration in nontransgenic mice. Science. 2012;338(6109):949-53.

174. Gate D, Saligrama N, Leventhal O, Yang AC, Unger MS, Middeldorp J, et al. Clonally expanded CD8 T cells patrol the cerebrospinal fluid in Alzheimer's disease. Nature. 2020;577(7790):399-404.

175. Bridel C, van Wieringen WN, Zetterberg H, Tijms BM, Teunissen CE, Alvarez-Cermeño JC, et al. Diagnostic Value of Cerebrospinal Fluid Neurofilament Light Protein in Neurology: A Systematic Review and Meta-analysis. JAMA Neurol. 2019;76(9):1035-48.

176. Giunti D, Borsellino G, Benelli R, Marchese M, Capello E, Valle MT, et al. Phenotypic and functional analysis of T cells homing into the CSF of subjects with inflammatory diseases of the CNS. J Leukoc Biol. 2003;73(5):584-90.

177. Pashenkov M, Söderström M, Link H. Secondary lymphoid organ chemokines are elevated in the cerebrospinal fluid during central nervous system inflammation. J Neuroimmunol. 2003;135(1-2):154-60.

178. Amin J, Boche D, Clough Z, Teeling J, Williams A, Gao Y, et al. Peripheral immunophenotype in dementia with Lewy bodies and Alzheimer’s disease: an observational clinical study. Journal of Neurology, Neurosurgery & Psychiatry. 2020;91(11):1219-26.

179. Mahnke YD, Brodie TM, Sallusto F, Roederer M, Lugli E. The who's who of T-cell differentiation: human memory T-cell subsets. Eur J Immunol. 2013;43(11):2797-809.

180. Kimura A, Kishimoto T. IL-6: regulator of Treg/Th17 balance. Eur J Immunol. 2010;40(7):1830-5.

181. Stylianou E, Saklatvala J. Interleukin-1. Int J Biochem Cell Biol. 1998;30(10):1075-9.

182. Yang J, Ran M, Li H, Lin Y, Ma K, Yang Y, et al. New insight into neurological degeneration: Inflammatory cytokines and blood-brain barrier. Front Mol Neurosci. 2022;15:1013933.

183. Watson MB, Richter F, Lee SK, Gabby L, Wu J, Masliah E, et al. Regionally-specific microglial activation in young mice over-expressing human wildtype alpha-synuclein. Exp Neurol. 2012;237(2):318-34.

184. Guo L, Li X, Gould T, Wang ZY, Cao W. T cell aging and Alzheimer's disease. Front Immunol. 2023;14:1154699.

185. Xiong Y, Bosselut R. CD4-CD8 differentiation in the thymus: connecting circuits and building memories. Curr Opin Immunol. 2012;24(2):139-45.

186. Churlaud G, Pitoiset F, Jebbawi F, Lorenzon R, Bellier B, Rosenzwajg M, et al. Human and Mouse CD8(+)CD25(+)FOXP3(+) Regulatory T Cells at Steady State and during Interleukin-2 Therapy. Front Immunol. 2015;6:171.

187. Lazarini F, Tham TN, Casanova P, Arenzana-Seisdedos F, Dubois-Dalcq M. Role of the alpha-chemokine stromal cell-derived factor (SDF-1) in the developing and mature central nervous system. Glia. 2003;42(2):139-48.

188. Timotijević G, Mostarica Stojković M, Miljković D. CXCL12: role in neuroinflammation. Int J Biochem Cell Biol. 2012;44(6):838-41.

189. Hatton RD, Weaver CT. Immunology. T-bet or not T-bet. Science. 2003;302(5647):993-4.

190. Strieter RM, Gomperts BN. CHEMOKINES, CXC | CXCL12 (SDF-1). In: Laurent GJ, Shapiro SD, editors. Encyclopedia of Respiratory Medicine. Oxford: Academic Press; 2006. p. 390-4.

191. Zheng W, Flavell RA. The transcription factor GATA-3 is necessary and sufficient for Th2 cytokine gene expression in CD4 T cells. Cell. 1997;89(4):587-96.

192. Bankhead P, Loughrey MB, Fernández JA, Dombrowski Y, McArt DG, Dunne PD, et al. QuPath: Open source software for digital pathology image analysis. Sci Rep. 2017;7(1):16878.

193. Hartnell IJ, Woodhouse D, Jasper W, Mason L, Marwaha P, Graffeuil M, et al. Glial reactivity and T cell infiltration in frontotemporal lobar degeneration with tau pathology. Brain. 2024;147(2):590-606.

194. Wang XN, McGovern N, Gunawan M, Richardson C, Windebank M, Siah TW, et al. A three-dimensional atlas of human dermal leukocytes, lymphatics, and blood vessels. J Invest Dermatol. 2014;134(4):965-74.

195. Schneider CA, Rasband WS, Eliceiri KW. NIH Image to ImageJ: 25 years of image analysis. Nat Methods. 2012;9(7):671-5.

196. Lier J, Streit WJ, Bechmann I. Beyond Activation: Characterizing Microglial Functional Phenotypes. Cells. 2021;10(9).

197. Walker DG, Lue LF. Immune phenotypes of microglia in human neurodegenerative disease: challenges to detecting microglial polarization in human brains. Alzheimers Res Ther. 2015;7(1):56.

198. Hopperton KE, Mohammad D, Trépanier MO, Giuliano V, Bazinet RP. Markers of microglia in post-mortem brain samples from patients with Alzheimer's disease: a systematic review. Mol Psychiatry. 2018;23(2):177-98.

199. Fuller JP, Stavenhagen JB, Teeling JL. New roles for Fc receptors in neurodegeneration-the impact on Immunotherapy for Alzheimer's Disease. Front Neurosci. 2014;8:235.

200. Noorani I, Sidlauskas K, Pellow S, Savage R, Norman JL, Chatelet DS, et al. Clinical impact of anti-inflammatory microglia and macrophage phenotypes at glioblastoma margins. Brain Commun. 2023;5(3):fcad176.

201. Zhao X, Wang H, Sun G, Zhang J, Edwards NJ, Aronowski J. Neuronal Interleukin-4 as a Modulator of Microglial Pathways and Ischemic Brain Damage. J Neurosci. 2015;35(32):11281-91.

202. Rakic S, Hung YMA, Smith M, So D, Tayler HM, Varney W, et al. Systemic infection modifies the neuroinflammatory response in late stage Alzheimer's disease. Acta Neuropathol Commun. 2018;6(1):88.

203. Moreno-Rodriguez M, Perez SE, Nadeem M, Malek-Ahmadi M, Mufson EJ. Frontal cortex chitinase and pentraxin neuroinflammatory alterations during the progression of Alzheimer's disease. J Neuroinflammation. 2020;17(1):58.

204. Ferreira SA, Romero-Ramos M. Microglia Response During Parkinson's Disease: Alpha-Synuclein Intervention. Front Cell Neurosci. 2018;12:247.

205. Choi YR, Kang SJ, Kim JM, Lee SJ, Jou I, Joe EH, et al. FcγRIIB mediates the inhibitory effect of aggregated α-synuclein on microglial phagocytosis. Neurobiol Dis. 2015;83:90-9.

206. Choi YR, Cha SH, Kang SJ, Kim JB, Jou I, Park SM. Prion-like Propagation of α-Synuclein Is Regulated by the FcγRIIB-SHP-1/2 Signaling Pathway in Neurons. Cell Rep. 2018;22(1):136-48.

207. Kramer ML, Schulz-Schaeffer WJ. Presynaptic alpha-synuclein aggregates, not Lewy bodies, cause neurodegeneration in dementia with Lewy bodies. J Neurosci. 2007;27(6):1405-10.

208. Kam TI, Song S, Gwon Y, Park H, Yan JJ, Im I, et al. FcγRIIb mediates amyloid-β neurotoxicity and memory impairment in Alzheimer's disease. J Clin Invest. 2013;123(7):2791-802.

209. Orr CF, Rowe DB, Mizuno Y, Mori H, Halliday GM. A possible role for humoral immunity in the pathogenesis of Parkinson's disease. Brain. 2005;128(Pt 11):2665-74.

210. Mak E, Reid RI, Przybelski SA, Lesnick TG, Schwarz CG, Senjem ML, et al. Influences of amyloid-β and tau on white matter neurite alterations in dementia with Lewy bodies. NPJ Parkinsons Dis. 2024;10(1):76.

211. Biernacki K, Prat A, Blain M, Antel JP. Regulation of cellular and molecular trafficking across human brain endothelial cells by Th1- and Th2-polarized lymphocytes. J Neuropathol Exp Neurol. 2004;63(3):223-32.

212. Gan J, Xu Z, Chen Z, Liu S, Lu H, Wang Y, et al. Blood-brain barrier breakdown in dementia with Lewy bodies. Fluids Barriers CNS. 2024;21(1):73.

213. Melzer N, Meuth SG, Wiendl H. CD8+ T cells and neuronal damage: direct and collateral mechanisms of cytotoxicity and impaired electrical excitability. Faseb j. 2009;23(11):3659-73.

214. Rhee JY, Ghannam JY, Choi BD, Gerstner ER. Labeling T Cells to Track Immune Response to Immunotherapy in Glioblastoma. Tomography. 2023;9(1):274-84.